

CHEMOTACTIC RESPONSES OF TETHERED BACTERIA

Thesis by

Steven M. Block

In Partial Fulfillment of the Requirements

for the Degree of

Doctor of Philosophy

California Institute of Technology

Pasadena, California

1983

(Submitted May 23, 1983)

i i

to Grandma Sue

ACKNOWLEDGEMENTS

It is a pleasure to be able to record, in print, my heretofore unsaid thanks to all those people who managed, in one way or another, to help me through graduate school.

I owe an enormous debt to the late Max Delbrück, who took me under his wing after I graduated Oxford and started me off in science. I am also indebted to Ed Lipson, with whom I worked closely during my tenure with Max, for starting me off on the right foot.

My sincerest thanks go to Howard Berg, my adviser, in whose tracks I have followed the last several years. I admire Howard for his strong scientific instincts, his technical skill, and his ability to write clearly. I hope I have learned from each of these. I also admire Howard as a truly likeable, warm person, who, with his wife Mary, extended hospitality and friendship; these have meant a great deal to me over the years.

Thanks also go to Jeff Segall, my colleague, with whom I have spent uncounted hours doing experiments, analyzing data, and arguing over the meaning of it all. It has been my fortune to be able to have someone close by to share the roller-coaster ride of experimental science, and Jeff has proved to be a stubborn and stalwart companion. Thanks, Jeff.

Thanks further to Mike Manson and his wife Lilly, who encouraged me, counseled me, consoled me, and transformed parts of my graduate experience from endurable to pleasurable. I love you both.

Back in Boulder, which I have dearly missed, I thank especially my teachers Dick McIntosh and Mike Yarus, whose combination of style and wisdom I so much enjoyed. Thanks to Paul Horowitz, on leave from Harvard, who undertook, by example and through his class notes and book, to teach me electronics. I also thank Peter Nielsen, my friend and colleague, who showed me the meaning of quiet

strength. And Evelyn Krohn, who served as graduate secretary and mother-to-us-all, soothing the hurts and sharing the triumphs. I wish every graduate student could have an Evelyn in his life.

Here in Pasadena, Nancy Gill has taken up where Evelyn left off, and I feel twice blessed. Thanks to Bill Lease for his help and support. Thanks to Mike Walsh, who solved all my electronics dilemmas and has been a great friend. Thanks also to Caren Oto and Candi Hochenedel for help in typing the manuscripts, to the J. Alfred Prufrock house and eating group (my graduate family), to those in the lab, especially Pat, Markus, and Paul, and to all others who helped.

Thanks to my faculty committee, Drs. Berg, Fender, Hopfield, Lester, and Revel for reading this thesis and serving on the committee.

I gratefully acknowledge the support of the University of Colorado, The California Institute of Technology, grants and traineeships from the NIH and NSF, as well as the support of a University of Colorado Fellowship and an NSF Fellowship during my graduate study.

ABSTRACT

Escherichia coli swim in a three-dimensional random walk of alternating runs and tumbles, using their flagella for propulsion. When moving in a gradient of an attractant or repellent, they bias the walk in such a way as to migrate into a favorable region; this is a basis for chemotaxis. Bacteria may be tethered to a glass surface by means of a single flagellum. When tethered, cell bodies spin alternately clockwise (CW) and counterclockwise (CCW) under the influence of the rotary motor that drives the flagellum. The CCW state corresponds to the run mode and the CW state to the tumble mode. Tethered bacteria remain fixed in place, thereby providing an opportunity to study chemotactic behavior by direct manipulation of attractant or repellent concentration near the cells. Two experimental approaches have been used to exploit this opportunity. In the first, a mixing device that provides programmable concentration changes was used to stimulate tethered cells with exponential temporal gradients or exponentiated sine waves of the attractant α -methyl-D,L-aspartate. Such changes cause chemo-receptor occupancy to be changed linearly or sinusoidally, respectively. Exponential temporal gradients (both positive and negative) were found to shift the rotational bias (defined as the fraction of time spent spinning CCW) by a fixed amount related to the steepness of the gradient. The bias shifts produced indicate that cells are exquisitely sensitive to small changes in chemo-receptor occupancy. Distributions of CW and CCW intervals remained exponential during such gradients. This result is inconsistent with a response regulator model in which rotational transitions are associated with level-crossings of a fluctuating, hypothetical intermediate. It is consistent with a model in which transitions occur at random between rotational states, the transition probabilities being governed by chemotactic signals. In the second approach, short bursts of an attractant or repellent were delivered iontophoretically, producing an impulse response in the tethered

bacteria. Properties of the impulse response show both adaptive and integrative behavior, and imply that cells respond maximally to changes in concentration which occur over times comparable with the length of a run. The impulse response can be used to predict the behavior of cells towards an arbitrary stimulus in the linear domain. Impulse responses from a series of chemotaxis mutants showed that some were defective in adaptation but not excitation; others were defective in both. Taken together, the experiments provide information about the spectral response of bacteria to concentration changes with frequencies ranging from 10^{-3} Hz up to almost 10 Hz. Both sets of data are consistent with the notion of a cellular "bias regulator" signal that sets the transition probabilities between two states; one representing CCW and the other representing CW rotation.

TABLE OF CONTENTS

	<u>Page</u>
Dedication	ii
Acknowledgements	iii
Abstract	v
Table of Contents	vii
Quotations	viii
Preface	1
General Introduction.	3
Chapter I Stimulation of Tethered Cells by Programmed Gradients	17
Adaptation Kinetics in Bacterial Chemotaxis (as printed in J. Bacteriol. 154:312-323. copyright 1983, Am. Soc. Microbiol.)	40
Additional Data and Summary	89
Chapter II Stimulation of Tethered Cells by Iontophoresis	98
Impulse Responses in Bacterial Chemotaxis (reprinted from Cell 31:215-226 copyright 1982, MIT)	101
Additional Data and Summary	114
References	128

We are here on earth to learn, I have concluded
(possibly because it's clear that I'm never
going to make any money)."

Noel Coppage

What is true for E. coli,
is true for elephants,
only more so."[†]

Jacques Monod

[†]I thank Jeff Mayne for bringing this quotation to my attention.

PREFACE

It has been said that theses are read only by a faculty committee (out of obligation), a few family relatives (out of a sense of loyalty), and by their own authors (for proofreading purposes). Begging the indulgence of this small readership, I hope to depart somewhat from the terse academic style reserved for the writing of journal articles. After all, a thesis is a bit like a diary—it is a chronicle of years of activity (alas, altogether too many years, in my case!). Seldom are those years devoted single-mindedly towards one purpose; even more seldom are the activities uniformly successful. Apparatus is built that proves unworkable. Theories are developed, tested and found wanting. Experiments are tried and fail, etc. Finally, due only to persistence, borne of either stubbornness or naïveté, a few things begin to go right. Building on these, the graduate student regains both the lost track and his sense of worthiness as a scientist. Both success and failure are a part of a graduate career. Only the successes, however, find their way into scientific publications. Seldom does anyone chronicle the failures. This is, arguably, the way it should be: the scientific community doesn't advance through the failures of its graduate students. But the graduate students themselves can, and do. It is a cliché, but nonetheless true, that we learn from our failures. The thesis is the one opportunity we have to document, albeit for a small readership, some of the things that didn't work.

With this notion in mind, I have included published, unpublished (but publishable), and downright unpublishable information in this thesis. A certain forbearance will be required by those readers put off by turgid prose, speculation, heuristics, etc. Failing that, they are requested to confine their reading to the two chapters containing articles that have already been submitted and accepted for publication. Readers bored by gadgets should skip the extended sections dealing with custom-built apparatus. Readers who dislike teleology would do well to pass

up sections that attempt to explain just why bacteria behave the way they do.

After all, this is my one chance to write some of this down. I'm going to use it.

INTRODUCTION

The bacterial system

Bacteria are remarkable creatures. Only microns in length, they perform the entire repertoire of functions traditionally associated with living things: they eat, grow, and reproduce; they move and respond to stimuli. In the case of a bacterium such as Escherichia coli, this vital activity takes place inside a cytoplasmic volume of less than one femtoliter. The bacterium is a metabolic jack-of-all-trades, obtaining most, if not all, that it requires from the surrounding milieu. Simple sugars, amino acids, salts, etc., are actively accumulated and anabolized into the compounds required to sustain life and support reproduction. The process by which this occurs is currently one of the better understood in biology: of the roughly 4000 proteins estimated from the coding capacity of E. coli DNA, nearly 3000 have been identified biochemically (Watson, 1977), while some 1300 have been genetically mapped (Bachmann and Low, 1980). Mapping has been aided by the relative ease with which mutant strains are identified and isolated in bacteria. Recent advances in recombinant DNA technology have also centered around bacterial genetics and biochemistry; most eukaryotic gene cloning operations are, in fact, performed using strains of E. coli.

Bacteria are more than tiny bags of enzymes and nucleic acids, however. In order to obtain food and to secure a competitive advantage, they have developed the ability to swim and to sense. Bacterial size imposes unique restrictions on the mechanisms they can use to generate useful behavior (Purcell, 1977; Berg and Purcell, 1977). Size also imposes restrictions on the means by which these mechanisms can be studied: prokaryotes are generally too small to yield to conventional neurophysiological approaches. Nonetheless, the power of bacterial genetics, taken together with the relative organizational simplicity of prokaryotes, have made bacteria attractive for the study of sensory behavior.

A brief history of chemotaxis

Anton van Leeuwenhoek, during the late 17th century, is generally regarded as the first man to observe bacterial behavior. Using a handheld, single-lens microscope of his own invention, he detailed observations of not only small "animalcules"—probably protozoa—but also of organisms only a fraction their size—probably bacteria (Dobell, 1958). He imagined them, like their larger counterparts, to be possessed of "paws withal," with which they presumably swam. Two centuries passed before scientific investigation of bacterial movement began in earnest with the work of Engelmann (1883) and Pfeffer (1884, 1888), who examined the ability of bacteria to accumulate in gradients of chemicals and oxygen. This movement towards chemicals—chemotaxis—remains a subject of study today.

The present renaissance of interest in bacterial chemotaxis dates from the 1960's, when Julius Adler took up the study of chemotaxis in E. coli as a model system for sensory transduction. Modifying techniques pioneered by Pfeffer, he was able to show that chemotaxis was effected through the sensation of an attractant (or repellent) per se, i.e., that neither transport nor metabolism of the sensed chemical were required (Adler, 1969). This implied that bacteria were equipped with peripheral chemoreceptors that monitored local concentrations of specific substances; information derived from these receptors modified cell movement.

The mechanism for bacterial motility itself remained a source of controversy over the years. Flagellated bacteria, such as E. coli, move by means of a bundle of long, wavy flagellar filaments. These bundles can be seen, for example, in phase-contrast images of bacteria having large numbers of flagella, such as C. okenii and S. volutans. They can also be visualized in dark field using extremely intense sources (Macnab, 1976). It is not possible, by simply viewing bundle movement, to

decide between a model in which bundled filaments propagate helical bending waves, as is the case for motility in some sperm, or a model in which the helical filaments literally rotate (e.g., Berg and Anderson, 1973; Berg, 1975). The issue of whether bacterial flagella bent or rotated was not resolved until about ten years ago. The wave-propagation hypothesis was placed in serious jeopardy by Berg and Anderson (1973), who based their arguments for rotation on the effects of mono- and divalent flagellar antibodies upon bundle movement. Bending wave theories were finally laid to rest when Silverman and Simon (1974) succeeded in tethering cells of *E. coli* to a glass surface by means of a flagellum. The cell bodies were observed to spin in circles from the torque generated by the cell on the filament, affirming the rotation hypothesis. The tethered cell paradigm, in which bacteria, attached via antibodies (or, in some cases, spontaneously) by a filament or hook to a surface, spin alternately clockwise (CW) and counterclockwise (CCW), has since become an invaluable preparation for studying flagellar responses in this and other laboratories.

The motor and its modulation

The flagellar basal body contains the rotary motor which supplies torque to the filament of a swimming cell (DePamphilis and Adler, 1971; Berg, 1974); this filament serves as a relatively rigid propellor which moves the cell through the fluid. The motor itself is exquisitely small: just 225 nm in diameter. It is capable of exerting torque in either rotational sense, i.e., it has a "reverse gear." Unlike the actin-myosin sliding interaction that powers muscle, or the analogous dynein-microtubule interaction that bends cilia, the bacterial motor does not utilize ATP as its energy source (Larsen et al., 1974). It is powered instead by a more fundamental "energy currency", the protonmotive force (pmf, Manson et al., 1977); this is the same energy source that drives ATP synthesis in bacteria, mitochondria, and chloroplasts, as well as a host of active transport systems. The mechanism by

which the pmf turns the motor, and the mechanism by which the motor is able to reverse, are unknown at present.

To perform chemotaxis, some communication must exist between the primary chemoreceptors, located in both the periplasmic space and inner membrane, and the flagellar motor. This signalling comprises a sensory transduction chain. Viewed in a broader sense, bacterial chemotaxis represents a stimulus-response system in which the input is a local concentration of attractant or repellent and the output is the motion of the cell through the medium. The problem, then, is to determine the sequence of molecular interactions which couple the input and output. Quite a bit of progress has been made along this line over the last decade, largely through the isolation and characterization of cells defective in chemotaxis.

Mutations that affect bacterial motility

When bacteria are mutagenized and selected for the loss of swimming ability, two broad classes of mutant are isolated. In the first class, cells are unable to synthesize one or more of the flagellar components, and therefore lack the equipment with which to swim. Such cells generally fail to produce flagellar filaments, and are designated as fla (and, more recently, also as flb). Those in the second class produce intact, morphologically normal flagella that are unable to rotate. Cells with this paralyzed phenotype map into one of two mot (for motility) loci. The mot gene products are not found in the basal body itself, but can be isolated from cell membrane fractions. Induction of mot synthesis in mutants missing the gene product restores swimming ability (Silverman, Matsumura, and Simon, 1976).

Close to thirty fla genes have been isolated. These genes include flaF, normally referred to as hag, which codes for flagellin, the sole constituent of the flagellar filament. The filament itself is joined to the basal body by means of a hook, which serves as a flexible joint to couple rotation off-axis (Berg and

Anderson, 1973). The hook protein is the product of the flaK gene. Mutations in the flaE gene give rise to long hooks, called polyhooks, implying that the flaE gene product is involved in hook termination. Most of the remaining fla genes code for elements of the basal body, and have undetermined functions. Flagellar synthesis is regulated by a series of complex, hierarchical controls: the absence of one or more fla genes usually leads to failure to synthesize or transcribe others. Partial assembly of basal bodies and incorporation of these parts into the cell membrane occurs only for certain fla gene combinations (Iino, 1977). At least two "executive" genes, flaI and flbB, control expression in clusters of other fla loci (Komeda, 1982). Flagellar synthesis is subject to catabolite repression through the CRP-cAMP complex as well through both positive and negative gene control mechanisms.

E. coli are peritrichously flagellated, i.e., the flagella arise at different sites on the cell body; normally 6-8 are made. For flagellar synthesis, proteins are required in vastly disproportionate number; basal bodies require only a few copies of minor fla gene products, each hook requires hundreds of monomers of flaK gene product, while the filament itself contains over 10,000 monomers of hag. The control system that governs the synthesis of bacterial flagella is one of the most complex that has been found in prokaryotes. (For reviews, see Iino, 1977; Silverman and Simon, 1977; Parkinson, 1982; Parkinson and Hazelbauer, 1983.)

Mutations that affect bacterial chemotaxis

Mutant cells can be found that are able to swim (or, at least, to rotate their filaments) but are unable to perform chemotaxis. Failure to execute chemotaxis towards one specific compound can be traced to mutation in a primary chemoreceptor, e.g., a sugar-binding protein (Hazelbauer, 1975). Cells that are generally non-chemotactic, however, define a class of mutants designated che (for chemotaxis-defective). Some che isolates run incessantly; others tumble

incessantly. All are believed to contain mutations in an element of the sensory chain. Less than a dozen che genes have been found.

A few nonchemotactic mutants, originally isolated as having the che phenotype, are in fact defective in taxis to a specific range of compounds, chemically unrelated. These include tsr (taxis to serine and certain repellents, also called cheD) and tar (taxis to aspartate and some repellents, also called cheM). Also defective in chemotaxis towards a range of compounds is trg (taxis to ribose and galactose). A gene closely related to these, tap, has been identified, although no specific taxis defects have been reported (Boyd et al., 1981). These four genes produce polypeptides known as methyl-accepting chemotaxis proteins (MCPs), which integrate information from receptor channels corresponding to a variety of compounds. The MCPs are membrane-spanning polypeptides that become methylated on the cytoplasmic side in proportion to the local concentration of attractant; they are demethylated by addition of repellent. They therefore serve as an internal measure of external concentration. MCPs are believed to mediate adaptation to chemicals; they are methylated and demethylated by the cheR and cheB gene products, respectively, over time spans corresponding roughly to those required for recovery to steps in concentration of attractants or repellents (Goy et al., 1977; Springer et al., 1979). The MCPs also behave as primary chemoreceptors. In the case of some compounds (e.g., serine, Clarke and Koshland, 1979; aspartate, Hedblom and Adler, 1980), they bind directly to substrate on the periplasmic face of the membrane. For other compounds, they serve as secondary chemoreceptors (e.g., ribose, Kondoh et al., 1979), interacting with periplasmic binding proteins that detect and transport metabolites. Possible interactions ("cross-talk") among the various MCPs have been reported (Springer et al., 1977). The MCPs are now being cloned and sequenced (Boyd et al., 1983); these proteins

are currently the subject of intense study. It is not known how communication is established between the MCPs and the motor.

Interactions among various other che gene products are equally crucial to signalling and adaptation. The methyltransferase, cheR, has been found to interact with the cheY gene product, while the methylesterase, cheB, interacts with the product of cheZ (Parkinson, 1981; Parkinson, 1982). The existence of such interactions has been established by a genetic approach involving interallelic suppression; the function of these interactions remains to be established. In addition, a form of adaptation not involving MCP methylation but instead related to an apparently irreversible MCP amino acid modification, performed by the cheB gene product, has been reported (Rollins and Dahlquist, 1981; Sherris and Parkinson, 1981). Space does not permit a full discussion of the genetics of chemotaxis. Interested readers are referred to recent reviews (Boyd and Simon, 1982; Parkinson, 1981, 1982).

The physiology of chemotaxis

Unstimulated bacteria swim in a three-dimensional random walk of alternating runs and tumbles. In the presence of a chemical gradient of an attractant or repellent, the random walk becomes biased in such a way that net drift occurs in the favorable direction (towards attractants, away from repellents). Specifically, runs with a component in the favorable direction are lengthened. Runs with unfavorable components and tumbles are largely unaffected (Berg and Brown, 1972, 1974). Swimming bacteria sense concentration gradients by means of a temporal, as opposed to a spatial, mechanism (Macnab and Koshland, 1972; Brown and Berg, 1974): the spatial concentration gradient is converted to a temporal one by the motion of the bacterium itself. It is doubtful that a spatial mechanism would be of any use to an organism the size of E. coli. Even if receptors were located maximally apart on opposite ends of a stationary cell, the concentration

difference set up between them by typical gradients would be only barely detectable over background noise: movement of the cell through the medium generates an apparent difference many times larger than the real one (Berg and Purcell, 1977).

When swimming cells are provided with abrupt increases in the concentration of an attractant, they run without tumbling for periods of minutes. Abrupt decreases in attractant concentration (or increases in repellent) lead to a much shorter period of tumbling behavior (Macnab and Koshland, 1972). When tethered cells are provided with similar abrupt increases in attractant concentration, they spin CCW for long periods. Abrupt decreases in concentration cause cells to enter a short period of CW rotation. Thus a one-to-one correspondence exists between motor rotational sense and running and tumbling (Larsen et al., 1974; Berg and Tedesco, 1975). However, the correspondence does not hold to the extent that mean run and tumble intervals equal mean CCW and CW intervals, respectively.¹ This breakdown in the relationship between tethered and swimming cells is poorly understood, and probably results in some way from interaction among the many flagella of free-swimming cells; tethered cells reflect the properties of the single rotary motor from which they are driven (Khan and Macnab, 1981; Ishihara et al., 1983).

Adaptation behavior

After the prolonged response induced by a rapid step in concentration, the swimming behavior of free cells or the rotational behavior of tethered cells returns to normal. This transient response to a tonic change in the chemical environment represents sensory adaptation. E. coli are able to sense and to completely adapt

¹ Runs and tumbles are distributed exponentially, with mean lifetimes of about 1 and 0.1 sec, respectively (Berg and Brown, 1972). CCW and CW intervals are also distributed exponentially, with mean lifetimes close to 1 sec for each direction (Block et al., 1982). Tumbles are therefore anomalously shorter than CW intervals.

out changes in attractant concentration covering almost five orders of magnitude (Berg and Brown, 1974; Berg and Tedesco, 1975; Spudich and Koshland, 1975). Adaptation and large dynamic range are the hallmark of sensory systems.² Sensory adaptation is observed almost universally in physiology, and yet it remains one of the most obscure phenomena. With the exception of trivial examples (such as the bleaching of photopigment at higher light levels), the molecular basis of adaptive processes is an outstanding mystery. One of the hopes in studying chemotaxis is that the mechanisms which mediate adaptation to chemicals in bacteria may have a greater generality.

The physiological range

Bacteria swimming in a natural habitat never experience stepwise concentration changes. They live in a world entirely dominated by thermal fluctuations and small numbers; these, in turn, give rise to diffusion, Brownian movement, and concentration "noise". Diffusion smooths out spatial irregularities in attractant concentration on the length scale of a bacterium in milliseconds. The drift of bacteria up chemical gradients, in itself a diffusive process, is too slow for cells to experience large variations in mean concentration over a short time scale. Moreover, rotational Brownian movement of the axis of motion in a swimming cell entirely prevents it from steering directly up a gradient, even in principle (Berg and Brown, 1974). Fluctuations in locally perceived concentration further complicate matters, requiring that some sort of signal averaging be performed in a successful chemotaxis strategy (Berg and Purcell, 1977): the gradients experienced by bacteria are noisy signals whose mean values change only slowly with time.

²For comparison, the dynamic range of vertebrate vision is around 10^9 , while audition has a dynamic range of around 10^7 . Most olfactory senses have dynamic ranges on the order of 10^{5-6} . Electroantennograms of the silk moth, *Bombyx mori*, show responses to the pheromone bombykol over a dynamic range of roughly 10^7 (Boeckh et al., 1965). All these senses show at least partial adaptation to stimuli over their entire dynamic range.

It is therefore somewhat ironic that so much of the major work in bacterial adaptation has been based on stepwise changes in concentration that are orders of magnitude larger than changes experienced during chemotaxis. Behavioral models developed from these studies have, until quite recently, guided the thinking of those in the field. The work undertaken for this thesis has been devoted to exploring the chemotactic responses of E. coli to signals in the physiological range.

Background for these experiments

Two previous groups have studied chemotactic responses to shallow spatial or temporal gradients. The experiments of Dahlquist et al. (1972, 1976) followed the movement of a population of cells in preformed one-dimensional gradients. Their inability to monitor the responses of individual cells complicated the analysis considerably, since a number of assumptions had to be made about details of cell movement (Lovely and Dahlquist, 1975); only the population density could be measured. Subject to the validity of these assumptions, models for the temporal response of bacteria to changing chemoreceptor occupancy were tested. An important result of their work was the confirmation that there is a regime of concentration where bacterial behavior obeys the well-known Weber-Fechner relationship (Boring, 1956): the change in bacterial response in this domain is proportional to the relative (spatial) change in concentration, i.e., cells respond in proportion to $d(\ln C)/dx$ (a behavior first reported by Pfeffer, 1888). Taking into account the fact that bacteria use a temporal sensing mechanism based on their movement, this implies that bacteria respond linearly to $d(\ln C)/dt$ in the Weber-Fechner region.

The experiments of Brown and Berg (1974) circumvented the problems associated with following cell populations through the use of the tracking microscope, which locks on to and follows the motion of individual cells (Berg, 1971). Spatial chemotaxis was simulated by producing isotropic temporal changes

in the concentration of an attractant in the medium; these changes were achieved by running an enzyme reaction which converted a substance that was chemotactically inert into an attractant (or, for repellent responses, by running a reaction that degraded an attractant to a chemotactically inert compound). The power of the experiment lay in its ability to measure the responses of single cells to controlled stimuli over time. The difficulty lay in the inability of the tracking microscope to follow the trajectory of a single cell for more than about a minute (the mean period of observation was approximately 30 sec). Thus, the experiment had to be repeated for a large number of cells; the enormous population variance found in the mean run length complicated the analysis and interpretation of the data. A further difficulty lay in the precise control over the stimulus timing, which was governed by the enzyme kinetics. Despite these drawbacks, results from the enzyme-gradient experiments argued persuasively that bacteria employ a temporal sensing mechanism. The data, when examined for a functional dependence of run length upon stimulus, supported a model in which bacteria monitor the temporal change in the fraction of chemoreceptor that has bound substrate. Data presented in Chapter I give new support for this model.

The tethered cell approach

With the advent of the tethered cell technique it was possible, for the first time, to make long-term observations of single cells. Using a miniature flow cell, Berg and Tedesco (1975) were able to record from tethered bacteria exposed to changes in concentration over extended periods; the stimulus could be brought to the cell, as it were, rather than vice versa. Although the recovery time³ to a step in attractant concentration varied widely from cell to cell, the responses of any given cell were accurately reproducible. In response to addition of an attractant (or the removal of a repellent), cells spun exclusively CCW for periods up to several minutes before regaining their prestimulus behavior (i.e., alternation of roughly

equal periods of CW and CCW rotation). They noted, in agreement with Brown and Berg (1974), that removal of an attractant (or addition of repellent) caused a substantially shorter period of CW behavior. This implied that the bacterial sensory system involved a kind of "rectification" of the response with respect to the rate of change of concentration.

The data of Berg and Tedesco were explained by a model in which adaptation to attractant increases took place slowly at a constant rate, independent of stimulus size. Adaptation to attractant decreases took place very rapidly. The independence of adaptation rate from the size of the stimulus meant that the sensory system was behaving in a manner analogous to a simple thermostat, in which the heat is turned on or off fully depending only upon whether the temperature was above or below the set point (and not by how much it was off). Since the size of the stimuli used were so large, Berg and Tedesco argued that this result may have been obtained purely because the bacterial signalling systems were being overloaded. To use language borrowed from electronics, the system was driven to its maximum slew rate by the input. Biochemically, this might correspond to some rate-limiting reaction (or set of reactions) involved in adaptation proceeding at V_{max} . The question naturally arose as to what was the functional dependence of adaptation upon stimulus history for less drastic

³Cells do not recover instantly to step changes in concentration, so the point of recovery must be carefully defined. Berg and Tedesco (1975) used the term "transition time" to denote the time taken for the relatively long period of exclusive CCW or CW behavior in tethered cells elicited by a step change, disregarding very short reversals that were seen in some cases. Spudich and Koshland (1975) used the term "recovery time" to denote the time at which half of a population of swimming cells had re-initiated tumbling behavior after a step up in attractant concentration. At the end of the transition time following a step up, cells reverse rapidly for a short while, generally spinning with increased probability in the CW direction; this period has been called the "response overshoot" by Berg and Tedesco.

concentration changes. The work reported in Chapter I of this thesis details a set of experiments undertaken to explore the question.

A programmable mixing apparatus was built and used to stimulate tethered E. coli with concentration changes in the range of a few percent per second. The results suggest that, in the domain of small changes, bacteria adapt at a rate roughly proportional to the difference between present and past receptor occupancy. Changes in receptor occupancy, in turn, are approximately proportional to changes in the logarithm of concentration; the response is therefore based on a calculation of the time-derivative of the bound receptor fraction. This can be shown to reflect a form of proportional control (as opposed to "thermostat" control).

High time resolution studies

The programmable mixer was capable of producing concentration changes which varied by an order of magnitude on a time scale from one hour down to tens of seconds. This includes a range over which, at the slow extreme, bacteria failed entirely to respond—being in a continuous state of adaptation with respect to their environment—and which, at the fast extreme, gave a completely saturated response—i.e., tethered cells spun exclusively in one mode. The response time of bacteria, defined as the time required to initiate a motor reversal in response to a chemotactic signal, is quite rapid: 0.2 sec (Segall et al., 1981). This short time scale is entirely outside of the domain that can be explored using the mixer.

Bacterial responses involve both an excitation and an adaptation phase. To examine these in detail, Jeff Segall and I employed iontophoretic techniques to administer tiny bursts of attractant in the neighborhood of tethered cells. The response to such bursts gives the impulse response for chemotaxis, which can be used to understand properties of the signalling chain. Both positive and negative stimuli were used. In addition to the wild type, a number of che mutants were also

examined. These experiments are covered in Chapter II. They show that bacteria can respond and adapt to small amounts of chemicals in seconds, and that the properties of the response system are nicely matched to the task at hand: the problem of whether cells must lengthen or terminate runs up (or down) noisy chemical gradients.

Taken together, the experiments of Chapter I and Chapter II are complementary, allowing us to chart the sensitivity of bacteria over four orders of magnitude in stimulus frequency. The measured impulse response can predict, quantitatively, many of the broad features seen in response to slow ramps of concentration. The ramp experiments offer an opportunity to examine nonlinearities in the response not revealed by linear (impulse response) analysis. The iontophoretic experiments, on the other hand, offer a new means of characterizing adaptation mutants, as well as fresh insight into how che genes might function in the signalling pathway.

Chapter I

STIMULATION OF TETHERED CELLS BY PROGRAMMED GRADIENTS

Background

This section covers background material related to the design of apparatus and experimental protocols for Block et al. (1983).

An early approach

Our original scheme for stimulating bacteria with slow changes in concentration involved the use of preformed gradients. Exponential gradients of an attractant in motility buffer were manufactured in a small gradient mixer and pumped into a Pasteur pipet. A sucrose density gradient was superimposed upon the attractant gradient in order to stabilize the gradient column against convective mixing. Several identical gradients were poured in a series of pipets and maintained for later use. Bacteria were tethered in a flow cell whose inlet tube ran from a two-way valve. The valve was fed by lines coming from either of a pair of reservoirs of motility buffer (containing fixed concentrations of attractant, arranged to equal those found at the top and bottom of the gradients) and from the outlet of a preformed gradient column. By switching the valve from a reservoir to the pipet and pumping in the contents of the gradient at a variable rate, exponential ramps in concentration of different time constants could be set up in the flow cell.

This plan proved unworkable for several reasons. First, the tethered cells became jittery in the presence of sucrose (probably an osmotic effect); this was remedied by changing to Ficoll, a long-chain polysaccharide. Second, it was impossible to arrange for the concentrations at the end-points of the ramp to exactly match the corresponding concentrations in the buffer reservoirs; although small, the experimental differences were sufficient to cause behavioral artifacts when the valve was switched at the start and end of the ramps. Third, the flows required to produce the appropriate ramp time constants were too high; cells were sometimes pulled off their tethers or pinned against the flow cell coverslip.

Finally, the pressure changes induced when the valve was switched caused the preparation to go out of focus for several seconds.

Programmable gradients

The preformed gradient approach was abandoned in favor of an on-line mixing apparatus that could produce continuous, programmable attractant concentrations. The device accommodated a slow, steady flow through the tethering chamber (independent of ramp rate), required no density gradients, generated no discontinuities in concentration at the ramp end-points, and allowed microscope focus to be maintained at all times. In addition, subject to restrictions on its dynamic range, any kind of concentration profile could be produced with the device, including sine waves. Despite its virtues, the apparatus was a plumber's nightmare of jumbled tubes and valves; successful experiments with it required fastidious attention to minor details, and it was inclined towards breakdown during the critical moments of an experiment. Detailed descriptions of the mixer and the associated pump programmer are given below.

Single cell observations

The experimental strategy involved recording for as long as possible from a single tethered bacterium. The experiments of Brown and Berg (1974) demonstrated a large variation in mean run length among a population of cells; runs were distributed log-normally. Analogous variations in CW/CCW intervals of tethered cells would have made analysis intractable. In contrast, the recovery (or transition) times of individual tethered bacteria are quite stereotyped and have a very much smaller variance (Berg and Tedesco, 1975). Hence more could be learned from looking at one cell for ten hours than ten cells for one hour. For the experiments described in this chapter, videotaped records were made from single fields of tethered cells which were subjected to multiple concentration changes over a

period of hours; emphasis was placed on finding those individual cells from which data could be taken for the entire duration of the experiment.

The tethering preparation

Tethered cell preparations have a finite lifetime. While tethered E. coli maintain endogenous energy reserves that allow them to rotate at several Hertz for days on end in simple buffer, their behavioral properties nevertheless change gradually; cells tend to become increasingly CCW-biased. An increase in CCW bias has been attributed to a drop in cellular pmf (Khan and Macnab, 1980). These changes begin surprisingly soon after tethering. Preliminary experiments in motility buffer (dilute phosphate buffer at pH 7.0 with EDTA) indicated changes in both CW/CCW interval properties and adaptation rate over the course of an experiment. An energy source (10 mM lactate) and methionine (10^{-6} M) were added to the buffer; this was found to alleviate the problem.

Another limiting factor was the tethering itself. In tethering E. coli with antifilament antibody, the antibody adheres nonspecifically to the glass surface. The glass must be exceedingly clean. The usual cleaning procedure involved treating coverslips with fuming nitric acid for a few minutes. I found that pre-cleaning coverslips in acetone, ethanol, and distilled water prior to the acid bath improved tethering lifetimes. Even so, tethered cells would, with time, become fixed at more than one point and thereby cease rotation. The problem was exacerbated by the fluid moving in the flow cell, which tended to force tethered bacteria closer to the glass. Worse, the tethering efficiency was low—the vast majority of cells in the field failed to spin. This was traced to the antibody then in use, which had been acquired from another lab. A second outside source of antibody was tried but it failed to give strong tethering as well. Finally, I isolated the flagella from a large population of bacteria and inoculated a rabbit; the antibody that was raised had the desired properties. With the new antibody,

tethering efficiency was improved and cells could be held for periods of six to eight hours while being perfused in the flow cell. At this point, preparation lifetimes were limited only by microscopic leaks and bubbles which formed in the system plumbing, coming mainly from around the greased seal which held the coverslip in place on the flow cell.

What to measure?

Given that cells were to be monitored for such long periods, it was necessary to ensure that the behavior was stationary in a statistical sense, i.e., that mean values of nominally fixed parameters were stable over the course of the experiment. As it turned out (notwithstanding the presence of methionine and lactate in the medium), mean unstimulated CW and CCW intervals were not constant (Fig. 3 of Block et al., 1983), but increased steadily. Neither was the reversal rate, which is a function of the sum of mean CW and CCW times. Fortunately, the ratio of mean CCW/CW times was maintained, and consequently so was the rotational bias of the cell, bias being defined as the fraction of time spent spinning CCW (or, equivalently, as the probability of CCW rotation). The reason for this stationarity is not known, but it implies that CW and CCW intervals are subject to a form of coordinate control that is relatively stable; more evidence for this will be developed later. Bias stationarity meant that differences in bias induced by identical chemotactic stimuli at the beginning and end of experiments were directly comparable.

The mean rotation rate of tethered cell bodies was also rather stable over time, maintaining its value to within ± 1 Hz for hours in some cases. However, chemotactic stimuli appear to have no effect upon rotation rate, only upon the direction of that rotation.

Apparatus

The remainder of this section is devoted to a description of the instruments used for stimulating tethered cells, recording data, and transferring data to computer records.

The mixing apparatus

The apparatus that manufactured time-varying concentrations underwent several major design changes. In the original incarnation, the cells were to have been sequestered from the moving fluid phase in the flow cell by a semipermeable membrane held close to the tethering surface; diffusion would then transport the changing attractant concentration across the membrane to the bacteria. In order not to introduce a long phase lag between the concentration at the tethered cell and in the moving fluid, such a membrane would have to be thin, transparent, and maintained within a few hundred microns of the tethering surface, a geometry that is obtained only with considerable effort. A number of schemes were tried. It later proved more practical to use a slow flow with no membrane barriers; the flow rates of less than 0.005 ml/sec used in these studies had no visible effect upon the motion of energized cells.

The top and supporting walls of the original flow cell were made mainly of glass and were extremely prone to breakage. A sturdier flow cell was designed whose body was machined from 316-stainless steel; top and bottom windows were made from circular coverslips and inlet and outlet pipes from 22 gauge stainless syringe needles.

The design of a suitable mixer posed problems. The time constant for mixing is given by the ratio of the volume of the mixer to the flow rate through it. To achieve a small mixing time constant therefore required a tiny chamber and/or a large flow rate. In order to accommodate a large flow rate into the mixer and the much slower rate needed in the tethering chamber, the mixer was designed with

two outlet ports. Through one port trickled a slow flow to the tethering chamber, while the remainder of the fast flow was discarded through the other. The mixer was fed approximately ten times the flow actually drawn off to the flow cell. This scheme had the additional advantage that the flow into the tethering chamber could be maintained constant, independent of the time-varying input to the mixer. A vacuum trap attached to the fast outlet port collected the excess. A needle valve (made originally from a model aircraft engine throttle, but eventually superseded by a more refined version) controlled flow to the vacuum trap and maintained the pressure at the slow port of the mixer just slightly below the pressure at the outlet of the tethering chamber. This adjustment was crucial insofar as it kept the coverslip sealed on the flow cell and in focus.

Originally, an active mixer was made inside the body of a four-way miniature valve (Hamilton #1-4-NNNN, internal volume approx. 0.1 cc). A tiny ferromagnetic bead, sealed in glass (1 mm OD), served as a stirring bar when oscillated at several Hertz by an external magnetic field produced by relay coils. Tests of this mixer using methylene blue dye (in place of attractant) at the desired flow rates showed that mixing was incomplete. The design was discarded and replaced by a passive mixer (internal volume 0.09 cc) packed with 0.5 μ -dia. glass wool (Corning Glass Works, Pyrex Wool #3950). The passive mixer gave homogeneous mixing at the experimental flow rates (judged spectroscopically with methylene blue dye), but, due to its construction, generated a large back pressure. The attractant pump, constructed from a glass syringe, was able to pump at a (slow) rate essentially independent of the back pressure (i.e., it acted as a good current source). However, the original buffer pump (a three-roller peristaltic pump manufactured by Holter), which ran ten times faster, was unable to provide flow independent of back pressure; it was replaced by a heavy-duty peristaltic pump (a

twelve-roller Gilson Minipuls II) that provided flow constant to within 5% over the required range.

Roller-to-roller transitions in the peristaltic pump caused small, periodic fluctuations in pumping pressure. Although this led to a negligible change in flow rates, the flow cell, with its sealed coverslip holding the tethered cells, acted as a sensitive manometer: the coverslip flexed up and down in response to the slightest variations in pressure. Since the microscope depth of field is only a few microns, it was impossible to keep the system in constant focus. Surge filters (hydrodynamic low pass filters) were constructed using 3 cc syringe bodies. Inlet and outlet pipes (made from 22-gauge needles) were added to the Luer-lock tip; the tip cavity was filled by fluid which passed through. The size of the sealed air chamber above was controlled by withdrawing the syringe plunger. In this fashion, the cavity could be tuned; the device behaved like a variable capacitor. Surge filters were placed on the output of the buffer pump and before the needle valve assembly. With the filters in place, the flow cell could be maintained in focus for minutes at a time, even when the attractant concentration was made to change over an order of magnitude.

The large pressure changes undergone by fluids moving through the mixing system caused them to outgas; small air bubbles would nucleate and slowly grow at the inlet and outlet pipes of the mixer and the tethering chamber. Such bubbles perturb the laminar flow pattern through the chamber. They proved even more disastrous to the tethering preparation when pin-prick sized bubbles (larger than the microscopic field of view) would break off and pass along the tethering surface, destroying the preparation. Autoclaving the buffer solution provided some relief, but not enough to be able to maintain observation for many hours. A successful remedy was provided by replacing the dissolved air with an 80:20 mixture of He and O₂; the greater solubility of He prevented the "bends" in the buffers.⁴

Design of the pump programmer

The attractant pump consisted of a glass syringe whose plunger was advanced by a micrometer driven via a timing belt off a stepping motor (see Fig. 1 of Block et al., 1983). The stepping motor, in turn, received input from drive circuitry clocked by pulses produced in the pump programmer. The device was set up to provide linear and exponential ramps in pumping rate between two preset holding levels, or sinusoidal (or exponentiated sinusoidal) changes in pumping rate of specified amplitude and frequency. See Text-figure 1.

Strip chart analysis

The rotational behavior of tethered cells was recorded on strip charts. For the impulse response experiments, these charts held records of the analog x- and y-outlets of the Linear Graded Filter apparatus⁵ (LGF), in addition to event markers indicating the timing of stimuli and the rotational sense of the cell, the latter being generated by electronics which used information from the LGF signals. Charts were produced in real time (i.e., during the experiment) using a 2-channel Gould Brush 220 recorder run at 25 mm/sec. For the adaptation experiments, the rotational sense was determined off-line (i.e., after the experiment) by an operator viewing a quarter-speed playback of a videotaped experiment who toggled an event

⁴I acknowledge Howard Berg's ingenuity for this solution. This may have had some influence on my subsequent decision to become a certified diver.

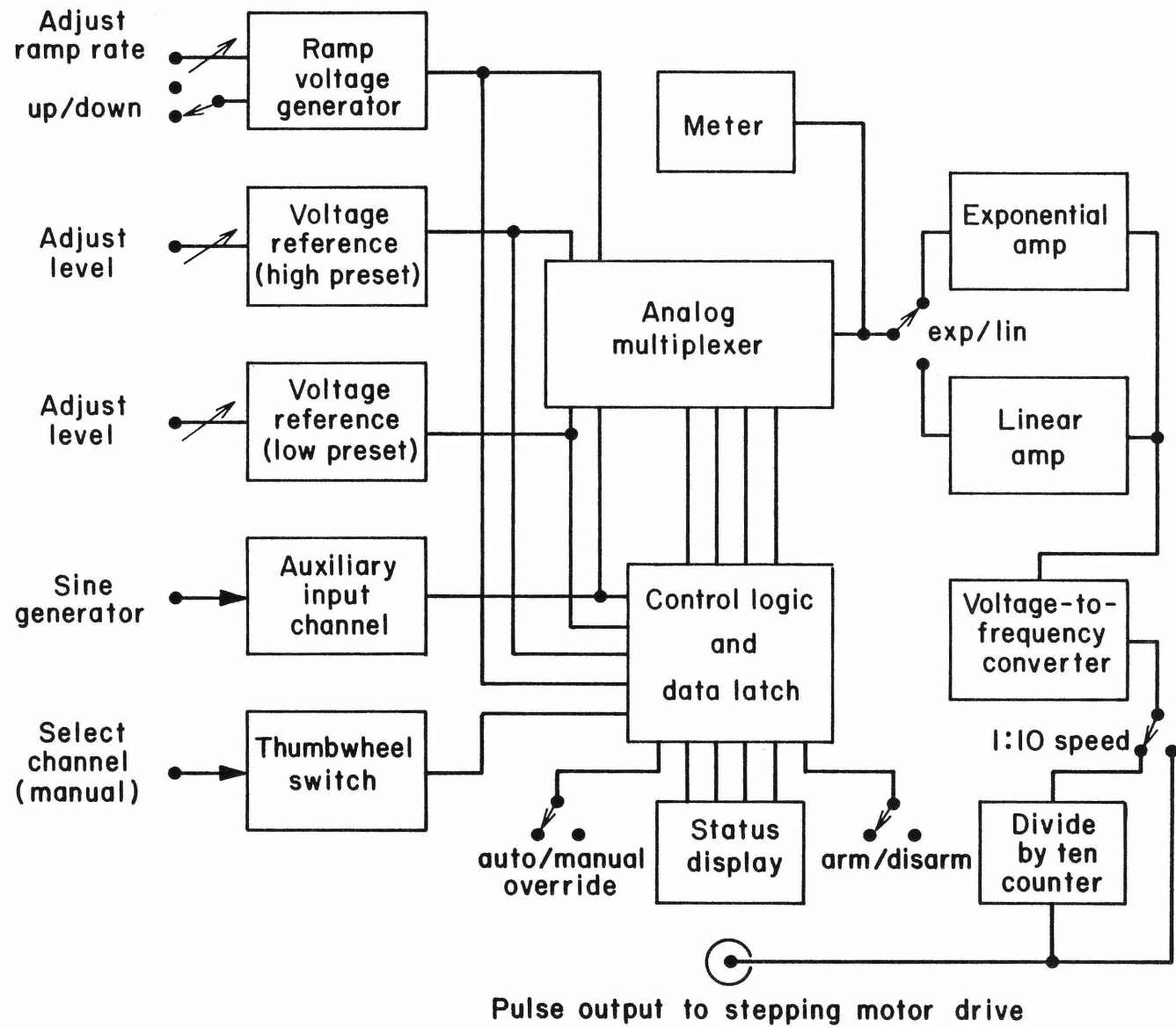
⁵The LGF is an optoelectronic device that derives signals which track the centroid of a rotating image (Berg et al., 1982). It passes identical images of the spinning cell, seen through a pinhole, to each of two inconel-coated "wedge" filters. These filters are designed to attenuate transmitted light as a linear function of the displacement across the filter; one is graded in the x-direction and the other in the y-direction. This has the effect of darkening each point in the image in proportion to its displacement in x or y. Photomultipliers over each filter integrate light coming from the cell and pinhole background. The signal from each photomultiplier is therefore proportional to one of the coordinates of the centroid of the image. For objects that execute circular motion, these signals are pure sine and cosine waves, regardless of the shape of the image. The relative phase of the signals gives the rotational handedness of the motion.

Text-figure 1. Logic diagram of pump programmer.

In the automatic mode (for a ramp up), control circuitry caused the voltage specified by the low preset level to be passed to the output of an analog multiplexer until such time as the ramp voltage had risen to the same level, at which point the ramp voltage was switched in. When the ramp rose to the high preset level, the multiplexer was switched to the latter level. For ramps down, the process was reversed. The ramp rate was selected with a three-position range switch, and was made continuously adjustable over each range by means of a vernier dial; ramps could swing full-scale in times ranging from a few seconds up to one hour. Ramp direction was set with a switch. The preset voltage levels were also adjusted with vernier dials.

In the manual mode, the input channel was selected by a thumbwheel switch and latched by control circuitry. When armed, the latched channel was passed to the output of the multiplexer; when disarmed, the multiplexer maintained its previous state until the arm/disarm switch was thrown: this feature allowed levels to be set without affecting the status of the output. An auxiliary input channel was fed sine waves from a function generator (Hewlett-Packard 3310A). Display lights connected to the control circuitry and an analog meter showed the status of the programmer and facilitated calibration.

The multiplexer output was passed to a voltage-to-frequency converter which produced pulse trains for the stepping motor drive. Before conversion, the signal was optionally exponentiated. The pulse output of the V-to-F converter was optionally divided by ten; this provided an extended pumping range for the apparatus. Additional features included a variable-delay trigger output at the end-points of each ramp that provided a timing signal for videotape purposes and a "rabbit speed" ramp switch; these have been omitted from the figure for clarity.



marker on the running chart by means of a pushbutton. These strip charts were produced on a Brush Mark II running at 5 mm/sec and held records of both the rotational sense of the cell and the timing of stimuli. The stimulus timing was encoded directly on the videotape, either on an audio channel or by toggling the color of an on-screen digital time display between black and white. In early experiments, this timing was transferred to the strip chart by an operator listening to the audio channel; in later experiments the signal was transferred by circuitry triggering on a color change encoded in the video time display.

A strip chart digitizer was built in order to measure and record rotational intervals from the chart records. The chart digitizer was interfaced to a lab computer and run in conjunction with a program that continuously displayed the total time, interval durations and senses of rotation. The digitizing program allowed the operator to select the exact chart position corresponding to each reversal. In addition, editing capabilities allowed deletion and insertion of intervals during input, as well as the ability to concatenate segments of the records containing valid data. Rotational intervals (and their associated senses of rotation) were accumulated in a buffer which could be written to disk in segments or as a whole for subsequent analysis. The design of the digitizer itself will be described below.

The sheer number of rotational intervals involved in these studies (over 150,000 events) required a computerized approach. Digitizing rotational intervals via the intermediate of a strip chart record, admittedly a cumbersome approach, was done for several reasons. First, it provided a convenient means of previewing the experimental data prior to computer analysis; this helped to remove unusable record segments. During the impulse response experiments, cells occasionally became stuck on the tethering surface, giving unreliable signals from the LGF apparatus. In addition, the phase relationship between x- and y-signals in the LGF

differed considerably from the theoretical values of $\pm 90^\circ$ as a result of changes in the position of the center of rotation of the spinning cell, again leading to unreliable signals. (Small drifts in position occurred routinely during long periods of observation, due to creep in the position of the flow cell. Changes also occurred, on a more rapid time scale, when the length of the tethering filament was long enough to allow the center of rotation to move with respect to the point of attachment; this happened frequently during reversals.) Periods of unreliable data were picked out by visual examination of chart records and eliminated.

Second, in the case of records bearing the x- and y-signals from the LGF, the strip chart records allowed the operator to estimate the position of a reversal to a precision not achievable with the electronic event marker, which was triggered by zero-crossings in the x-signal and consequently limited to a resolution equal to the time required for the cell to complete half a revolution. Reversals could be seen directly in the LGF signals as small peaks or inflection points in either one or both channels; under favorable conditions these were digitized with a precision corresponding to better than one-tenth of a revolution.

Third, for the adaptation experiments, the hours-long periods of continuous observation completely precluded the use of the LGF apparatus, which proved intolerant of small variations in focus or stage creep. It was also desirable to record from many tethered cells in a single field experiencing the same stimulus, since it was impossible to tell a priori which cells would last for the duration of the experiment. This led to recording the experiment on videotape. Under these conditions, the simplest means of determining reversals was by eye. However, human operators can record such reversals reliably only for relatively short periods of time before fatigue sets in and reaction time is degraded. By placing reversal information on strip chart records, several such periods could be concatenated to yield long, relatively accurate representations of tethered cell behavior. Here

again, the strip chart records enabled preview and editing of the data that could not have been readily accomplished with an on-line digitizing scheme.

One drawback to placing the rotational records on strip chart is that it is a time-consuming process. Strip charts must be edited, digitized, and stored as computer files in a separate step after each experiment; this involves many hours of painstaking work. Furthermore, digitized charts cannot reflect the accurate timing possible with electronic signals, although in practice errors related to using a strip chart intermediate were not a major source of experimental error. In the case of videotaped data, the strip charts must first be prepared off-line during slow-motion playback, a step that required four times again the amount of time devoted to the original experiment. Nonetheless, the data acquired in this manner are rather trustworthy, and the data files, once in the computer, are easily accessed and manipulated.

Most of the problems inherent in strip chart analysis can, in principle, be avoided by the development of an instrument that would automatically record reversals in tethered cells, and yet which would have an error rate low enough to dispense altogether with an editing step involving a human operator. Such an instrument must reliably determine the rotational handedness of a bacterial image spinning at up to 20 Hz (real-time). Microscope images of tethered cells only microns long are far from ideal: they are surrounded by diffraction rings, and their size varies from cell to cell. Moreover, images of bacteria tethered in flow cells are often degraded by light scattered from other cells and the flow chamber itself. As discussed, the image of the cell is subject to slow drift (creep), and the exact center of rotation may vary considerably from moment to moment with the handedness of rotation. The microscope depth of field is comparable to the length of a bacterium, and it is not unusual for the image to wander somewhat from good

focus, particularly if fluid is being passed through the flow cell. Finally, a tethered cell may stop rotating altogether for a period.

These conditions make the determination of rotational handedness a complex problem in pattern recognition. The human brain is remarkably good at solving this problem, since an observer can detect and respond to a change in handedness in 70-200 msec, depending on the circumstances.⁶ An electronic device that would perform real-time analysis of rotational handedness for tethered bacteria is under development in this laboratory. As with many problems in real-time pattern recognition, a great deal of pictorial information must be collected rapidly, after which the instrument must reject information that is either irrelevant or redundant, saving for analysis a reduced representation of the original image. The algorithm that performs the calculation of rotational handedness must be robust enough to survive changes in center of rotation, illumination, focus, etc.

Current development plans call for using a high-speed video scan followed by a frame buffer interfaced to a dedicated PDP 11/23 computer. A high-contrast representation of the x-y coordinates of the periphery of the cell image would be digitized and used to fit a straight line through the image. Slopes of this line in successive frames are compared to determine the sense of rotation. If these slopes are acquired rapidly enough (so that one revolution occupies several successive

⁶For events occurring at random, responses are significantly slower than for anticipated changes. Bacterial reversals are exponentially distributed (i.e., follow a Poisson process) and therefore represent a more difficult task. For these experiments, reaction times to slow-speed video playback of tethered cells were measured with a microcomputer simulation. For long intervals, reaction delays at the start and the end of each interval simply shift its phase somewhat; it is the spread in reaction time (and not its mean value) which contributes to an error in the recorded time. The standard deviation in reaction time is generally less than one quarter of its mean. For short intervals (i.e., comparable to the mean reaction time) both the mean and variance come into play. Operators will generally record the presence of such intervals without fail, but they are stretched in time. See Block et al. (1983).

frames), then this approach can be used to assign unambiguously a direction of rotation to the cell, even under conditions where the center of rotation or focus changes. The construction of this instrument will require a considerable amount of custom hardware and software; about five milliseconds will be available between frames for data reduction and computation.

The design of the strip chart digitizer

Strip charts were digitized by passing the chart through a system of rollers attached to an electronic device which measured the total angle through which one of the rollers had turned. The apparatus was constructed from old belt dictaphone rollers mounted on a large plate held vertically. The chart was lightly clamped between two such rollers held together by spring tension. The paper path width was adjustable to accommodate the different sizes of chart paper used in the two Brush recorders. Chart paper was tensioned by automatic takeup reels (again, made from belt dictaphone parts) driven with DC servomotors; these also helped to align the chart and to prevent paper slippage. One of the rollers on the paper path had a precision potentiometer mounted on its axis. This pot was used to compute the angle by counting both the integral number of turns made and the fraction of a turn from a trigger point. Distance traveled, d , is given simply by

$$d = 2\pi r[\Delta n + (V_t - V)/\Delta V]$$

where r is the radius of the roller, Δn the number of integral turns from the starting point, V the wiper voltage, V_t the voltage at which the turns counter triggers, and ΔV the total voltage excursion of the pot.

The chart paper was passed under a transparent acrylic reticle inscribed with a hairline. To digitize an event, the corresponding point was placed under the hairline and the space bar on the computer terminal depressed. A program running on the computer then acquired data from the digitizer, computed the distance traveled, and converted it to time using a value for the chart speed.

The chart digitizer ran in both forward and reverse directions; this was essential for error recovery and in order to measure back a known distance from stimulus times. To do this, it had to be able to count the number of turns made by the roller bidirectionally, the reverse direction corresponding to negative turns. In an earlier scheme, a mechanical turns counter, driven by a timing belt, was used in conjunction with the wiper voltage on the pot. The mechanical counter suffered from considerable hysteresis which limited the accuracy of the device. An electronic turns counter was subsequently built that triggered directly off the wiper voltage on the pot, which was stable to 0.02%. The problem was to design a turns counter with negligible hysteresis that would signal for a count up or down at precisely the same point on each cycle.

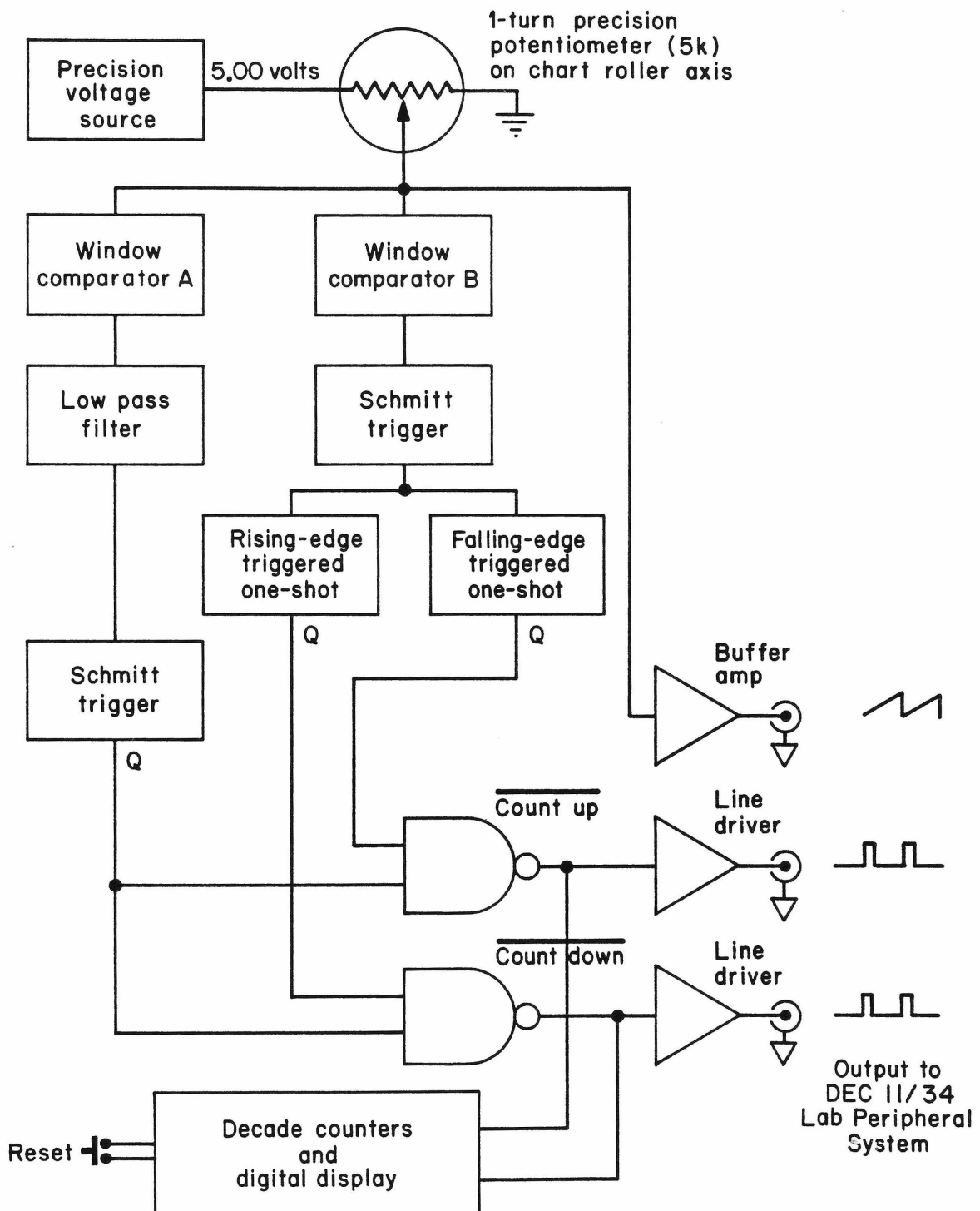
A diagram of the electronic turns decoder is shown in Text-figure 2. Three signals were passed to the computer: one digital line signaled that a turn had been completed in the forward (positive) direction, another digital line signaled a completed turn in the reverse (negative) direction, and the third signal carried the analog voltage from the pot wiper for determining the angle within a given turn. This voltage was digitized to 12-bit accuracy by a data-acquisition unit attached to the computer (Digital Equipment LPS-11). An LED display on the digitizer showed the turns count; this feature was used primarily to calibrate the digitizer and to measure ahead long distances. The digitizer, when calibrated, could resolve points separated by less than 0.2 mm. For long distances, the precision was limited not by errors associated with the turns counter nor the wiper voltage but by small amounts of chart slippage, and was typically on the order of one-half of one percent.

The algorithm used for decoding the direction of rotation from the wiper voltage is shown in Text-figure 3. The voltage is monitored as it passes through two overlapping window comparators; one is level-triggered while the other is edge-triggered. This information is sufficient to determine the rotational

Text-figure 2. Logic diagram for the strip chart digitizer.

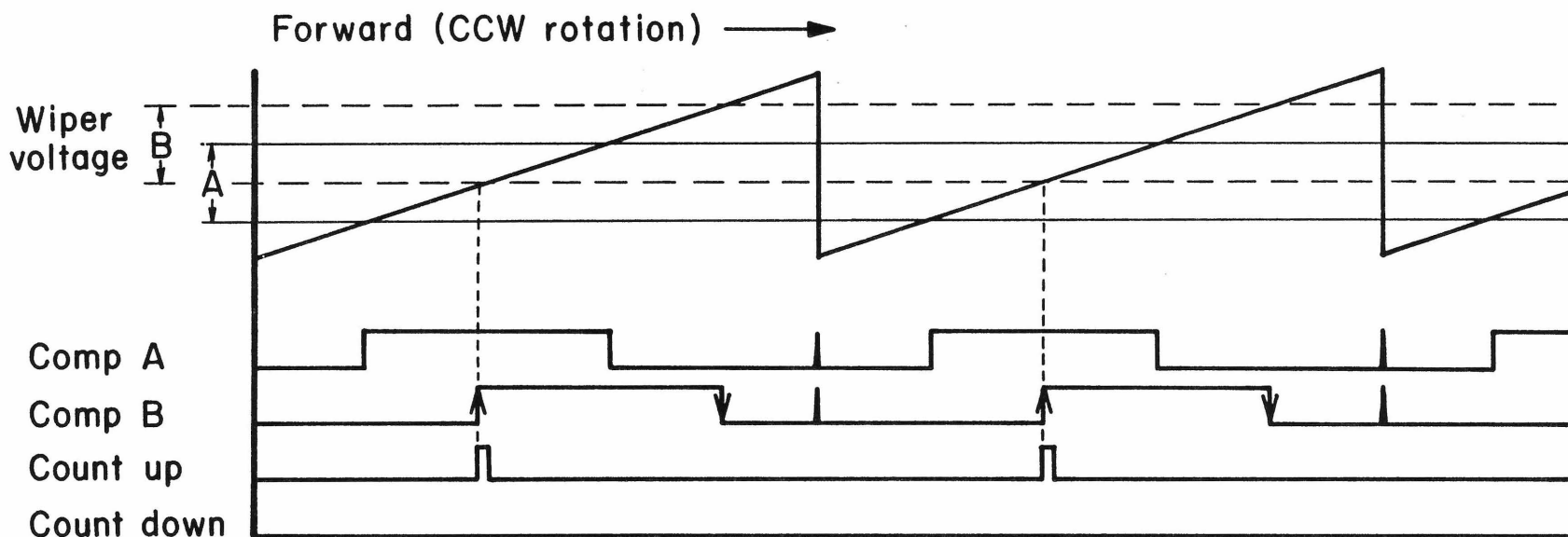
A precision voltage source, consisting of a stabilized reference and buffer amplifier, delivered 5.00 volts to a one-turn, 5K-ohm wire-wound potentiometer. The pot was coupled to the axis of a chart roller, so that the wiper voltage traced out a sawtooth waveform during each revolution of the roller. The potentiometer had a "dead zone" subtending less than half a degree, corresponding to the point where the wiper made the transition from the low end of the resistance to the high end. Although quite small, the finite size of the dead zone made it a poor candidate for a place to trigger the turns counter (due to hysteresis). The circuitry was arranged to trigger on a point away from the extremes of resistance.

The wiper voltage was buffered and passed to an A/D converter interfaced to the computer. Two overlapping window comparators, designated A and B, triggered over the ranges (1.80-2.20 V) and (2.00-2.40 V), respectively. To eliminate the glitch which can appear on the comparators during passage through the dead zone, a low pass filter with time constant 300 μ sec was inserted in the signal line from one comparator. The output of comparator B was passed to a dual edge-triggered one shot which fired a pulse on either a positive- or negative-going edge. These pulses were NAND'ed with the output of the level-triggered signal from comparator A in order to generate count up or count down signals, then fed to the computer via balanced 75- Ω line drivers. An interrupt was generated on either line that caused the computer to update the line count. See Figure 2.

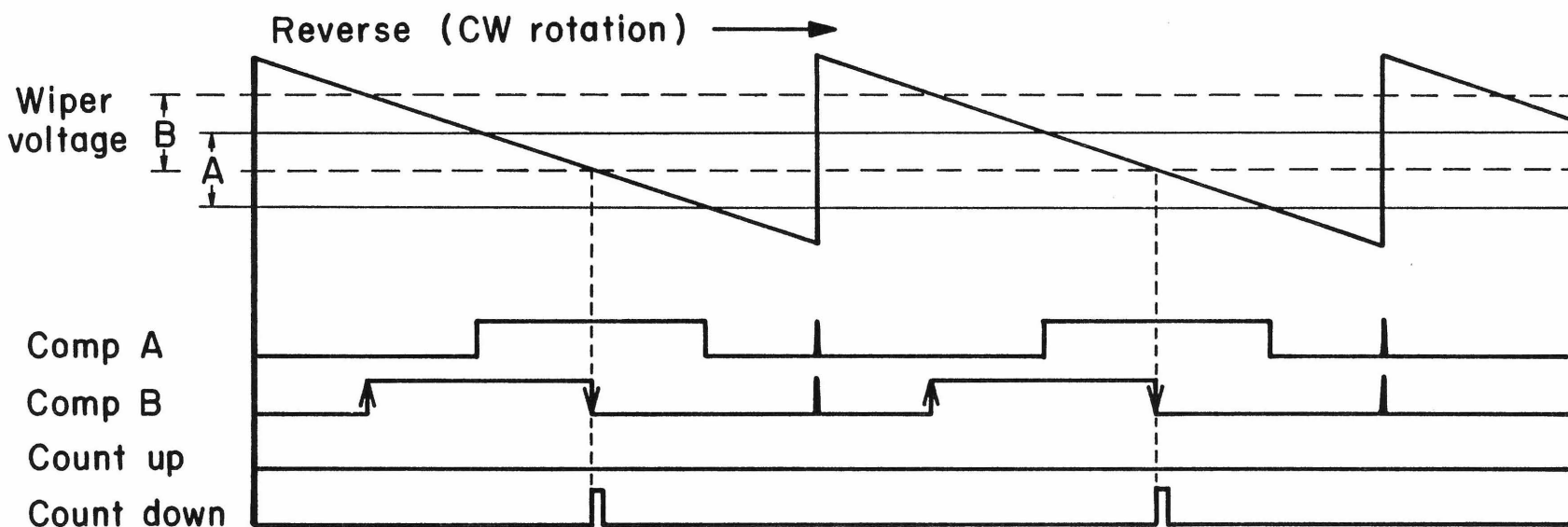


Text-figure 3. Scheme for determining the direction of rotation.

If the chart roller is turned continuously, the pot wiper voltage describes a sawtooth wave function. The shape of the sawtooth depends on the direction of rotation; the two possible waveforms are displayed in the top and bottom panels, above. Two overlapping window comparators, A and B, go high when the wiper voltage is within the window ranges; the size of the windows has been greatly exaggerated for the purpose of illustration. Comparator B is connected to an edge-triggered one-shot which pulses one of two lines depending on whether the transition was positive-going or negative-going (shown by arrows). These lines are enabled only when comparator A is concurrently high; this point occurs only once in each cycle (shown by the vertical dashed line). If the transition in comparator B is positive-going, the count up line is pulsed; if the transition is negative-going, the count down line is pulsed. The scheme successfully counts both CW and CCW turns of the chart roller regardless of the speed with which it is turned, and with negligible hysteresis. Occasional noise arising from the dead zone of the pot, shown as glitches at the full-scale transition points, is removed by a filter.



37



direction. Apparently, the scheme is not original: the same decoding method is used to read "gizzi-wheel" digital position encoders such as those used to measure head displacement in dot-matrix printers.⁷ These encoders replace the overlapping window comparators used here with a positionally-staggered pair of photodiodes that illuminate a rotating disk bearing alternate black and white sectors. By edge-triggering on the reflection of one photodiode, and level-triggering on the other, the two photosensors can be used to increment and decrement counters which keep track of print head movement bidirectionally.

Digital video time display

A video display module that generates a digital readout of time and experiment number was built. Suggested by a similar device built by Aneshanesley (1980), the module encodes a six-digit time display and a two-digit channel number into the composite video signal from the camera. In contrast to the Aneshanesley device, this module contains on-board circuitry for decoding horizontal and vertical synchronization signals directly from the composite input (rather than requiring signals from inside the camera), as well as a dual time base and some other features that proved convenient.

The digital display appears on the television screen at x-y coordinates set with two knobs. The size of the digits and their transparency are also adjustable. Channel number is selected manually by means of thumbwheel switches, and was used to represent experiment, record, or tape number. The timebase for the clock circuit may be set to either 1 Hz or 60 Hz. In the former case, the display shows [hours:min:sec], while in the latter case the display shows [min:sec:1/60 sec]. The use of the fast timebase permits each video frame to be labeled with a distinct

⁷In am grateful to Andy Moiseff and to Mike Walsh for pointing out that I had reinvented the wheel.

number. The adaptation studies were performed using the slow time base. An additional feature toggles the digital video display to black or white, for use as an event marker. The color can be selected through a switch on the front panel or toggled by means of an external TTL trigger. For the ramp experiments, a delayed trigger on the pump programmer was used to signal times at which the end-points of the ramps reached the flow cell. The display device was based on a CMOS integrated circuit used for time/channel display in home TV (National Semiconductor MM58106).

ADAPTATION KINETICS IN BACTERIAL CHEMOTAXIS

Steven M. Block, Jeffrey E. Segall and Howard C. Berg

Division of Biology 216-76, California Institute of Technology
Pasadena, California 91125

Running title: **Adaptation in Bacterial Chemotaxis**

As printed in: **Journal of Bacteriology** 154:312-323.

copyright 1983 by American Society for Microbiology

ABSTRACT

Cells of Escherichia coli, tethered to glass by a single flagellum, were subjected to constant flow of a medium containing the attractant α -methyl-D,L-aspartate. Its concentration was varied with a programmable mixing apparatus over a range spanning the dissociation constant of the chemoreceptor at rates comparable to those experienced by cells swimming in spatial gradients. When an exponentially increasing ramp was turned on (a ramp that increases the chemoreceptor occupancy linearly), the rotational bias of the cells (the fraction of time spent spinning counterclockwise) changed rapidly to a higher stable level, which persisted for the duration of the ramp. The change in bias increased with ramp rate, i.e., with the time rate of change of chemoreceptor occupancy. This behavior can be accounted for by a model for adaptation involving proportional control, in which the flagellar motors respond to an error signal proportional to the difference between the current occupancy and the occupancy averaged over the recent past. Distributions of clockwise and counterclockwise rotation intervals were found to be exponential. This result cannot be explained by a 'response regulator' model, in which transitions between rotational states are generated by threshold crossings of a regulator subject to statistical fluctuation; this mechanism generates distributions with far too many long events. However, the data can be fit by a model in which transitions between rotational states are governed by first-order rate constants. The error signal acts as a 'bias regulator', controlling the values of these constants.

Bacteria respond in a transient manner to abrupt changes in their environment: they adapt. When exposed to a large stepwise increase in the concentration of an attractant (or decrease in the concentration of a repellent), cells swim smoothly—or if tethered, rotate counterclockwise (CCW)—for minutes before resuming their normal mode of behavior (6, 19, 20, 28, 29). When exposed to a large stepwise increase in the concentration of a repellent (or decrease in the concentration of an attractant), they tumble—or rotate clockwise (CW)—for several seconds before recovery. These responses are asymmetric: the flagellar motors remain in the CCW mode much longer than in the CW mode. 'Recovery times' (28) or 'transition times' (6) are proportional to the net change in the occupancy of specific chemoreceptors. The stimuli used in these experiments saturate the sensory system: they are much larger than stimuli encountered in nature, where bacteria swim slowly through spatial gradients that have been smoothed by diffusion. Chemotaxis evolved under the latter condition: it is important, therefore, to define the properties of the chemosensory system in the small-signal domain.

It was evident from tracking cells in spatial gradients of L-aspartate and L-serine (5) that the run (or CCW) bias increases when cells swim in favorable directions, but it was not possible to characterize the response accurately over a wide dynamic range. When cells were uniformly distributed in an exponential gradient of L-serine, they moved up the gradient with a uniform migrational velocity, indicating a net response proportional to the spatial change in the logarithm of concentration, $d(\ln C)/dx$ (10, 11). Data from cells tracked in spatially-isotropic temporal gradients of L-glutamate indicated a response proportional to the time rate of change of chemoreceptor occupancy (9). At concentrations near the dissociation constant of the chemoreceptor, this reduced to a response proportional to the temporal change in the logarithm of

concentration, $d(\ln C)/dt$. Over a broader range, it explained results obtained from 'sensitivity assays', in which the number of cells swimming from a pond into a capillary tube containing attractant at a fixed concentration ratio varied with concentration (22).

Recently, we measured the response of tethered cells to short iontophoretic pulses of attractants and repellents (8). The impulse response had a finite width, indicating that cells integrate sensory inputs over a period of a few seconds. It also was biphasic, indicating that the cells take time derivatives of these inputs. The sensory system is maximally tuned to concentration changes that occur over a span of about 4 s, an interval over which changes normally occur when cells swim in spatial gradients.

Do bacteria, in fact, continually compute and respond to the time derivative of their chemoreceptor occupancy? How might they do so? Previous work on temporal stimulation of free-swimming bacteria was limited to measurements made for a short period of time on a large number of different cells, whose responses varied widely. The tethered-cell approach offers the possibility of sustained observation of the responses of one cell to different, precisely defined stimuli. The large amount of data that can be collected in this manner permits more rigorous tests of models of flagellar behavior.

In the experiments described here, we exposed tethered cells to gradual changes in the concentration of a non-metabolizable attractant, α -methyl-D,L-aspartate (21). The results complement and extend those obtained from measurements of the impulse response. Changes in rotational bias can be accounted for by a model for adaptation in which an error signal, proportional to the difference between the current receptor occupancy and the occupancy averaged over the recent past, modulates the probabilities for transitions between discrete flagellar states.

MATERIALS AND METHODS

Reagents. α -Methyl-D,L-aspartate was obtained from Sigma, all other amino acids (A grade) from Calbiochem, lactic acid (reagent grade) from Mallinckrodt, and EDTA from Fisher.

Tethered cells. Wild-type *E. coli* strain AW405 (2) was grown and tethered as described by Block et al. (8), except that the motility medium was 0.067 M NaCl, 0.01 M potassium phosphate (pH 7.0), 0.01 M sodium lactate, 10^{-4} M EDTA, and 10^{-6} M L-methionine. The anti-filament antibody was preadsorbed against a hag⁻ derivative of strain AW405.

Apparatus. A stainless-steel flow cell holding a coverslip with tethered cells was placed on a temperature-regulated stage (32.0 °C) of an inverse phase-contrast microscope (Nikon S-Ke, 400x), as shown in Fig. 1. The buffer reservoir also was held at 32.0 °C. Images of the cells were recorded with a video camera (Sanyo VC1620X, 2:1 interlace) and cassette recorder (Sanyo VTC7100) and displayed on a 23-cm monitor (Hitachi VM910). The amount of attractant reaching the cells was controlled by a pump (adapted from a Radiometer SBU1 syringe burette) driven by a stepping motor (Rapid-Syn 23H-05A) controlled by an electronic programmer built for the purpose. This pump fed a concentrated solution of attractant (4×10^{-3} M α -methyl-D,L-aspartate in motility medium) to a small mixing chamber (a plexiglass cylinder of volume 0.09 ml packed with 0.5 μ m-dia. glass wool) at a variable rate, α . Connections were made with polyethylene tubing (0.58 mm i.d.) and sections of stainless steel needles (22 gauge). A 12.5-cm length of polyethylene tubing connected the mixer to the flow cell, which had an internal volume of about 0.05 ml. The flow rates β and γ were generated by peristaltic pumps I and II, which comprised different pumping tubes on a 4-stage head of a Gilson Minipuls II; for all experiments, β and γ were fixed at 0.028 and 0.0032 ml/sec, respectively, the latter level being low enough

to allow free rotation of the tethered cells. Small surges in pumping speed arising from roller-to-roller changes were suppressed with surge filters made from 3-ml syringe bodies: the air cavities could be tuned by sliding the plungers in or out. The excess fluid was carried away at the rate $\delta = (\alpha + \beta - \gamma) \approx 10\gamma$ by a vacuum line via a needle valve adjusted to maintain a slight negative pressure at the flow cell, which ensured that the coverslip maintained a proper seal. In order to prevent air bubbles from destroying the preparation, the solutions used in the experiment were autoclaved and then saturated with a mixture of 80% He, 20% O₂.

When α is constant, the concentration of attractant in the flow cell is $C = C_\alpha \alpha / (\alpha + \beta)$, where C_α is the concentration of attractant in the syringe. If $\beta \gg \alpha$, $C = C_\alpha \alpha / \beta$, and the concentration is proportional to α . The values used for α ranged from about 0.0003 to 0.0035 ml/sec, giving a worst-case mixing nonlinearity of 11%. The mixer behaves as a low-pass filter for concentration according to the relation $dC/dt = (\alpha C_\alpha - \beta C)/V$, where V is the effective volume of the mixer. When α changes abruptly, C slews exponentially to a new value with a mixing time constant $\tau_{mix} = V/\beta = 11$ s. This constant was determined experimentally by varying α sinusoidally and measuring the phase and amplitude of the changes in concentration at the output. The calibration was done by replacing the attractant with methylene blue, placing an orange bandpass filter in front of the microscope lamp to enhance contrast, and replacing the video camera with a photodiode (United Detector Technology PIN6), which converted the microscope into a microspectrophotometer. As a final check to ensure that the system was free of surges of concentration and that mixing was complete, the apparatus was converted to its normal configuration, and adjacent tethered cells were followed at fixed α . Variations in concentration above threshold would be expected to result in cross-correlated rotational behavior. No such correlation was observed.

Data acquisition. For measurements of rotational bias, the video tapes were played back at quarter speed while an operator scored rotational periods by eye, holding a pushbutton down for CW events and releasing it for CCW events. This button toggled an event marker on a strip-chart recorder running at 5 mm/sec. Strip charts were digitized (8), and the data, a list of numbers representing the times of CW-to-CCW or CCW-to-CW transitions, were stored as records in a PDP 11/34 computer for subsequent analysis. The accuracy of the method was checked by slightly displacing the image of a spinning cell up or down at exponentially-distributed random times, with the operator scoring up as CW and down as CCW. Interval distributions computed from these records were nearly exponential, but as expected, operators tended to miss or stretch the shortest events. This effect was significant only for intervals in operator time of less than 0.6 s, which scales to a real time of 0.15 s due to quarter-speed playback. The resolution for real-time intervals longer than 0.4 s was better than 0.05 s. For measurements of angular velocity, the tapes were played back into a system linked to an Apple computer that timed pulses generated whenever the image of a rotating cell crossed a video cursor.

Data analysis. CW or CCW interval distributions were constructed by sorting intervals into bins and counting the number of events in each bin. In the interest of learning whether these distributions were exponential, as suggested by earlier work (6), we combined data from different cells obtained either before or during ramps. If the distribution for each cell is exponential, then it is possible to combine data from different cells in a systematic fashion by normalizing the intervals of each cell to the mean for that cell. This produces another exponential distribution, of unit mean, which can be added to (i.e., binned together with) normalized distributions derived from other cells. Such a procedure relies on the property that all exponential distributions are identical up to a scaling factor.

The final global distribution can be rescaled to yield a plot with a mean equal to the average of the means of the original distributions.

Unfortunately, as noted above, the finite resolution of the digitizing technique limited our ability to record the shortest intervals with high fidelity. Therefore, events lasting less than 0.4 s were eliminated from each histogram, and a mean was computed from the remaining intervals. This mean was adjusted downwards by 0.4 s to compensate for the cut-off (a procedure that yields an accurate mean for any exponential distribution). The remaining intervals were scaled to the adjusted mean, combined with normalized data from other cells in a histogram containing 100 bins, and rescaled to yield a plot with a mean equal to the average of the adjusted means of the original distributions. This plot was tested for exponentiality by a non-linear least squares program (7) that returned a value for the reduced χ^2 (χ^2 divided by the number of degrees of freedom). This allowed a test of the hypothesis that the parent distribution, the distribution from which the data for each cell were derived, was exponential (for intervals exceeding 0.4 s). The corresponding p-value is an estimate of the probability that a reduced χ^2 of that value or greater would be expected to occur by chance. In making this test, bins were ignored for intervals extending out to about 1 s. When a truncated record with a relatively small adjusted mean is scaled upwards, no contribution is made to bins corresponding to times equal to 0.4 s times the scale factor, which can be a number greater than 1; therefore, the final distribution is anomalous for bins corresponding to times even longer than 0.4 s.

The probability of CCW rotation was estimated by calculating the fraction of time that a cell spent rotating CCW. For computing values of this parameter for periods before or during ramps, the time that the cell spent rotating CCW in the period of interest was divided by the total time in that period. For looking at variations in this fraction as a function of time, the following procedure was used.

First, the total time spent CCW up to a given reversal was computed. This sum, considered as a function of t , has a time derivative (slope) constrained to lie between 0 (if the cell spun exclusively CW) and 1 (if the cell spun exclusively CCW). The derivative provides a measure, at time t , of the fraction of time spent spinning CCW. The sum was computed, then digitally filtered with a cubic spline-fit smoothing routine (24, 25), which smooths the fit curve in a least-squares sense and generates coefficients that define the derivative. For the derivative to be well behaved, the smoothing must span several adjacent rotation intervals. Thus, while the derivative provides an estimate of the rotational bias at time t , its value depends on the behavior of the cell at adjacent times. As a result, abrupt changes in bias are rounded off.

The reversal rate was computed from the density of data points, as described by Block et al. (8).

The Montecarlo simulation of the response-regulator model was done by arranging for a counter (representing the amount of regulator, X) to be incremented by one exponential process and decremented by another, with probabilities obtained from random-number generation. The program kept track of those intervals for which the counter was above or below a critical value (corresponding to X_{crit}) and compiled the corresponding interval histograms.

RESULTS

It is known from earlier work with free-swimming cells (9, 10, 11, 22, 28) that *E. coli* is maximally sensitive to an attractant at a concentration equal to the apparent dissociation constant of its chemoreceptor, K_D . For α -methyl-D,L-aspartate, $K_D \approx 1.4 \times 10^{-4}$ M (6, 22). At an attractant concentration C , the fraction of receptor bound is $P = C/(K_D + C)$, and the time rate of change of this fraction is $dP/dt = [K_D C/(K_D + C)]^2 (dC/dt)/C$. The term in square brackets is a

bell-shaped function centered at K_D , the factor measured in sensitivity assays (9, 22). By limiting changes in concentration to a range logarithmically centered around K_D , from $C_{\text{low}} = 0.31 K_D$ to $C_{\text{high}} = 3.2 K_D$, the variation in this factor is reduced to less than 20% about the mean, and $dP/dt \approx \frac{1}{4}(dC/dt)/C = \frac{1}{4}d(\ln C)/dt$. If the response of the cells is proportional to dP/dt , then it should be linear in the logarithm of concentration, a type of behavior specified by the Weber-Fechner law (10). We tested exponential ramps of the form $\exp(at)$, with ramp rates, a , of either sign, and exponentiated sine waves of the form $\exp[\sin(\omega t)]$. These stimuli generate changes in P that are linear and sinusoidal, respectively.

Behavior at fixed concentration. The cells were allowed to adapt to C_{low} or C_{high} for at least 5 min before data were taken. They were monitored for 3 to 5 min before and immediately after each ramp. The interval distributions for data obtained prior to the ramps are shown in Fig. 2. These distributions were accurately fit by single exponentials. The interval distributions at C_{low} were indistinguishable from those at C_{high} (data not shown), indicating that the cells fully adapt.

The cells were continuously perfused with buffer containing lactate (an energy source; cf. 1) and L-methionine (required for adaptation in cells that do not synthesize it; cf. 27). They were well oxygenated but deprived of other amino acids and nutrients. The cells continued to rotate and respond for at least six hours, the longest period investigated. During this period, both CCW and CW intervals became progressively longer, increasing as much as 3-fold, Fig. 3A. However, the intervals varied in such a way that the fraction of time spent spinning CCW (the probability of spinning CCW) tended to remain constant, Fig. 3B. The probability of spinning CCW was chosen as a measure of the response because it has this stability. Rotational velocities also remained nearly constant. The cell shown in Fig. 3 averaged 10 Hz for the first hour, slowed to 7.5 Hz by the

end of the second hour, and maintained that speed (to within ± 0.5 Hz) for the remaining four hours. Another cell increased its speed by about 30% over a comparable period. Variations in speed of other cells were smaller than this. Changes in speed were not correlated with changes in rotational bias.

Behavior during exponential ramps. If the response of a cell is proportional to the rate of change of chemoreceptor occupancy, dP/dt , and a ramp of the form $C = C_{\text{low}} \exp(at)$ or $C = C_{\text{high}} \exp(-at)$ is switched on, then the response should shift by an amount proportional to a and remain nearly constant for the duration of the ramp. This behavior is shown in Fig. 4. The baseline fluctuations represent the normal statistical variation in rotational bias. When the ramps were turned on, the rotational bias changed rapidly to a new level, as predicted. The rate at which this level was established provides a measure of the time required by the cell to evaluate dP/dt : this time was relatively short, less than the mixing time constant, τ_{mix} . When the ramps were turned off, there was an 'overshoot' in rotational bias that persisted for about 1 min, analogous to the overshoot observed during recovery from large step stimuli, described earlier (6). With the exception of this period, the rotational bias faithfully mirrored changes in dP/dt , shown schematically at the bottom of each graph. To obtain a comparable change in rotational bias, down ramps had to be two to three times faster than up ramps, limiting the period of time during which data could be collected. Therefore, our conclusions for down ramps are more tentative.

The interval distributions remained exponentially distributed during up and down ramps. Results for up ramps of one particular rate are shown in Fig. 5. In this case, stimulation caused a slight decrease in the mean CW interval and a large increase in the mean CCW interval. The interval distributions remained exponential at all ramp rates tested, provided that the response did not saturate (data not shown).

Figure 6 shows the changes in rotational bias observed as a function of ramp rate. Since there was a large variation in bias from cell to cell, these experiments were done with single cells. The responses of two cells to ramps up are shown in Fig. 6A, and the responses of one cell to ramps down are shown in Fig. 6B. The response threshold, i.e., the ramp rate required to cause a measurable change in bias from the unstimulated value, is relatively low for ramps up, Fig. 6A, but relatively high for ramps down, Fig. 6B. The slopes of the linear parts of these curves have roughly the same magnitude.

The lengths of both CW and CCW intervals changed during the ramps. For ramps up, CCW intervals lengthened while CW intervals shortened. For ramps down, CCW intervals shortened while CW intervals lengthened. During ramps up, CCW intervals were more sensitive to change than CW intervals: the relative increase in the mean CCW interval was greater than the relative decrease in the mean CW interval in virtually all cases (31 out of 34 ramps on a total of 4 cells). However, during ramps down, the relative increase in the mean CW interval was sometimes greater than, sometimes smaller than the relative decrease in the mean CCW interval (CW increase greater in 12 out of 25 ramps on a total of 8 cells). In order to obtain the results shown in Fig. 6, it was necessary to collect a large amount of data on a small number of cells, cells that remained tethered to the glass and continued to spin while subjected to flow over a period of several hours. One could learn more about relative changes in interval lengths by exposing a large number of cells to only a few ramps.

Behavior during exponentiated sine waves. The response to an exponentiated sine wave of intermediate frequency is shown in Fig. 7. At this frequency, the response is unsaturated, even at peak values of dP/dt . The response tracks dP/dt , not P ; compare Fig. 7A and B. The response waveform is periodic but not quite sinusoidal, as expected from the up-down asymmetry noted in Fig. 6. The reversal

rate leads dP/dt in phase, but only slightly, Fig. 7C.

Figure 8 is a Bode (log-log) plot of the amplitude of the response as a function of frequency. Such plots are widely used in the analysis of linear systems to determine response characteristics; linear domains with slopes of $20n$ dB/decade represent n th-order filters. The responses at the lowest frequencies (the first three data points) were lost in the noise due to the normal statistical variation in baseline bias. At the highest frequencies, the cells spun exclusively CCW during the positive phase of the stimulus. The linear intermediate domain implies a power-law dependence of amplitude on frequency; the value of the slope is indicative of a first-order high pass (adaptive) process; see Block et al. (1982).

With increasing frequency, the baseline (DC) bias of the cells shifted in the CCW direction (data not shown). This is another consequence of the up-down asymmetry noted in Fig. 6. It would not occur were adaptation equally fast for changes on concentration in either direction. The response continued to track dP/dt at the highest frequencies tested.

DISCUSSION

Evidence for a bias regulator. The interval distributions shown in Figs. 2 and 5 and those obtained earlier with swimming cells (5, 9) or tethered cells (6, 8) can be fit accurately by single exponentials. This implies that reversals of the flagellar motors are generated by a Poisson process (6), a process with a constant probability per unit time. The possibility remains that the distributions are non-exponential for times shorter than 0.4 s. There is some indication of this in data collected with the linear-graded filter apparatus; see Fig. 2A of (26). To find out, we need to use methods with even better time resolution.

Two models that suggest mechanisms for the generation of spontaneous

reversals are diagrammed in Fig. 9. The first is the response regulator model of Koshland (17, 18). As noted in Fig. 9A, it exploits the notion of a fluctuating intermediate to account for rotational transitions (18): "The steady-state level of response regulator (X_{ss}) varies in a Poissonian manner relative to a critical value (X_{crit}). When ($X_{ss} - X_{crit}$) is slightly less than zero, tumbling is generated. When ($X_{ss} - X_{crit}$) is greater than zero, smooth swimming results." Variations in which X_{ss} stays put and X_{crit} fluctuates or in which both fluctuate also are acceptable. The model assumes that X is raised transiently when cells are exposed to an attractant; this leads to tumble suppression, which subsides when X returns to its original level. This model must be correct, a priori, in the sense that some signal controls the changes in rotational bias that occur during a chemotactic response, but, as we shall now show, variations in this signal do not generate exponential interval distributions.

The problem reduces to the question of how level crossings of such a regulator are distributed. Fluctuations expected in the amplitude of X are simply derived, but level-crossing (or zero-crossing) times are not (4). Many random functions have exponentially distributed amplitudes, but very few have exponentially distributed zero crossings. We simulated the response regulator model by computer using a Montecarlo method. The histogram shown in Fig. 10 was obtained for the case of a cell whose average steady-state value $\langle X_{ss} \rangle = X_{crit} = 1000$, with mean generation and destruction rates given by $\lambda = 1 \text{ s}^{-1}$. This histogram is not exponential; it has a very long tail, with some intervals lasting many thousands of seconds. The analytical solution, shown by the solid line, is derived in Appendix A. We also simulated cells with different rotational biases, i.e., with $\langle X_{ss} \rangle \neq X_{crit}$, or with X displaced relative to X_{crit} , as during a chemotactic response. These distributions were skewed but remained far from exponential (data not shown). Changes in the level of $\langle X_{ss} \rangle$ had virtually no

effect on these results, until $\langle X_{ss} \rangle \approx 1$. With $\langle X_{ss} \rangle = 1$, the CW distribution was exponential, but the CCW distribution was not. An exponential distribution for CW intervals is obtained when $\langle X_{ss} \rangle = 1$, because CW rotation occurs only for one state ($X = 0$), and the probability per unit time of leaving this state is constant. This feature is exploited for both rotational modes in the two-state model (8).

The exponential fits to the data shown in Figs. 2 and 5 all map onto the dashed line shown in Fig. 10. The long intervals predicted by the response-regulator model are not observed. Note, Appendix A, that this distribution has a tail that decays as $t^{-3/2}$, which cannot be fit by an exponential. Thus, we can rule out mechanisms in which flagellar reversals are generated by level crossings.

In the two-state model, Fig. 9B, transitions between binary states occur with constant probability per unit time and yield exponential distributions for either state, with mean lifetimes given by $1/k_r$ and $1/k_t$. These states might represent alternate conformations of a protein, occupancies of a receptor, or the like. In the absence of chemotactic stimulation, both k_r and k_t can drift with time, as indicated in Fig. 3A, but in this case they do so proportionately, so that the function $k_t/(k_r + k_t)$, the fraction of time spent spinning CCW, remains approximately constant, Fig. 3B. The drift shown in Fig. 3A cannot be explained by a reduction in protonmotive force, which has been found to lengthen CCW intervals and shorten CW intervals (15), i.e., to decrease k_r and increase k_t . The data given in the legend of Fig. 5 indicate that the chemotactic signal shifts k_r and k_t in opposite directions, but not by a proportionate amount; k_r changes by more than k_t . The chemotactic signal may well be an intermediate, X , of the sort envisaged by Koshland (17, 18), but it controls the bias of the flagellar motors, not individual transition times; therefore, we refer to it as a 'bias regulator'. In the two-state model, fluctuations in X become largely irrelevant.

Evidence for proportional control. We have found that the change in bias is a function of the time rate of change of chemoreceptor occupancy, dP/dt , Fig. 4. This function is linear over a wide range, except for a small threshold seen for ramps up, Fig. 6A, and a larger threshold seen for ramps down, Fig. 6B. The magnitudes of the slopes of the linear portions of these curves, which relate to the gain of the system, are not as different as might have been expected, given the marked asymmetry in rates of adaptation to large step stimuli (6); however, they are consistent with predictions based on measurements of responses to impulse and small step stimuli (8 and unpublished results). Results obtained when dP/dt was varied sinusoidally, Fig. 7, confirm that the response depends on dP/dt , not P itself. The data summarized in Fig. 8, while consistent with that of Fig. 6, are of limited value, because of the up-down asymmetry and saturation. Because the relative phase of the response was not observed to vary as the frequency increased (data not shown), the high-frequency cutoff, apparent in Fig. 8, must result from saturation, not from a limit set by any characteristic adaptation time. As noted earlier, Fig. 4, this time is of the same order of magnitude as the mixing time constant (11 s) or less. We know from measurements of the impulse response that the longest time constant operative in wild-type cells in the small-signal domain is about 4 s (8).

How can the cell generate a response proportional to the time rate of change of chemoreceptor occupancy? Somehow it must make a running comparison between the present chemoreceptor occupancy, P , and the occupancy in the recent past. A comparison of this kind was proposed in a theory developed some years ago by Delbrück and Reichardt to explain light-adaptation in Phycomyces (12). Expressed in language appropriate to chemotaxis, this theory asserts that an internal variable, A , representing the virtual occupancy to which a cell is adapted, changes at a rate proportional to an error signal, $(P-A)$. Formally:

$dA/dt = (P-A)/\tau$, where τ is an adaptation time constant. In general, A will track P but will be filtered by a time constant τ . When $A = P$, $dA/dt = 0$, and the cell is fully adapted. Consider, for example, the case in which P is first held constant and then increased at a constant rate, a . A lags P by an increasing amount for the first few time constants, until $(P-A)$ reaches $a\tau$, whereafter $(P-A)$ remains constant. Thus, the main features of the ramp experiments can be explained if the change in rotational bias is proportional to the error signal $(P-A)$. If this is so, the change in bias is proportional to the ramp rate, a .

The level of adaptation, A, is equivalent to the receptor occupancy averaged over the past with a weighting factor (memory) that decays exponentially with time; see Appendix B. Information about receptor occupancy is relevant only if it is recent on the scale of the time constant, τ . In general, the memory of the cell cannot be characterized by a single exponential; however, when changes in concentration occur at low enough frequency, it can be: the system behaves as a first-order high pass filter (8). The gradual changes imposed in the ramp experiments fall in this low-frequency domain.

The Delbrück-Reichardt model does not account for the response thresholds evident in Fig. 6. A biochemically explicit model that can do so is outlined in Appendix C. In this model, the biochemical correlate for A is the level of methylation of a methyl-accepting chemotaxis protein, which, in the case of α -methyl-aspartate, is also the receptor (30; for a review, see 27). The error signal is generated by an imbalance between receptor occupancy and methylation. This signal controls both the behavior of the flagellar motors and, via a feedback loop, the activities of the methylation enzymes. Nonlinearities in this activation produce response thresholds.

Data obtained earlier with large step stimuli were explained by assuming that adaptation occurs at a constant rate (6). In the model described in

Appendix C, this happens when the methylation enzymes are fully activated. Adaptation to large downward steps in the concentration of α -methylaspartate is much faster than adaptation to upward steps (6). This appeared to explain the asymmetry observed when cells were tracked in spatial gradients of aspartate, in which changes in run length were much larger when cells swam up the gradients than when they swam down the gradients (5). The data shown in Fig. 6 suggest that these differences are due, instead, to an asymmetry in response thresholds.

The overshoots that occur when ramps are switched off, Fig. 4A,B, are not explained by the models presented. These overshoots, although of smaller magnitude than those seen earlier during recovery from large step-changes in the concentration of attractants or repellents (6), last for similar times. In both sets of experiments the cells sustain a monotonic change in bias for a relatively long period of time. It is likely that an intermediate accumulates during this time that affects the rotational bias when adaptation is nearly complete. One candidate for this intermediate is an incorrectly methylated or demethylated methyl-accepting chemotaxis protein, i.e., one that signals the presence of chemoattractants other than the one used as a stimulus.

General conclusions. Distributions of CW and CCW intervals remain exponential, even when cells are subject to continuous chemotactic stimulation. This behavior implies that transitions between motor states occur at random, at rates controlled by signals whose amplitudes depend on sensory input. Adaptation to changes in concentration occurs via proportional control: the signal that determines the transition rates is proportional to the difference between current and past receptor occupancy. This control can be imposed by biochemical pathways that involve negative feedback.

ACKNOWLEDGMENTS

We thank Gary Lorden for consultations on probability theory, Robert Smyth for providing the cubic spline-fit routine, and Greg Matthews for digitizing. This work was supported by grant AI 16478 from the National Institute of Allergy and Infectious Diseases. S.M.B. and J.E.S. acknowledge support as NSF predoctoral fellows during some of this work.

APPENDIX A

Mathematical analysis of a response regulator model. Consider the model diagrammed in Fig. 9A. The problem is to derive the probability distribution functions for intervals when X is above (or below) X_{crit} . For simplicity, we examine the case in which $X > X_{\text{crit}}$ exactly half the time, on average. Symmetry then requires that $X_{\text{crit}} = \langle X_{\text{ss}} \rangle$, the average steady-state level of X . At steady-state, $\langle X_{\text{ss}} \rangle = k_f/k_d$. If the value of X is reasonable (say, 100 or greater), then fluctuations in the amplitude of X will be given by a Gaussian distribution with spread proportional to \sqrt{X} . In this case, the flux out of state X varies only slightly, and we can treat the fluxes which create and destroy X as essentially constant. The probability density function for the creation of X is given by $\lambda e^{-\lambda t}$, with $\lambda = k_f$. An identical relation holds for the destruction of X .

The problem may be thought of as a series of successive events in which the number of X -molecules (i.e. the concentration, X) is increased or decreased by one. These events describe a random walk in the concentration, X . Let X start at $\langle X_{\text{ss}} \rangle$. The probability density function for the times of excursions of X below (or above) $\langle X_{\text{ss}} \rangle$ will be given by the convolution

$$\rho(t) = \sum_{k=1}^{\infty} p_k g_k(t) \quad (\text{A1})$$

where p_k is the probability that a random walk over the integers, starting at 0, will reach the value 1 in exactly k steps—known as a 'first passage time'—and $g_k(t)$ is the probability density function which represents the distribution of the sum of k separate times, each drawn from an exponential distribution, i.e., the density function for the time it takes to make k steps. The probability p_k is given by

$$p_k = \frac{1}{k} \binom{k}{\frac{k+1}{2}} 2^{-k}, \quad (\text{A2})$$

where k is an odd integer (13). Now, $g_k(t)$ is a probability density representing the sum of times, each of which will be distributed with exponential density $h(t)$. Since an event (a change in X) arises as a result of one of two concurrent Poisson processes— X is created or destroyed—these events will be distributed as $h(t) = 2\lambda e^{-2\lambda t}$. Therefore, by the convolution theorem, $g_k(t)$ is the k -fold convolution of $h(t)$ with itself. This convolution yields the Gamma distribution

$$g_k(t) = \frac{(2\lambda)^k t^{k-1} e^{-2\lambda t}}{\Gamma(k)}. \quad (A3)$$

Insertion of these expressions into Eq. A1 yields

$$\rho(t) = \sum_{k \text{ odd}} \frac{1}{k} \binom{k}{\frac{k+1}{2}} \frac{\lambda^k t^{k-1} e^{-2\lambda t}}{(k-1)!}, \quad (A4)$$

which, after some manipulation, can be reduced to a form representing a standard series (23):

$$\rho(t) = \frac{e^{-2\lambda t}}{t} \sum_{r=0} \frac{\left(\frac{(2\lambda)t}{2}\right)^{r+1}}{r! (r+1)!}. \quad (A5)$$

Eq. A5 is equivalent to

$$\rho(t) = \frac{e^{-2\lambda t} I_1(2\lambda t)}{t}. \quad (A6)$$

where I_1 is a modified Bessel function of the first kind. This density function is shown as the solid line in Fig. 10. Equation A6 is actually a special case of the general formula for the distribution of first-passage times in a birth and death process (a so-called 'queuing' problem) in which events occur with fixed probability (3). For short times, $\rho(t)$ decays rapidly as $e^{-2\lambda t}$; for long times, it decays slowly as $t^{-3/2}$. The integral of $\rho(t)$ can be calculated by recourse to standard forms. As expected for a probability distribution, the area equals 1; however, the slowness of the decay for large t gives an expectation value for t that is infinite. This kind of

counter-intuitive behavior is common for certain types of random walks and represents the fact that lead changes occur surprisingly infrequently, even in games with balanced odds. For example, in a coin-tossing game with balanced stakes and a fair coin tossed n times, the average lead for one or the other player increases roughly as n (13). Therefore, as n goes to infinity, the length of the average lead does also, and so the expectation value for a lead is infinite.

APPENDIX B

Equivalent statements of a model for adaptation. The version of the Delbrück-Reichardt model presented in the text contains two assumptions about the behavior of the system. 1) The response, R , is proportional to an error signal

$$R = g(P - A), \quad (B1)$$

where g is a constant of proportionality specifying the gain, P is the receptor occupancy, and A is an adaptation level. 2) A follows P according to the first-order differential equation

$$dA/dt = (P - A)/\tau, \quad (B2)$$

where τ is an adaptation time constant. The variable A can be eliminated from these equations by solving Eq. B2 for A and substituting the result into Eq. B1. The solution of Eq. B2 for $t \gg \tau$ is

$$A(t) = \frac{e^{-t/\tau}}{\tau} \int_0^t P(t') e^{t'/\tau} dt', \quad (B3)$$

which can be rewritten and substituted into Eq. B1 to yield

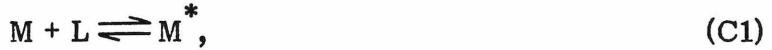
$$R(t) = g \left[P(t) - \frac{1}{\tau} \int_0^t P(t') e^{-(t-t')/\tau} dt' \right]. \quad (B4)$$

The first term in the brackets, $P(t)$, is the current receptor occupancy. The second term is an average of P over past times with a weighting factor that decays exponentially with time. The response is proportional to the difference of these terms.

APPENDIX C

A model for adaptation that can account for response thresholds. We make the usual assumption that the signal generated when an attractant binds a receptor is switched off when the receptor is methylated (27). We identify P, Eq. B1, with the fraction of receptors that have bound attractant and A with the fraction of receptors that have bound attractant and are methylated. If the total number of receptors is N_0 , then the number that have bound attractant but are not methylated is $(P-A) N_0$, which we call S (for signal). Methylation of S is carried out by a methyltransferase; let the total number of these molecules be M_0 . We assume that the enzyme is activated by the error signal (or the response), e.g., by association with a ligand $L = fS$, where f is a feedback constant. This reaction sequence comprises a negative feedback loop: if S increases, L increases; more M is activated, and S decreases.

The Delbrück-Reichardt model follows when the feedback is proportional to the signal. If M is activated by association with L, i.e., if



where M is the number of free enzyme molecules and M^* is the number bound to L, then

$$M^* = LM_0 / (K_d + L), \quad (C2)$$

where K_d is the dissociation constant for the enzyme-ligand complex. For $L \ll K_d$, $M^* = fSM_0 / K_d$, and activation is proportional to the signal. We assume that methylation proceeds by Michaelis-Menten kinetics, i.e., at a rate

$$kM^*S / (K_m + S), \quad (C3)$$

where k is the rate constant for conversion of the enzyme-substrate complex to enzyme and product and K_m is the Michaelis-Menten constant. Now, in the middle

of an up ramp, the response is constant; therefore, S is constant. The rate at which the receptor is methylated, Eq. C3, must be equal to the rate at which additional attractant is bound to the receptor; since $dP/dt = a/4$, this quantity is

(a/4) N_o :

$$kM^*S/(K_m + S) = aN_o/4. \quad (C4)$$

Substituting the relation $L = fS$ and Eq. C2 into Eq. C4 gives a quadratic in S , which can be solved to yield S as a function of a . If $L \ll K_d$ and $S \gg K_m$, S is proportional to a , as required. If $L \gg K_d$, $M^* = M_o$, and methylation occurs at a constant rate. In this limit, the response saturates (Eq. B1 breaks down), and S is not proportional to a .

A response threshold arises when there is some methyltransferase activity even at very low levels of S . This allows the cell to adapt without generation of a sizeable error signal. This hypothesis is plausible, given the turnover of methyl groups that occurs in the absence of stimulation (14). To cite an extreme example, suppose that some of the methyltransferase, M' , is active even in the absence of ligand, i.e., that

$$M^* = M' + LM_o/(K_d + L), \quad (C5)$$

where M_o now is the total number of molecules subject to activation and inactivation. For $L \ll K_d$, $M^* = M' + fSM_o/K_d$, and Eq. C4 leads to an expression that predicts a response threshold of order $a = 4kM'/N_o$. An alternative possibility is that more than one molecule of L binds to M , but that activation due to binding of the second or subsequent ligands is relatively less effective. Such an allosteric interaction would introduce the necessary nonlinearity.

In a more realistic model, methylation would be offset by demethylation, and the signal, S , would activate the methyltransferase and inactivate the methyl-esterase. Differences in thresholds for up ramps and down ramps then could be

accounted for by differences in the activation of these two enzymes.

LITERATURE CITED

1. **Adler, J.** 1973. A method for measuring chemotaxis and use of the method to determine optimum conditions for chemotaxis by Escherichia coli. *J. Gen. Microbiol.* **74**:77-91.
2. **Armstrong, J. B., J. Adler, and M. M. Dahl.** 1967. Nonchemotactic mutants of Escherichia coli. *J. Bacteriol.* **93**:390-398.
3. **Bailey, N. T.** 1964. The elements of stochastic processes, chpt. 11, John Wiley and Sons, New York.
4. **Bendat, J. S.** 1958. Principles and applications of random noise theory, chpt. 10, John Wiley and Sons, New York.
5. **Berg, H. C., and D. A. Brown.** 1972. Chemotaxis in Escherichia coli analysed by three-dimensional tracking. *Nature* **239**:500-504.
6. **Berg, H. C., and P. M. Tedesco.** 1975. Transient response to chemotactic stimuli in Escherichia coli. *Proc. Nat. Acad. Sci. USA* **72**:3235-3239.
7. **Bevington, P. R.** 1969. Data reduction and error analysis for the physical sciences, chpt. 11, McGraw-Hill, New York.
8. **Block, S. M., J. E. Segall, and H. C. Berg.** 1982. Impulse responses in bacterial chemotaxis. *Cell* **31**:215-226.
9. **Brown, D. A., and H. C. Berg.** 1974. Temporal stimulation of chemotaxis in Escherichia coli. *Proc. Nat. Acad. Sci. USA* **71**:1388-1392.
10. **Dahlquist, F. W., P. Lovely, and D. E. Koshland, Jr.** 1972. Quantitative analysis of bacterial migration in chemotaxis. *Nature New Biol.* **236**:120-123.
11. **Dahlquist, F. W., R. A. Elwell, and P. S. Lovely.** 1976. Studies of bacterial chemotaxis in defined concentration gradients. *J. Supramol. Struct.* **4**:329-342.

12. **Delbrück, M., and W. Reichardt.** 1956. System analysis for the light growth reactions of Phycomyces, p. 3-44. In D. Rudnick (ed.), Cellular mechanisms in differentiation and growth, Princeton University Press, Princeton, New Jersey.
13. **Feller, W.** 1968. An introduction to probability theory and its applications, vol. 1, chpt. 3, John Wiley and Sons, New York.
14. **Goy, M. F., M. S. Springer, and J. Adler.** 1977. Sensory transduction in Escherichia coli: Role of a protein methylation reaction in sensory adaptation. Proc. Nat. Acad. Sci. USA **74**:4964-4968.
15. **Khan, S., and R. M. Macnab.** 1980. The steady-state counterclockwise/clockwise ratio of bacterial flagellar motors is regulated by protonmotive force. J. Mol. Biol. **138**:563-597.
16. **Khan, S., R. M. Macnab, A. L. DeFranco, and D. E. Koshland, Jr.** 1978. Inversion of a behavioral response in bacterial chemotaxis: Explanation at the molecular level. Proc. Nat. Acad. Sci. USA **75**:4150-4154.
17. **Koshland, D. E., Jr.** 1977. A response regulator model in a simple sensory system. Science **196**:1055-1063.
18. **Koshland, D. E., Jr.** 1980. Bacterial chemotaxis as a model behavioral system, p. 64-68, Raven Press, New York.
19. **Larsen, S. H., R. W. Reader, E. N. Kort, W.-W. Tso, and J. Adler.** 1974. Change in direction of flagellar rotation is the basis of the chemotactic response in Escherichia coli. Nature **249**:74-77.
20. **Macnab, R. M., and D. E. Koshland, Jr.** 1972. The gradient-sensing mechanism in bacterial chemotaxis. Proc. Nat. Acad. Sci. USA **69**:2509-2512.
21. **Mesibov, R., and J. Adler.** 1972. Chemotaxis toward amino acids in Escherichia coli. J. Bacteriol. **112**:315-326.

22. **Mesibov, R., G. W. Ordal, and J. Adler.** 1973. The range of attractant concentrations for bacterial chemotaxis and the threshold and size of response over this range. *J. Gen. Physiol.* **62**:203-223.
23. **Olver, F. W.** 1968. Bessel functions of integer order, p. 358-433. In M. Abramowitz and I. A. Stegun (ed.), *Handbook of mathematical functions*, Dover Publications, New York.
24. **Reinsch, C. H.** 1967. Smoothing by spline functions. *Numerische Mathematik* **10**:177-183.
25. **Reinsch, C. H.** 1971. Smoothing by spline functions II. *Numerische Mathematik* **16**:451-454.
26. **Segall, J. E., M. D. Manson, and H. C. Berg.** 1982. Signal processing times in bacterial chemotaxis. *Nature* **296**:855-857.
27. **Springer, M. S., M. F. Goy, and J. Adler.** 1979. Protein methylation in behavioural control mechanisms and in signal transduction. *Nature* **280**:279-284.
28. **Spudich, J. L., and D. E. Koshland, Jr.** 1975. Quantitation of the sensory response in bacterial chemotaxis. *Proc. Nat. Acad. Sci. USA* **72**:710-713.
29. **Tsang, N., R. Macnab, and D. E. Koshland, Jr.** 1973. Common mechanism for repellents and attractants in bacterial chemotaxis. *Science* **181**:60-63.
30. **Wang, E. A., and D. E. Koshland, Jr.** 1980. Receptor structure in the bacterial sensing system. *Proc. Nat. Acad. Sci. USA* **77**:7157-7161.

FIG. 1. Apparatus for subjecting tethered cells to programmed changes in concentration. A concentrated solution of attractant was combined with buffer in a small mixing chamber. Part of the mixture was passed through a flow chamber holding the tethered bacteria, and the rest was collected in a trap in a vacuum line (not shown). The concentration of attractant was controlled with a programmed pump. Other flow rates were adjusted to give linearity in the mixing and a fast mixing time, with the flow past the cells held constant.

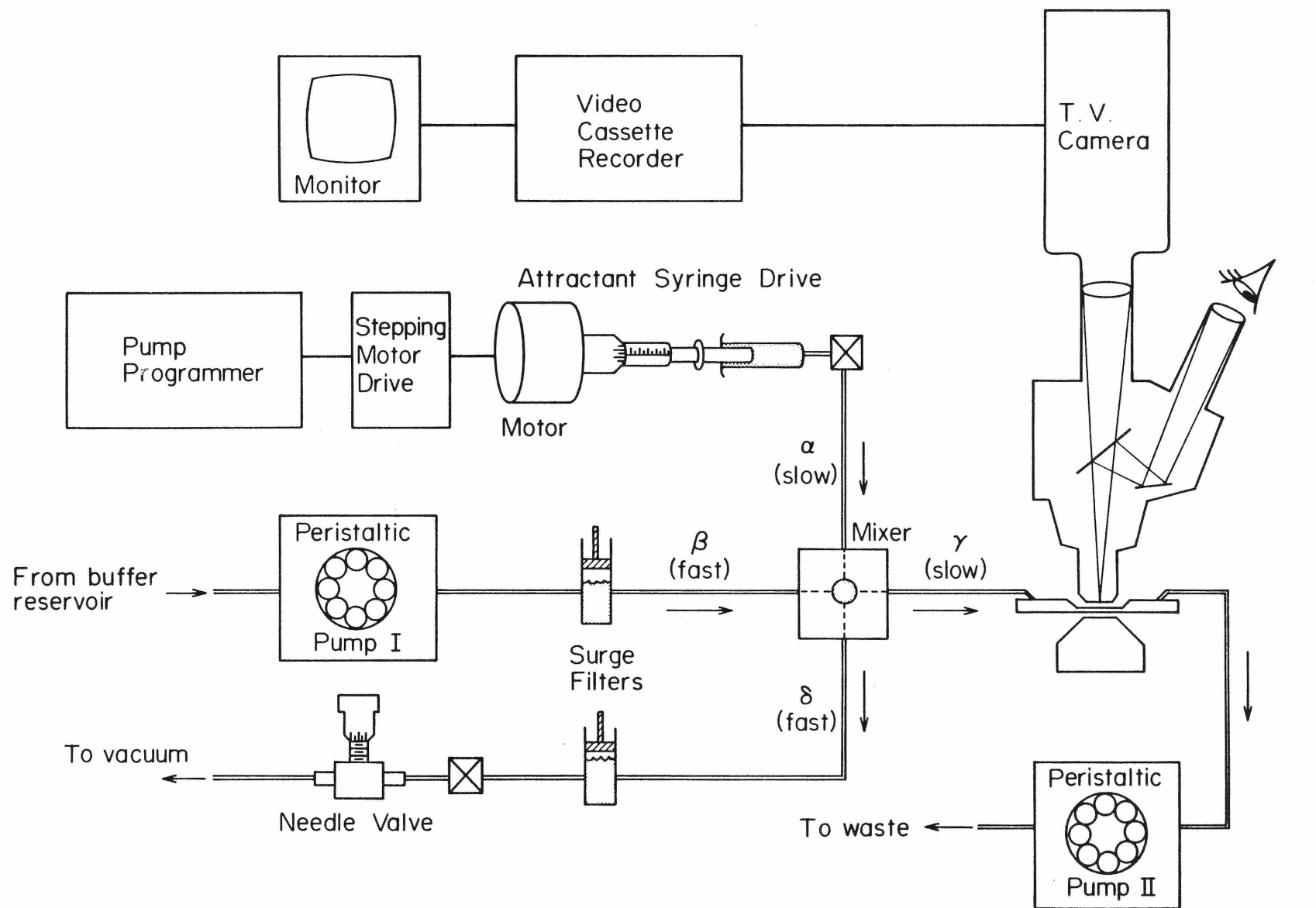


FIG. 2. CW and CCW interval distributions of adapted cells. Histograms for each record were scaled, combined, and fit by an exponential, as described in Materials and Methods. (Left) CW interval distribution computed from the 5,237 events longer than 0.4 s in 108 records on 24 cells; 4 events are off scale. Range of adjusted means for each record: 0.14 to 4.4 s. Global adjusted mean: 1.06 s. Decay time for the exponential fit: 1.33 s; reduced χ^2 1.06, 51 degrees of freedom, p-value 36%. (Right) CCW interval distribution computed from the 7,255 events longer than 0.4 s in 108 records on 24 cells; 13 events are off scale. Range of adjusted means for each record: 0.47 to 5.2 s. Global adjusted mean: 1.20 s. Decay time for the exponential fit: 1.22 s; reduced χ^2 1.05, 54 degrees of freedom, p-value 37%.

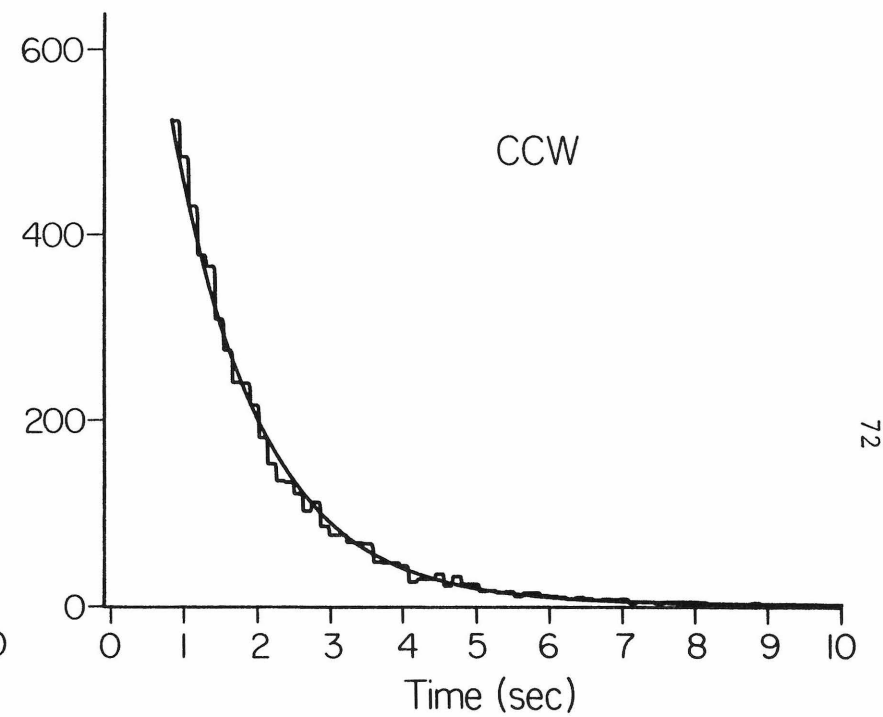
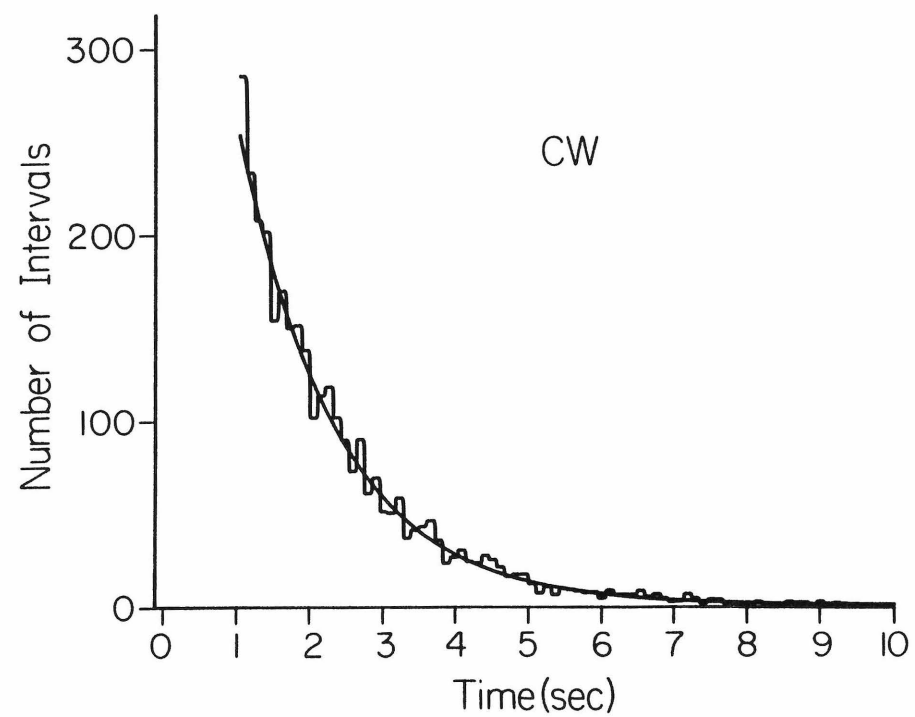


FIG. 3. Behavior of an adapted cell over a period of several hours. (A) Mean CW (o) and CCW (●) intervals. (B) Probability of spinning CCW (Δ). Each point shown was computed from data collected over a period of 3 to 5 min.

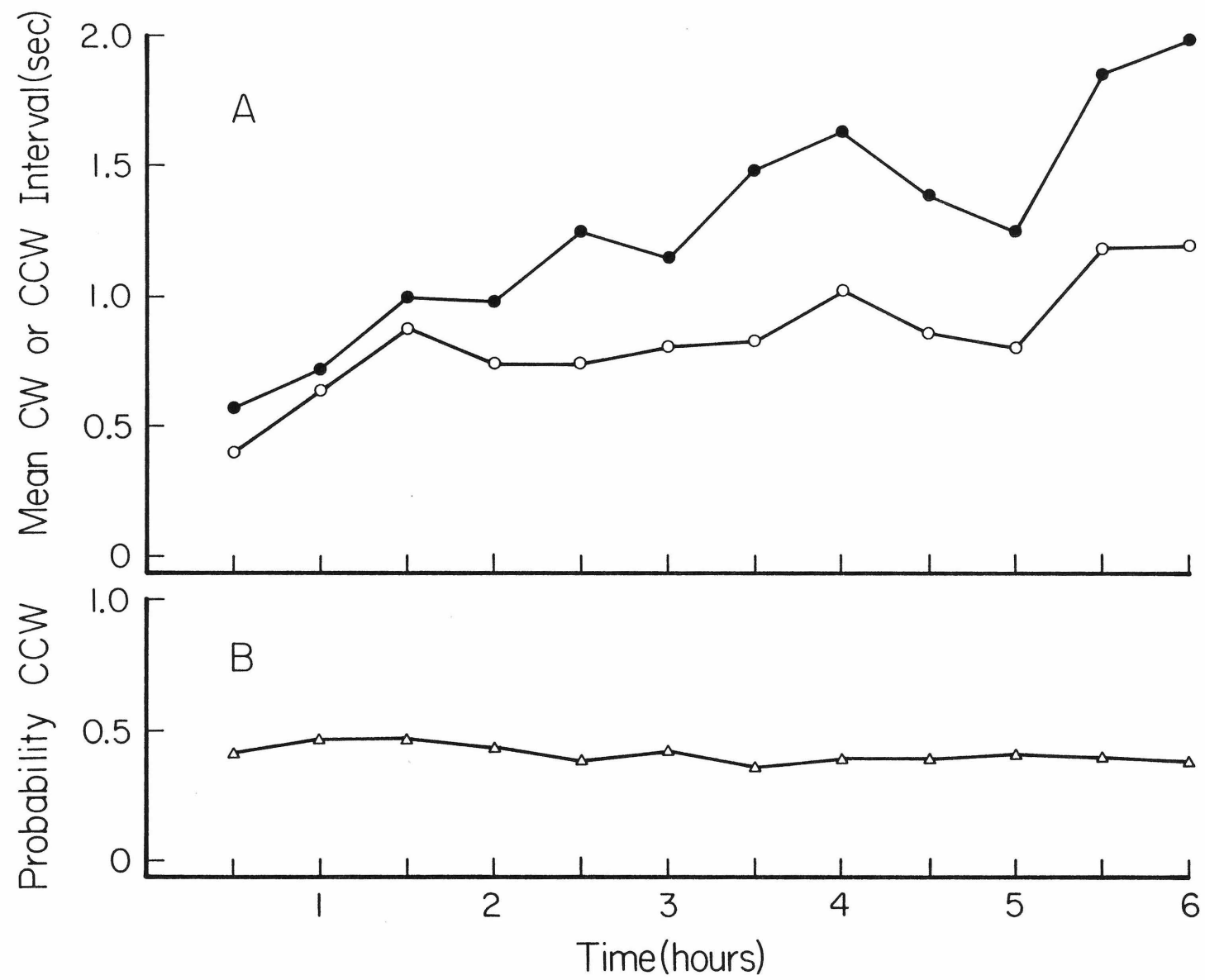


FIG. 4. Response of a typical cell to exponential ramps up or down. (A) A ramp from C_{low} to C_{high} at rate $a = 0.015 \text{ s}^{-1}$, beginning at $t = 177 \text{ s}$ and ending at $t = 339 \text{ s}$. (B) A ramp from C_{high} to C_{low} at rate $a = -0.037 \text{ s}^{-1}$, beginning at $t = 184 \text{ s}$ and ending at $t = 248 \text{ s}$. The arrows indicate the times that the ramps began or ended at the flow cell. The changes in bias shown in the figure do not coincide precisely with the arrows, in part because of fluctuations in bias, in part because the spline smoothing spans a finite interval; see Materials and Methods.

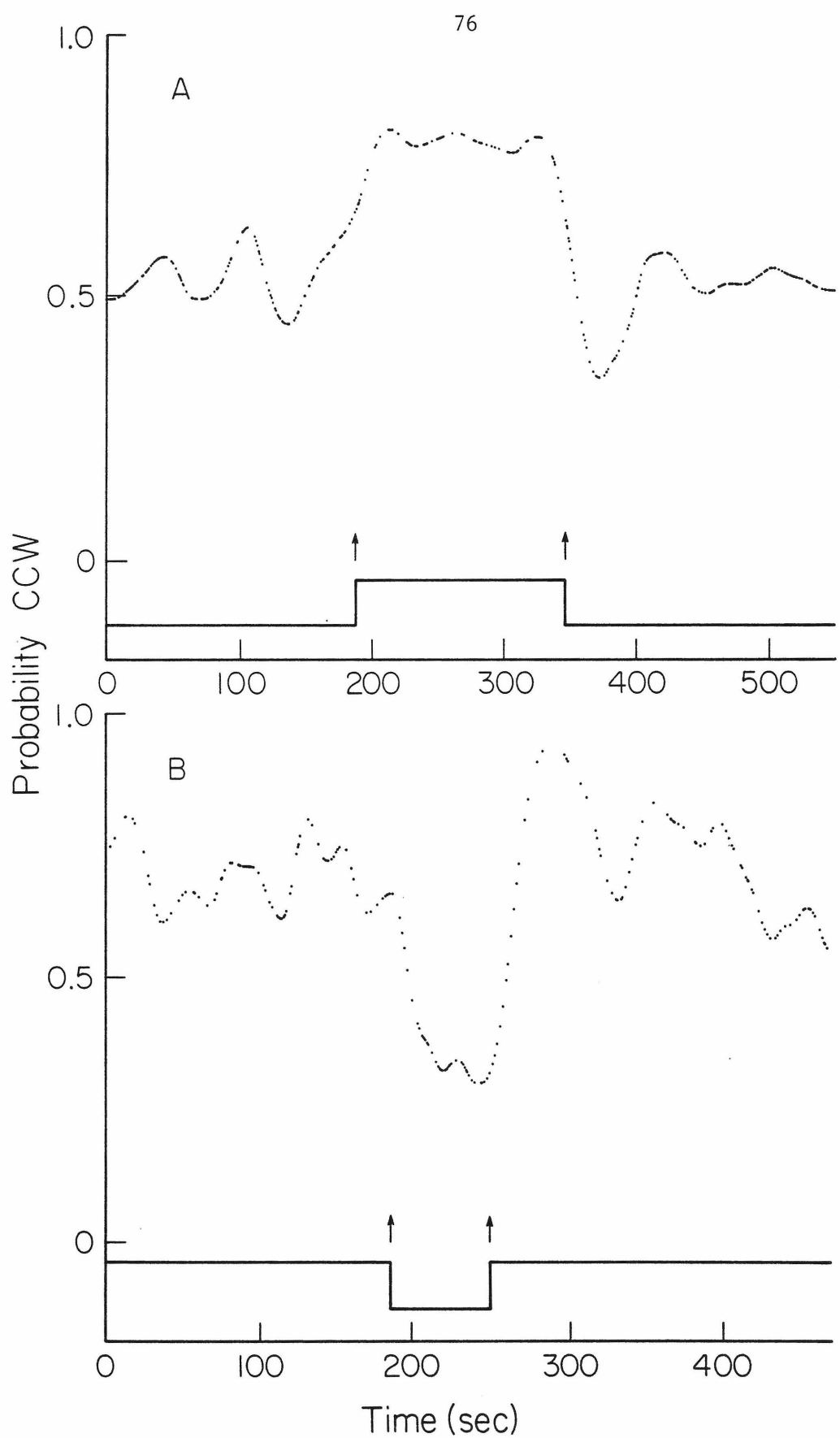
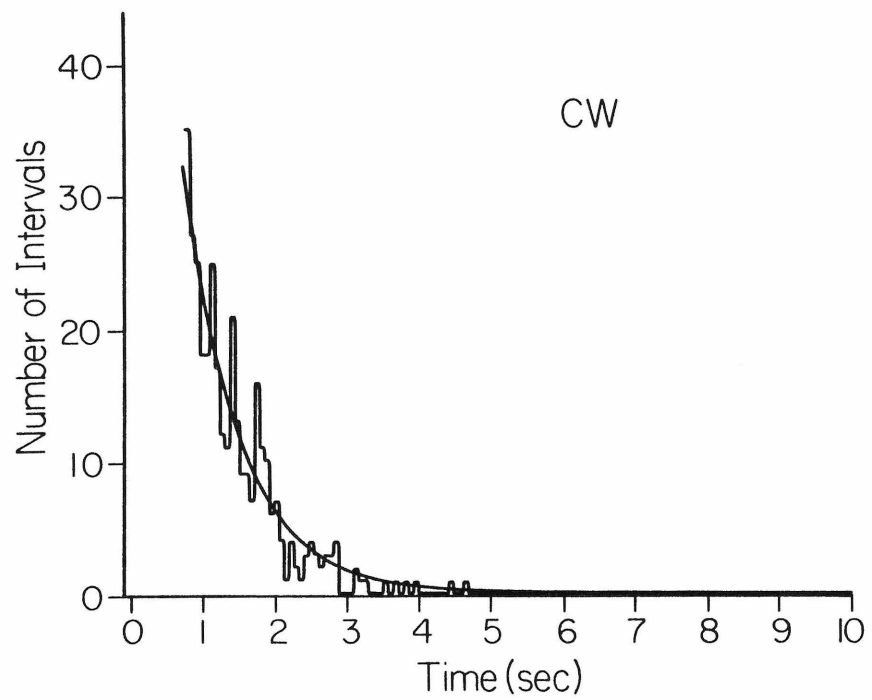
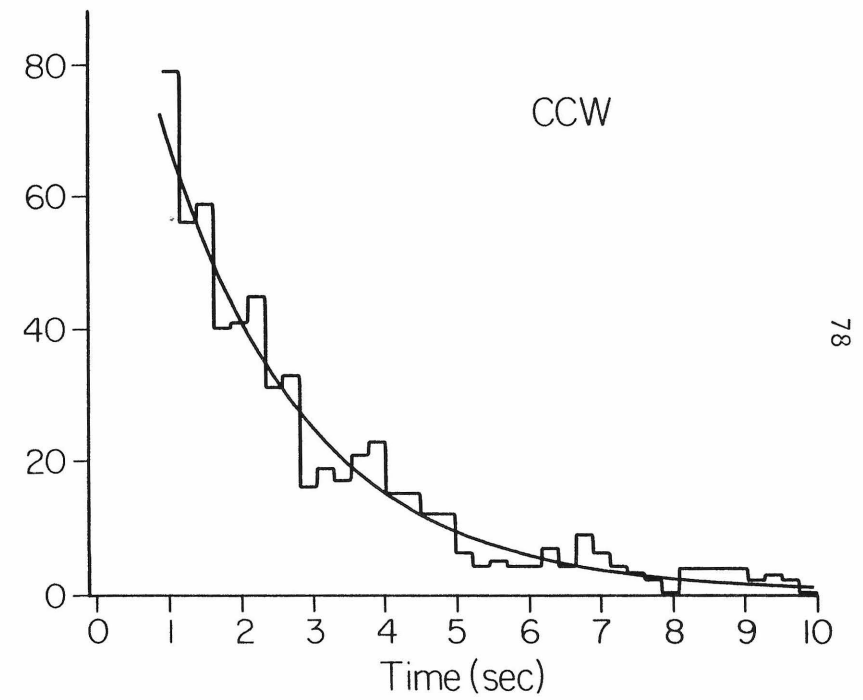


FIG. 5. CW and CCW interval distributions of cells during an exponential ramp up. Histograms for 13 records from 6 cells exposed to ramps of rate 0.013 sec^{-1} were scaled, combined, and fit by exponentials, as described in Materials and Methods. (Left) CW interval distribution computed from 534 events longer than 0.4 s. Range of adjusted means for each record: 0.30 to 1.5 s. Global adjusted mean: 0.69 s. Decay time for the exponential fit: 0.78 s; reduced χ^2 0.913, 17 degrees of freedom, p-value 56%. (Right) CCW interval distribution computed from 795 events longer than 0.4 s; 32 events are off scale. Range of adjusted means for each record: 0.75 to 12.0 s. Global adjusted mean: 2.38 s. Decay time for the exponential fit: 1.99 s; reduced χ^2 1.18, 19 degrees of freedom, p-value 27%. (Not shown) CW and CCW interval distributions for the same cells prior to each ramp. CW global adjusted mean computed from 740 events longer than 0.04 s in 13 records: 0.76 s. CCW global adjusted mean computed from 948 events longer than 0.4 s in 13 records: 0.89 s. Exponential fits were not made to these data.



CW



CCW

78

FIG. 6. Rotational bias as a function of ramp rate for exponential ramps up or down. Note the break in scale. (A) Responses of two cells to ramps up. The solid lines are least-squares fits to all but the first and last data points. The slopes of these lines are 21.5 ± 4.6 s (o) and 18.7 ± 4.1 s (●). The dashed lines were drawn by eye. The first data point, shown with error bars, is the mean and std. dev. of the bias prior to the ramps: 0.43 ± 0.06 , 16 determinations (o); 0.41 ± 0.04 , 12 determinations (●). The last data point was taken at the maximum rate attainable with the apparatus, at a time constant of about 12 s. (B) Responses of one cell to ramps down (□). Solid and dashed lines: as above. Slope of solid line: -16.0 ± 3.6 s. Mean and std. dev. of first data point: 0.64 ± 0.06 , 10 determinations.

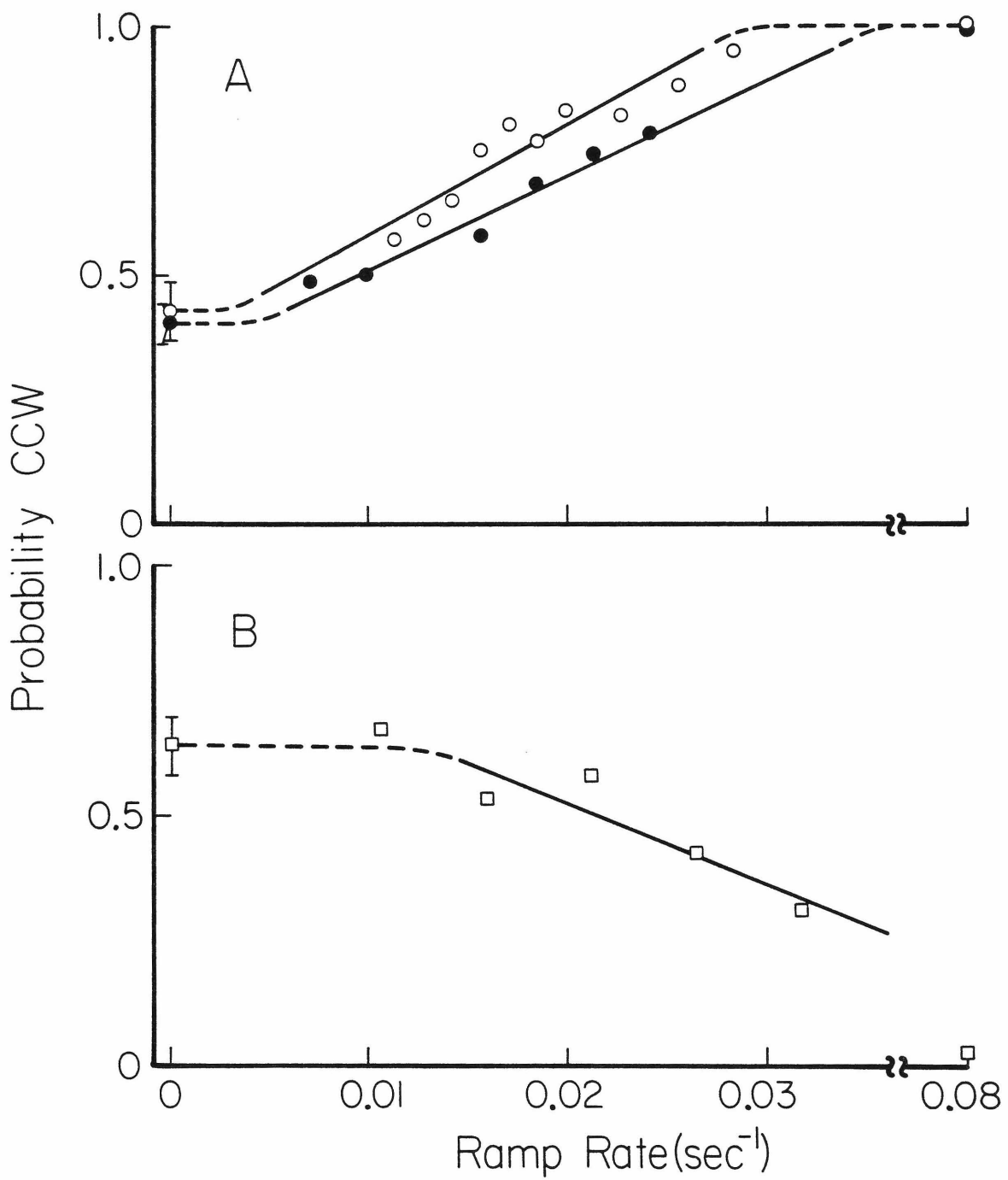


FIG. 7. Response of a cell to an exponentiated sine wave of frequency 0.005 Hz. The concentration varied from C_{low} to C_{high} . (A) Changes in rotational bias. The mean bias during this response was 0.71. The mean bias prior to stimulation was 0.64. (B) Changes in the fraction of receptor bound, P (---), and its time derivative, dP/dt (—). (C) Changes in reversal rate.

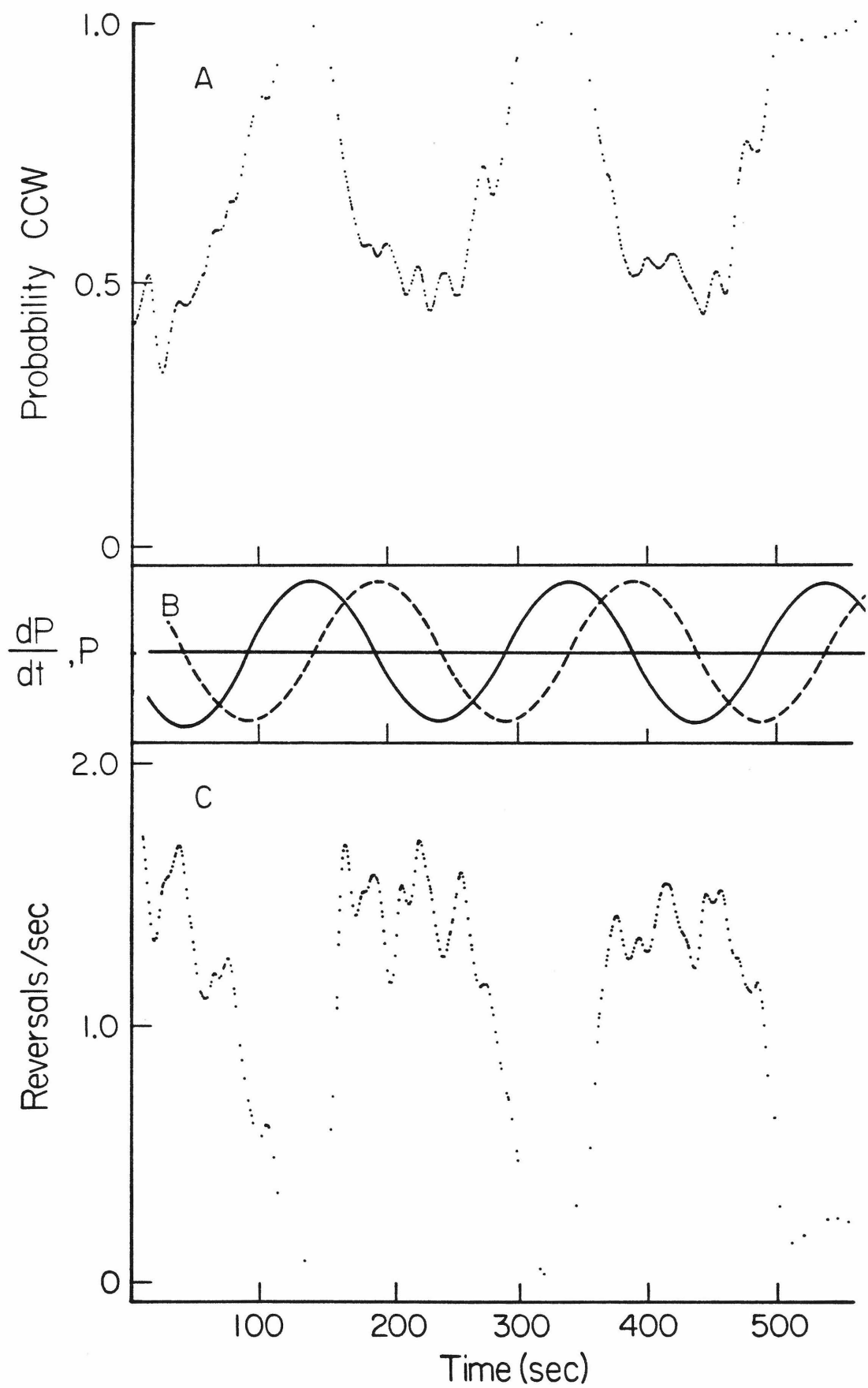


FIG. 8. Bode plot of response amplitude versus frequency for exponentiated sine waves. The concentration always varied between C_{low} to C_{high} . The peak-to-peak changes in rotational bias of two cells were normalized to the values obtained with saturating stimuli, averaged, and plotted as a function of frequency on a log-log scale. A reference line of slope 20 dB/decade (characteristic of a first order high-pass filter) is shown for comparison.

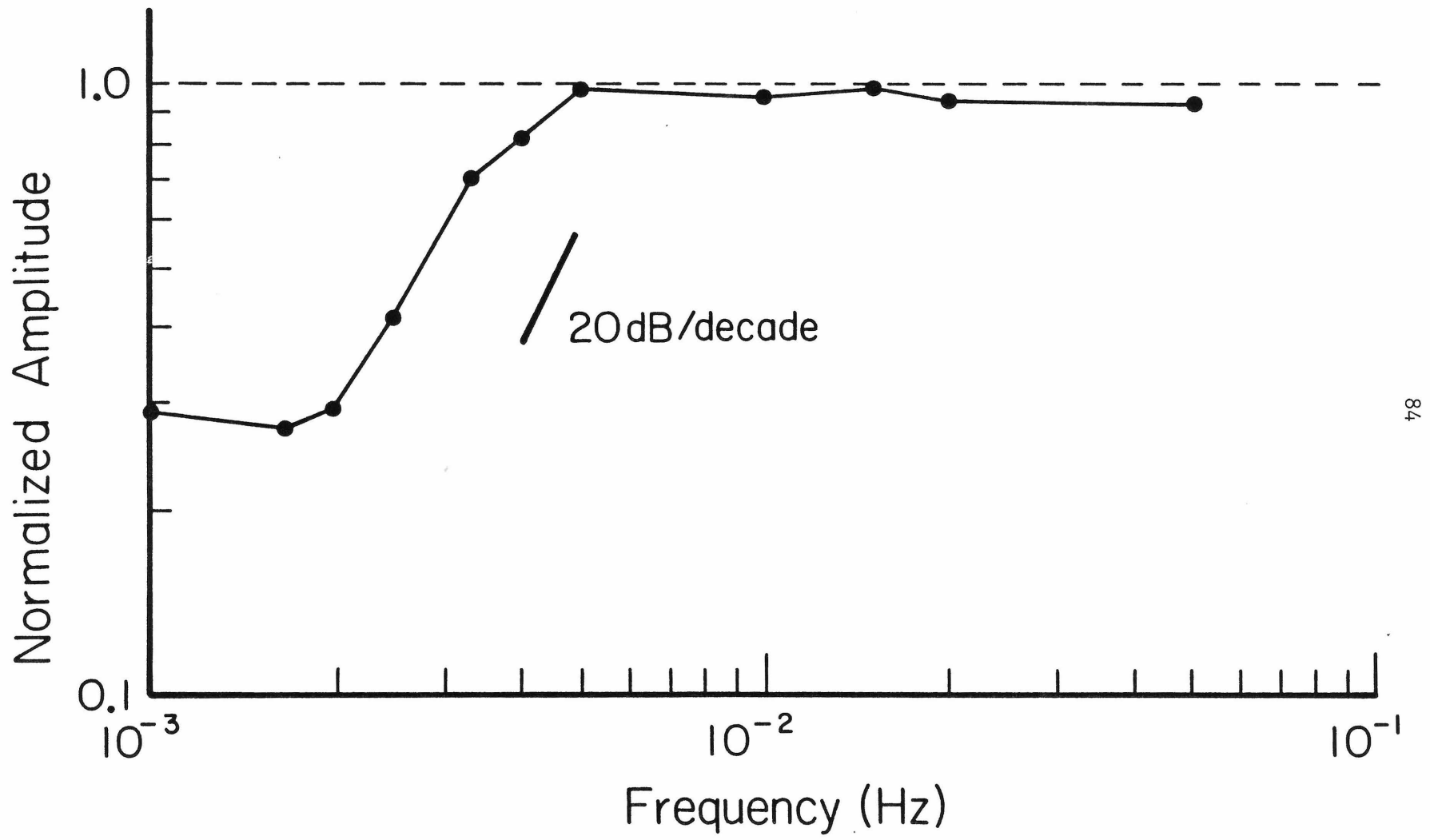
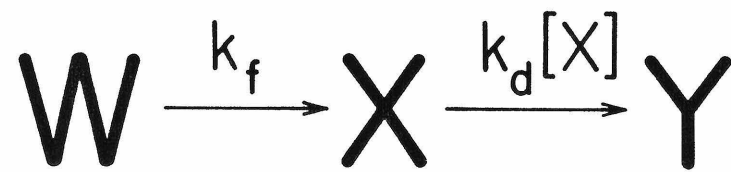


FIG. 9. Models for the generation of spontaneous reversals. (A) The response regulator model. An intermediate, X , is produced by one reaction and degraded by another. At steady state, the concentration of X is constant, on average, but fluctuations occur. A mechanism exists that compares the instantaneous value of X with a reference level, X_{crit} . CCW intervals (runs) occur when X is larger than X_{crit} , and CW intervals (tumbles) occur when X is smaller than X_{crit} . (B) The two-state model. Two states, representing CCW rotation (a run) or CW rotation (a tumble), are connected by first-order rate constants k_r and k_t , which are the probabilities per unit time of terminating these events. In the interest of using the common nomenclature, we assume a one-to-one correspondence between CCW intervals and runs (smooth segments in the track of a free-swimming cell) and between CW intervals and tumbles (short erratic segments) established in (19). Exceptions occur in cells with an extreme CW bias, which can move in a slow quasi-smooth manner while rotating their flagella CW (16).

A)



{ Run when $[X] > [X]_{\text{crit}}$
Tumble when $[X] < [X]_{\text{crit}}$

98

B)

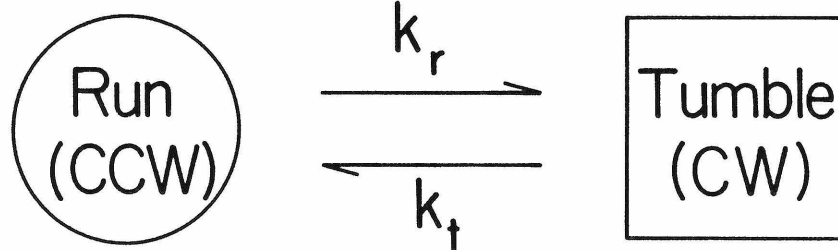
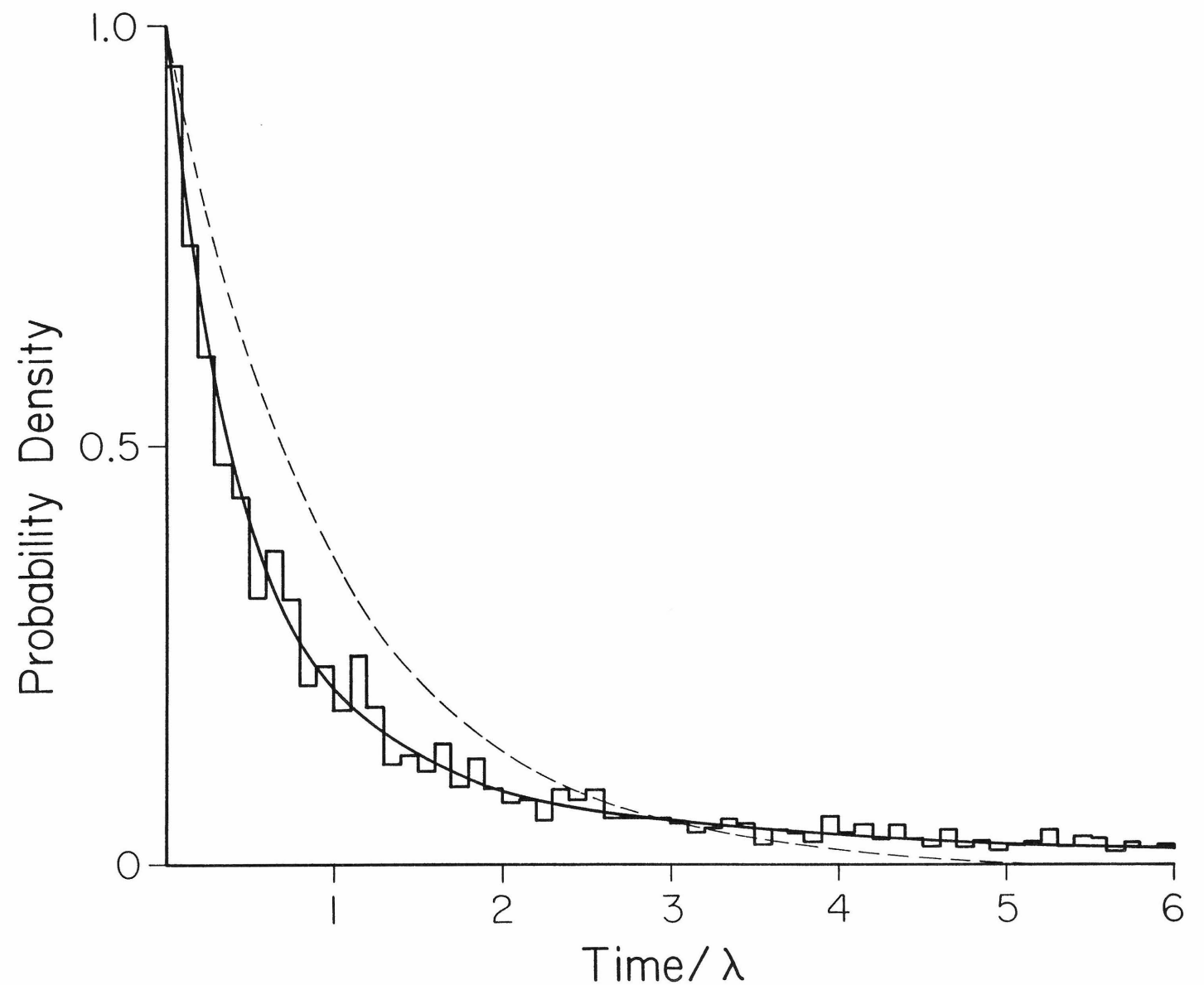


FIG. 10. Interval distribution predicted by the response regulator model (—) compared to an exponential distribution of the same area (---). The solid line is the analytical solution given by Eq. A6. The histogram is the result of a Montecarlo simulation. We assumed an average steady-state concentration $X_{ss} = 1000 = X_{crit}$, corresponding to a probability $CCW = 0.5$, and that X is generated at a rate $k_f = 1 \text{ s}^{-1}$ and destroyed at a rate $k_d = 0.001 \text{ s}^{-1}$, yielding a mean flux $\lambda = 1 \text{ s}^{-1}$. Twenty-three percent of the events predicted by the analytical solution and found in the simulation are off scale, as compared to 0.3% for the exponential distribution. The mean interval predicted by the analytical solution is infinite. The longest interval found in the simulation was 5,985 s.



General conclusions

Text-figure 4 shows a summary of the behavior of E. coli in exponential gradients of an attractant. An exponential increase in concentration leads to a linear change in P, the fraction of bound receptor. The time derivative of this function makes discrete steps to non-zero values during the course of the ramps. The rotational behavior of tethered cells resembles the time derivative of P, stepping from the unstimulated bias level to new levels dictated by the sign and magnitude of dP/dt. Several points of departure from exact proportionality are seen. First, the asymmetry in the response means that a steeper ramp down than up is required to generate the same change in bias; the ramps shown differ by a factor of two in rate. Second, a response overshoot occurs at the trailing edge of the ramps; its origin is unknown. Third, the rise in bias at the leading edge of ramps is not instantaneous; it occurs, however, over a time span too short to be investigated using the apparatus, which filters concentration changes with a time constant of 11 sec. Data from the impulse response (Chapter II) indicate that changes in bias should be complete within about 4 seconds.

This form of behavior is characteristic of a first order high pass filter process, or, equivalently, of models of the type presented by Delbrück and Reichardt (1956). The high pass characteristic can be seen in a Bode plot of the response to sinusoidal changes in P, but the asymmetric (i.e., nonlinear) character of the response severely limits the use of this approach.

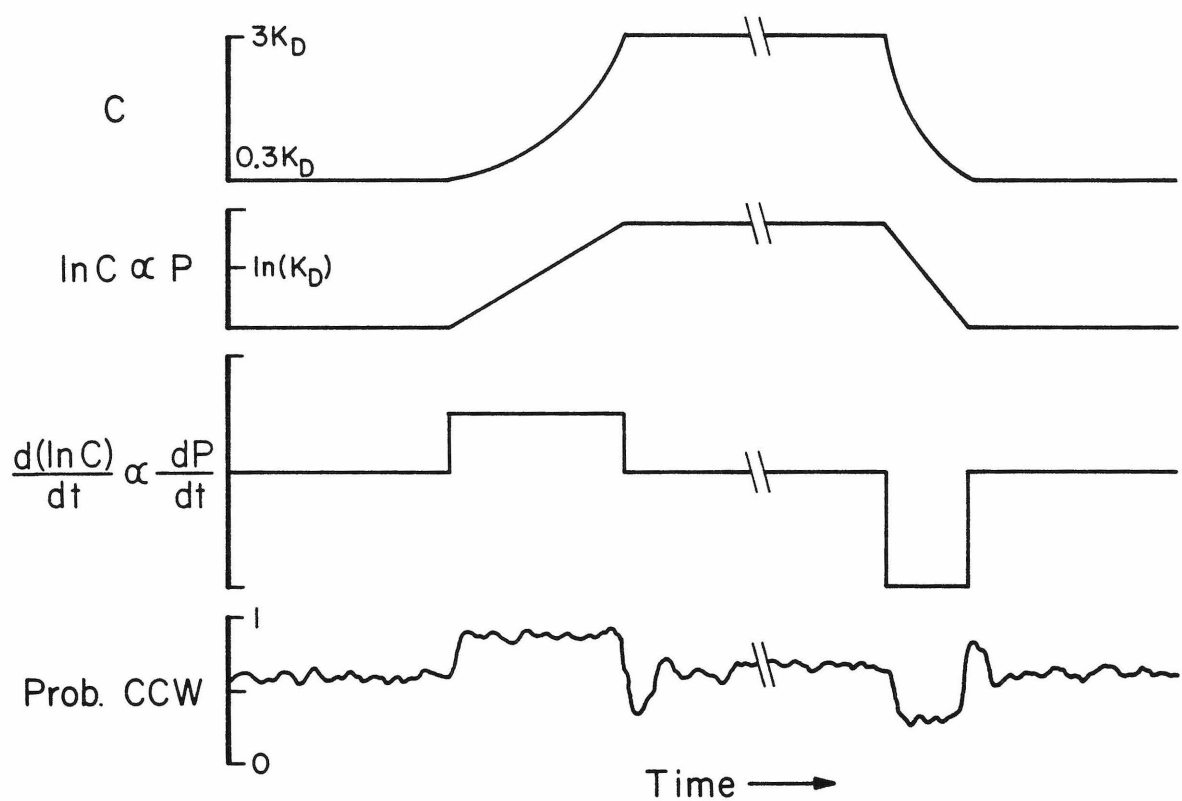
The problem of short events

Several aspects of the adaptation data bear further discussion. First, I would like to address the problem of interval distributions. The time resolution of any measurement puts limits on the fidelity with which events are recorded; this resolution is particularly evident when recording exponential distributions, since the most frequent events lie near $\Delta t=0$, i.e., right at the limit of resolution.

Text-figure 4. Gradient behavior.

The diagram summarizes the response of tethered cells to shallow exponential gradients of an attractant. Cells are initially adapted to C_{low} , then experience an exponential gradient to C_{high} , where they re-adapt. The process is then run in reverse.

From top to bottom: i) the exponential concentration profile experienced by cells, ranging in these experiments from 0.3 to 3 times the apparent dissociation constant of the receptor for α -D,L-methylaspartate; ii) the logarithm of concentration, which is proportional to P over this range of concentration (note that ramps run between values bracketing $\ln[K_D]$); iii) the time derivative of the above, which is proportional to dP/dt , showing steps of different magnitude up and down, and iv) an idealized response of a tethered cell, showing changes in bias during the ramps up and down (note also the overshoot and effects of rectification). See text.



Inability to measure small time intervals leads to histograms lacking short events; the histograms compiled in these experiments showed this paucity of short events. What was surprising was the apparent time out to which events continued to be missing. In principle, the effect should have been strong for times less than or comparable to the resolution of the digitizing process. These times, in turn, are set by the response of the human operator reacting to slow-motion playback of the videotapes. Considerable care was taken to get an accurate estimate of the errors introduced with this procedure. However, in the global histograms that were produced, the "missing" events were clearly seen out as far as one-half second or more, nearly three times the measured resolution of the digitizing technique.

This led me to believe that the phenomenon was real (as opposed to an artifact of the measurement process), and that some mechanism in the bacterium inhibited reversals for times less than around 0.2 sec. Such a mechanism might correspond, for example, to a new, short-lived intermediate between the "CCW" and "CW" modes of the two-state model. A number of elaborate models with multiple states were constructed having the desired properties. These models all predicted an interval distribution described by a convolution of two exponentials, one with a short time constant (of order 0.2 sec) and one with a longer time constant (of order 1 sec). Least-squares fits gave reasonable-looking curves which matched the data well for long times and more-or-less well for short times. Imperfections in the fit at short times were attributed to limited time resolution, especially for the first histogram bin.

It turned out that the departure from a single exponential out to times as great as one-half second was an artifact of the global averaging procedure used to combine histograms. Two nominally exponential histograms cannot be simply binned together if the time constants of the processes that generate them are not equal. However, if these histograms are first normalized in time to their

respective means, such an addition is permissible. Advantage was taken of this property in order to combine the many experimental histograms.

The problem was that the individual histograms had a large variation in mean time, ranging from about 0.6 sec to over 5 sec. Histograms with shorter time constants, when scaled to their means, appeared to have events missing at greater intervals than those with longer time constants. The overall effect of this phenomenon was to increase the number of bins in the summed histogram which had entries from the "missing" regions of individual histograms, thus enlarging the zone with fewer events when the final histogram was rescaled to the global mean. The involved averaging procedure described in the previous paper, which eliminated short time bins prior to averaging, was designed to circumvent aspects of this problem. Properly combined, the distributions follow a single exponential for times somewhat beyond the 0.4 sec cut-off. However, the interval chosen for this cut-off is still relatively long compared with the measurement error; it remains possible that a paucity of events does exist for times less than this value. The data from these experiments are just not reliable enough to decide the issue.

Hints that a genuine lack of very brief events exists come from data collected using the LGF detector, which also had fewer events than predicted by a single exponential out to times in the range of 0.1 to 0.2 sec; this is greater than the estimated measurement error contributed by the digitizing process (Block et al., 1982). This effect, however, may be attributed to an inability of the electronic event marker to pick up reversals lasting only a fraction of a revolution, thereby failing to trigger the rotational event in all cases. These brief events are generally scored by the operator of the chart digitizer directly from their signatures in the analog x- and y-signals, but it is entirely possible that enough are still missed to account for the observed distributions.

Analogous problems have plagued experimenters looking for single-channel lifetimes in patch clamp preparations—the finite bandwidth of the head-stage amplifier prevents the shortest events from being seen, and consequently limits their ability to fit models involving relatively short time constants. As in our case, the questions cannot be answered until an instrument of higher time resolution is built.

Nonlinearities in the response

Plots of rotational bias as a function of ramp rate (Fig. 6 of Block et al., 1983), although linear over a considerable range, have distinct offsets. The offsets mean that cells are unresponsive to rates of change in receptor occupancy below threshold levels. In the case of ramps up in α -methylaspartate, the threshold occurs at roughly 0.8% per sec, while for ramps down the corresponding value is close to 1.5% per sec. If behavior were described by a strictly linear proportional control mechanism (e.g., by the Delbrück-Reichardt model or equivalently, by a first-order high pass filter), such offsets would not be seen.

The presence of the offsets is also reflected in the response to exponentiated sine waves (Fig. 7 of Block et al., 1983). The combined effect of the different thresholds for response to dP/dt introduces a rectifying nonlinearity. This produces harmonic distortion in the response to a sinusoidal input, flattening it whenever dP/dt is near zero or slightly negative. The nonlinearity also introduces a DC offset in the mean response; both of these are evident in the records: the mean value of bias during response to exponentiated sine waves is greater than the mean unstimulated bias.

The asymmetry of response for small values of dP/dt is not nearly as severe as that observed for large-step stimuli. However, the asymmetry seen here is of an entirely different origin, in that for large steps the asymmetry reflects an underlying difference in the maximal rates of adaptation, whereas for shallow

ramps the asymmetry reflects the minimal onset of adaptive processes. In fact, the nonlinearities in the domain of small signals are not terribly severe, especially for dP/dt positive, suggesting that a reasonable representation of the response system can be accomplished using linear methods; the experiments described in the next chapter employ such an approach.

The gain of the response system

If cells sense dP/dt and respond by altering their rotational bias, then the slope of the curves in Fig. 6 provides a measure of the gain of the signalling chain. A slope of 20 sec on this plot of bias versus time rate of concentration increase corresponds to a sensitivity of 80 sec when bias is considered as a function of dP/dt (since $dP/dt = \frac{1}{4}d(\ln C)/dt$).⁸ In the linear approximation, a change in bound receptor amounting to 0.625% over one second (the average run time) is sufficient to produce a shift of one-half unit in the bias. Considering that the number of aspartate receptors on a cell is probably less than 1000, a change in 0.6% of that number producing such a large modulation in bias indicates an exquisite sensitivity, approaching the theoretical limit.

A previous estimate of the dependence of behavior upon dP/dt was made by Brown and Berg (1974) based on data collected by tracking cells swimming in enzymatically-generated temporal gradients of L-glutamate. In their work, the logarithm of the mean run length ($\ln \tau$) was found to depend on dP/dt according to the linear relation: $\ln \tau = \ln \tau_0 + \alpha dP/dt$, where $\ln \tau_0$ and α are fit parameters. The best value for α reported was 660 ± 70 sec.⁹ It is difficult to compare this

⁸ Measured slopes were 21.5 ± 4.6 sec, 18.7 ± 4.1 sec for ramps up, -16.0 ± 3.6 sec for ramps down. Units are seconds since they represent the dimensionless change in bias per unit time rate of (relative) concentration increase. P. Meyer was responsible for pointing out that these "times" do not represent any system time constants, but are instead measures of system gain.

⁹ Other values, representing determinations based on fewer cells, were $\alpha = 420 \pm 140$ and $\alpha = 1300 \pm 900$ sec.

number with the sensitivity found in the ramp experiments. First, the use of a different compound, although signalling through the same MCP (MCP II, the tar gene product), may influence sensitivity. Second, the mutant strain used in their experiments was tsr⁻ (this was done to prevent cells from sensing alanine, a substrate for the enzyme reaction). Methylation levels of MCP II in response to compounds sensed by tar in tsr⁻ strains are 1.5- to 2.7-fold greater than in wild type strains (Springer et al., 1977) and it appears that adaptation times in tsr⁻ strains are correspondingly longer (J. Segall and L. Flitz, personal communication). Third, the correspondence between the logarithm of mean run length (their measure) and rotational bias (our measure) is poorly understood. Nevertheless, a rough comparison may be obtained as follows.

In the enzymatically generated temporal gradients, the mean run length doubled (increased from 0.67 to 1.34 sec) for $dP/dt = 0.00105 \text{ sec}^{-1}$ (Fig. 1 of Brown and Berg; as cited by Berg and Purcell, 1977). To achieve correspondence with rotational intervals, let us assume that mean run times equal mean CCW interval times. This assumption is likely to be valid (Ishihara et al., 1983). Assume also that for small values of dP/dt , mean CW intervals remain largely unaffected (this is a reflection of the asymmetry in the response). For a cell with unstimulated CW and CCW intervals both equal to 1.0 sec (initial bias = 0.5), a doubling of the mean CCW interval to 2.0 sec with no change in CW interval would shift the bias by about 0.17 (final bias = 0.67). Using the sensitivity value of 80 sec from above, this implies that the corresponding value of dP/dt required to produce such an effect on a tethered cell would be $(.17/80) = 0.0021 \text{ sec}^{-1}$, a number that differs from the actual value by factor of about two. In view of the apparent 1.5- to 2.7-fold increase in sensitivity of tsr⁻ mutants, the two measures of sensitivity would appear to be in good agreement.

An independent test of sensitivity has been made using data from the step and impulse responses of wild type E. coli; this will be taken up in the second chapter.

Chapter II

STIMULATION OF TETHERED CELLS BY IONTOPHORESIS

Background

In late 1981, Jeff Segall was finishing up a series of experiments designed to measure the "reaction time" of bacteria (Segall et al., 1982), using an iontophoretic set-up and the LGF apparatus that had been constructed earlier by Howard Berg. Micropipets containing a solution of charged attractant could be brought within a few microns of a tethered cell spinning in motility buffer. By passing current through the pipets, a small amount of attractant was ejected from the tip, raising its concentration in the region of the cell. The cell would respond, if it happened to be spinning CW, by reversing to the CCW direction in about 0.2 seconds. Jeff had spent months of hard work tracking down the source of an artifact that caused cells to respond when only buffer was placed in the pipet: it turned out that surface charge on the glass had to be cancelled. At this point, the pipet technology was all worked out, the controls with buffer alone in the pipet gave no response, and Jeff was busy gathering data for publication.

It occurred to me that the diffusive process which carried the attractant rapidly from the region of the pipet tip to the cell would just as rapidly carry it away, were the stimulus current to be turned off; this would allow us to generate impulsive stimuli for tethered bacteria. With luck, enough chemical could be delivered in a short enough time to get a response from the cell. If the change in concentration could be made in a time comparable with, say, the 0.2 sec response time, then I felt we would be on safe ground. I approached Jeff with the idea, who had been using long current pulses in the 1-sec range for the reaction time experiments. I asked if he would try some really short pulses, over ten times shorter than those he had been using. We discussed the possibility that one record of an impulse response would probably not tell us much: some kind of signal averaging would need to be done. He agreed to grant me several pulses (out of the hundred or so) in his next experiment. I spent most of that night writing a signal-

averaging program that could be used, together with software scavenged from the ramp experiments, to extract an impulse response signal from the stochastic background behavior of our cells.

The next day, Jeff presented me with eight records, using 120 msec pulses. Only eight. And the pulses were a bit on the long side. I had (foolishly) insisted that he collect data on the cells for an entire minute following each impulse. I digitized the chart records using hardware that had also been scavenged from the ramp experiments and ran my new program. On a scale of one minute, nothing was to be seen. But if one looked very closely, and with considerable prejudice, at the first ten or so seconds of the averaged response, there was a suggestion of a peak. Not that it was statistically significant; it just looked suspicious. I took a photo of the response on the oscilloscope and showed it to Jeff. From that point, we were both hooked. He tried twenty-three pulses in his next experiment, and when he had finished the data collection for the earlier work, we both went full-time into the impulse business. It was a fruitful collaboration. Jeff ran the iontophoresis set-up and I digitized charts and wrote analysis programs. We both argued about the interpretation. Our current pulses kept getting shorter and shorter, down to 20 msec. We pulsed up, we pulsed down. Since then, over 1600 impulses and small steps have been digitized for the wild type and nearly 1400 for various chemotaxis mutants. Peaks now look quite respectable in comparison to the background noise.

The impulse response has turned out to be a useful way of measuring behavioral properties, and information obtained from it nicely complements the conclusions drawn from using finnicky programmable gradients. Jeff is continuing with the work, examining new mutants and different chemicals.

IMPULSE RESPONSES IN BACTERIAL CHEMOTAXIS

Steven M. Block, Jeffrey E. Segall and Howard C. Berg

Division of Biology 216-76, California Institute of Technology
Pasadena, California 91125

Reprinted from: **Cell** **31**:215-226.

copyright 1982 by MIT

Impulse Responses in Bacterial Chemotaxis

Steven M. Block, Jeffrey E. Segall and
Howard C. Berg
Division of Biology
California Institute of Technology
Pasadena, California 91125

Summary

The chemotactic behavior of *Escherichia coli* has been studied by exposing cells tethered by a single flagellum to pulses of chemicals delivered iontophoretically. Normally, wild-type cells spin alternately clockwise and counterclockwise, changing their direction on the average approximately once per second. When cells were exposed to a very brief diffusive wave of attractant, the probability of spinning counterclockwise quickly peaked, then fell below the prestimulus value, returning to baseline within a few seconds; repellent responses were similar but inverted. The width of the response indicates that cells integrate sensory inputs over a period of seconds, while the biphasic character implies that they also take time derivatives of these inputs. The sensory system is maximally tuned to concentration changes that occur over a span of approximately 2 sec, an interval over which changes normally occur when cells swim in spatial gradients; it is optimized to extract information from signals subject to statistical fluctuation. Impulse responses of cells defective in methylation were similar to those of wild-type cells, but did not fall as far below the baseline, indicating a partial defect in adaptation. Impulse responses of *cheZ* mutants were aberrant, indicating a serious defect in excitation.

Introduction

Flagellated bacteria swim in a purposeful manner. They move up gradients of some chemicals (attractants) in search of food and down gradients of other chemicals (repellents) to avoid noxious substances. The cells are propelled by thin, helical flagella, each driven at its base by a reversible rotary motor. The behavioral repertoire of *Escherichia coli* and *Salmonella typhimurium* consists of runs and tumbles. During a run, the flagellar filaments rotate in concert in a helical bundle, pushing the cell steadily forward. Each run is terminated by a tumble, during which the filaments change their direction of rotation, the bundle flies apart and the cell moves erratically, with little net displacement. At the end of a tumble, the cell runs again, moving off in a new direction. The direction of rotation of a flagellar motor is determined in part by sensory inputs. In a chemically isotropic environment, changes in the direction of rotation occur at random, and a cell executes a three-dimensional random walk. Run and tumble intervals are each distributed exponentially, with time constants on the order of 1 and

0.1 sec, respectively. In a gradient of an attractant (or repellent) the rotational bias is altered in such a way that runs that happen to carry the cell in a favorable direction are extended. This imposes a drift on the random walk that carries the cell up (or down) the gradient. Temporal changes in concentration experienced by the cell as it moves in a gradient lead to variations in the occupancy of chemoreceptors that, in turn, alter the rotational bias of the flagellar motors. (For recent reviews on bacterial chemotaxis see Macnab, 1978; Springer et al., 1979; Koshland, 1981; Parkinson, 1981; Boyd and Simon, 1982.)

What is the pathway linking the receptors to the flagella? How does it function? While many of the components of this pathway have been identified genetically and some of their biochemical interactions are known, most of the events that occur during signal processing remain obscure. The work reported here defines the physiological properties of the sensory-transduction pathway in detail, both in the wild-type and in certain mutant cells. It is based on a method that provides means for systematic analysis of chemotactic behavior at the level of an individual flagellar motor.

The output of a single motor can be monitored by tethering the flagellar filament to a glass surface (Silverman and Simon, 1974). When the filament is held fixed, the motor spins the cell body alternately clockwise (CW) and counterclockwise (CCW). Rotation in the CCW direction (as viewed from a point in the external medium above the cell) corresponds to the run mode, while rotation in the CW direction corresponds to the tumble mode (Larsen et al., 1974). This preparation is particularly useful for the study of behavior: the cell remains at a fixed position for observation, while the chemical milieu may be changed at will. When properly energized, cells remain active for hours. A tethered cell can be stimulated by mixing in an attractant or a repellent (Larsen et al., 1974), by displacing one medium with another containing an attractant or a repellent (Berg and Tedesco, 1975) or by positioning an iontophoretic micropipette containing a charged attractant or repellent near the cell and passing an electric current (Segall et al., 1982).

The first two methods have been used in studies of adaptation, wherein cells exposed to the sudden addition of a large amount of attractant spin CCW for minutes, spin CW for a somewhat shorter time and then gradually relax to their initial mode of behavior (Berg and Tedesco, 1975). Cells exposed to the sudden removal of attractant spin CW for many seconds, spin CCW for a shorter time and then resume their initial mode of behavior. Similar responses are observed when repellents are removed or added, respectively. The biochemical basis for this adaptive behavior appears to be the reversible carboxymethylation of proteins found in the cytoplasmic membrane called methyl-accepting chemotaxis proteins (MCPs;

Kort et al., 1975). Individual polypeptides are multiply methylated in a sequential fashion, the final steady-state level of methylation reflecting the external concentration of attractant or repellent (Boyd and Simon, 1980; Chelsky and Dahlquist, 1980; DeFranco and Koshland, 1980; Engström and Hazelbauer, 1980). The time course for methylation in response to addition of attractant closely parallels that for physiological adaptation (Goy et al., 1977). When the concentration of an attractant increases (or that of a repellent decreases), methyl groups are added gradually; when the concentration of an attractant decreases (or that of a repellent increases), they are removed rapidly. These steps are catalyzed by two cytoplasmic enzymes: a methyltransferase, the product of the *cheR* gene (Springer and Koshland, 1977), and a methylesterase, the product of the *cheB* gene (Stock and Koshland, 1978); *che* refers to generally nonchemotactic. The MCPs also serve to integrate information from different sets of receptors and to relay that information to the flagellar motors. Accordingly, their genes have been designated *tar* (taxis to aspartate and some repellents), *tsr* (taxis to serine and other repellents) and *trg* (taxis to ribose and galactose) (Silverman and Simon, 1977; Springer et al., 1977; Kondoh et al., 1979).

Several other gene products are involved in signal processing. Direct interactions between some of these components have been demonstrated by reversion analysis and interspecies complementation. For example, the *cheY* gene product interacts with the methyltransferase and with components of the flagellar motor involved in controlling the direction of rotation (the *cheC*, or *flaA*, and the *cheV*, or *flaB*, gene products). The *cheZ* gene product interacts with the methylesterase and with these components of the motor as well. The functions of these and other *che* gene products, such as *cheA* and *cheW*, are not known (see Parkinson, 1981).

The iontophoretic method has been used in studies of excitation, in particular, to measure response latencies (Segall et al., 1982). When cells are exposed to rapid step changes in the concentration of attractants or repellents, responses to these stimuli occur in about 0.2 sec. This is true both for wild-type cells and for cells carrying a *cheR-cheB* double deletion. Response latencies of *cheZ* mutants are much longer. These latencies are relatively insensitive to the magnitude of the stimulus, provided that the change in chemoreceptor occupancy is above the threshold level. The response latency is a measure of the time required for signals to be processed by the complete transduction pathway. Given the small size of the organism, the latency of wild-type cells is surprisingly long, suggesting that the excitation pathway is complex.

There are two serious problems with the studies of tethered cells made thus far. The first is that measurements

of adaptation times and response latencies provide only a limited amount of information about the transduction machinery. The second is that the stimuli used are so large that this machinery is driven into saturation; the information that is obtained may not be relevant to the behavior of the cell in the real world, where stimuli are much smaller. Cells swimming in spatial gradients do not experience large temporal stimuli, because discontinuities in concentration are smoothed out by diffusion.

We have used the iontophoretic technique to expose cells to impulsive stimuli rather than to large-step stimuli, and we have followed each cell's behavior for many seconds, not just to the next flagellar reversal. In these experiments, a small amount of chemical is ejected from the micropipette over a period of a few milliseconds. The chemical spreads outwards as a diffusive wave, passing over the tethered cell and rapidly dissipating in the external medium. If the time course of the wave is sufficiently short, it can be treated as an idealized impulse. The behavior of the cell toward this stimulus is an impulse response. Impulse responses have two very useful features. The first is that they reflect only the time constants of processes occurring in the system under study, not the time constants of the stimulus itself. A simple analogy is a bell struck by the percussive impulse of a clapper: a characteristic tone is generated that decays with time. The fundamental frequency of the tone and its rate of decay reflect intrinsic properties of the bell itself, not properties peculiar to the clapper. The second feature is that the impulse response contains all the information necessary to predict the behavior of the system when it is exposed to an arbitrary stimulus. One need only decompose the arbitrary stimulus into a series of impulses of appropriate magnitude and timing and compute the sum of the responses that would be observed, were these impulses applied separately. However, for this computation to work, the stimulus must be small enough that there are no nonlinear effects: the response to each impulse must remain independent of whether or not the cell is still responding to previous impulses (see Papoulis, 1977; Marmarelis and Marmarelis, 1978).

The early events in chemotaxis occur on a time scale of tenths of a second, and cannot be resolved by methods previously used to explore bacterial behavior. The iontophoretic technique has allowed us to generate stimuli that are short enough to be impulsive. By monitoring the rotation of tethered cells with an optoelectronic device accurate to a fraction of a cycle, we have achieved the temporal resolution necessary to characterize the response to these stimuli. The response has properties that imply that the sensory system in *E. coli* is optimally designed to allow cells swimming in spatial gradients to extract information about changes in concentration from signals subject to statistical fluctuations.

Results

Computation of the Impulse Response

Cells were tethered to a glass window and viewed through the water-immersion lens of a phase-contrast microscope. The microscope was equipped with linearly graded optical filters that extract the x and y coordinates of the centroid of the image of a spinning cell; sensors viewing these filters generate signals that contain information about the cell's angular velocity and direction of rotation. A micropipette was positioned within about $4 \mu\text{m}$ of the cell, and the cell was stimulated by short iontophoretic pulses, repeated at intervals of about 1 min. Time records of the x and y signals were made on a strip-chart recorder, together with event markers indicating the direction of rotation of the cell and the timing of the stimulus current. The size of the stimulus to which the cell was exposed could be varied by adjusting either the magnitude of the current passed through the pipette or its duration. These parameters were adjusted by hand during the experiment to ensure that responses occurred, but under conditions in which the stimuli were impulsive (see below). Records of 20 sec duration bracketing each iontophoretic pulse were digitized and stored in a computer for subsequent analysis.

The rotational behavior of a tethered bacterium is a binary, stochastic process: it is the probability of spinning CW or CCW that is modulated by the sensory

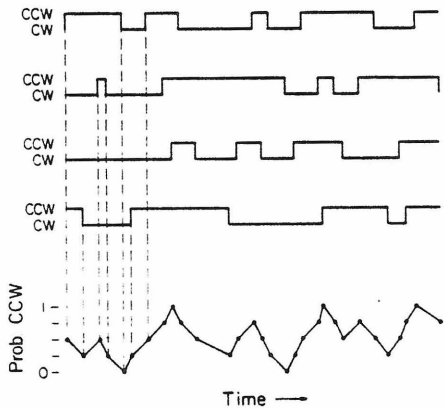


Figure 1. Scheme for Averaging Data Records

Individual binary records of rotational behavior (four are shown) were placed in register at the time of stimulation. A value of +1 was assigned to each record when the direction of rotation was CCW and 0 when it was CW. The average value of these numbers was computed each time a transition (an event) occurred in any one of the individual records. The result (bottom) is a function that can assume any one of $n + 1$ values between 0 and 1 inclusive, where n is the number of records. The value of this function provides an estimate of the probability of CCW rotation, and the density of points along the time axis gives an estimate of the average reversal rate. The algorithm actually used to perform this computation is described in the Experimental Procedures.

apparatus. Therefore, we took as our measure of the response the probability that a cell spins CCW. We obtained an estimate of this probability by taking the average of a series of records, each containing data obtained with a single stimulus. The procedure is outlined in Figure 1. A typical result obtained with 25 records from a single cell is shown in Figure 2. The fluctuation about the baseline before and after the stimulus results from the averaging of binary signals. Its amplitude obeys the binomial distribution; the mean amplitude decreases as the inverse square root of the number of records. To verify this fact and to test our data-reduction procedures, we used a Monte Carlo method to construct records of an "artificial cell" whose CW and CCW rotation intervals were given by exponential distributions. These records were processed in the same way as the real data. The probabilities computed from artificial and real data had similar statistical properties, which agreed with theory.

Impulse Responses of Wild-Type Cells

The impulse response to attractant stimuli is shown in Figure 3A. The same response was observed with aspartate and α -methylaspartate; only the threshold concentrations differed. Prior to stimulation, the directional bias of the cells averaged 64% CCW. After the pulse at time zero (5 sec on the scale shown in the figure), the probability of spinning CCW rose sharply to a maximum value at 0.4 sec, then fell in a smooth manner, crossing the baseline at 1 sec and reaching a minimum value at 1.5 sec, and finally returning to its initial value at approximately 4 sec. The excursion below baseline (the response undershoot) is important, because it implies that the chemosensory system has adaptive properties in the 1 sec time domain (see below). The areas of the two lobes of the response were equal.

The impulse response to repellent stimuli is shown

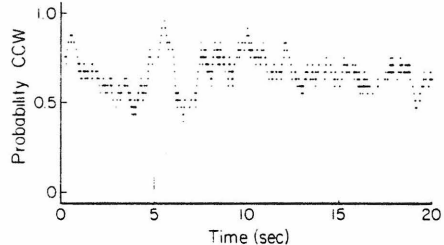


Figure 2. Impulse Response of a Single Cell

A single cell was stimulated 25 times by a pulse given at 5 sec (vertical line). The graph shows the probability of CCW rotation as a function of time, estimated as described in the legend to Figure 1. The pipette contained 100 mM α -methyl-D,L-aspartate, a negatively charged attractant. Pulses were generated by switching the current from 0 to -100 nA for a period of 100 msec. The discrete layer lines that appear in the data are determined by the 26 quantized values obtained when 25 binary records are averaged. Data were not smoothed.

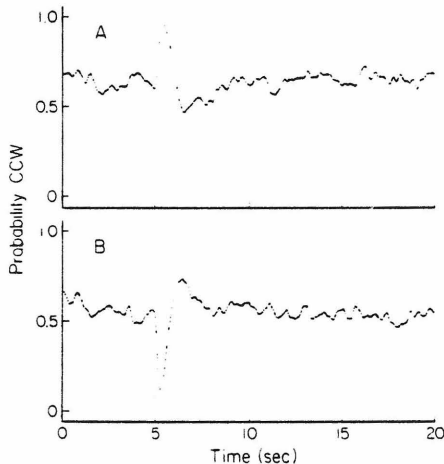


Figure 3. Impulse Responses of Wild-Type Cells

The probability of spinning CCW is shown as a function of time, with stimuli given at 5 sec (vertical line). The data were smoothed, as described in the Experimental Procedures.

(A) Attractant response. The pipettes contained either 1 mM L-aspartate or 7 mM α -methyl-D,L-aspartate. Pulses were generated with currents ranging from -1 to -100 nA switched on for periods of 20–100 msec. The graph was constructed from 172 records containing 3193 events obtained with nine different cells; 399 points are displayed; 115 of the records were from stimulation by L-aspartate, 57 from stimulation by α -methyl-D,L-aspartate.

(B) Repellent response. The experiment was carried out as described in (A), but with pipettes containing 200 mM benzoate or 1 mM L-aspartate. Benzoate was injected at -100 nA for 20–50 msec. L-aspartate was added continuously at -2 to -3 nA, and the addition was interrupted by switching to +3 to +10 nA for 20–40 msec. Addition of repellent or removal of attractant gave the same response. The graph was constructed from 169 records containing 2785 events obtained with seven different cells; 397 points are displayed; 86 of the records were from addition of repellent, 83 from removal of attractant.

in Figure 3B. The responses to the addition of benzoate and to the removal of aspartate were similar. The repellent response resembled an inverted attractant response, with a similar time course and biphasic character. The cells responded to the addition of benzoate and nickel chloride on a slightly shorter time scale than they did to the removal of aspartate (data not shown).

The pulses used represented true impulses, as indicated by the following experimental criteria: pulses were adjusted to be close to, but generally above, threshold for a response; in a trial experiment, stimuli of lower amplitude resulted in a smaller probability of a change in directional bias, but gave an impulse response with the same time course; and cells with different thresholds, exposed to pulses of different amplitude and duration, also gave an impulse response with the same time course. Finally, a theoretical calculation of the diffusive wave (Segall et al., 1982) showed that for the 20–40 msec pulses used

with wild-type cells, the change in chemoreceptor occupancy had fallen to less than 3% of its maximum value by 200 msec after the onset of the pulse, long before the end of the response was observed.

As stated above, the impulse response has predictive value when the system operates in a linear domain—that is, when responses to different stimuli add algebraically to give the overall response. In this domain, the response to an arbitrary stimulus is given by the convolution of that stimulus with the impulse response (Papoulis, 1977), a process that decomposes the stimulus into an infinite set of impulses of appropriate magnitude and timing and adds their responses together. For the simple case of the response to a step, the convolution reduces to the integral of the impulse response with time. The extent to which such a convolution predicts the system response is a measure of the linearity. In Figure 4, the measured response of wild-type cells to a small step change in concentration of an attractant is compared with the response predicted by integration of the impulse response; the agreement is satisfactory.

Does the response to an impulse depend on the initial state of the flagellar motor? That is, does it matter in which direction a cell happens to be spinning when it is stimulated? To answer this question, we separated the data into two parts: one containing those records for which the cell was spinning CW at a given instant, and another containing those for which the cell was spinning CCW at that instant. If this is done for an arbitrary time, t_0 , the records will be autocorrelated around that time in both directions. For example, if a cell happened to be spinning CCW at time t_0 , it is likely that it was also spinning CCW for times close to t_0 . For CCW intervals that are distributed as $\exp(-k_r t)$ and CW intervals distributed as $\exp(-k_t t)$, where k_r and k_t are the run and tumble rate constants, respectively, the autocorrelation function decays as $\exp[-(k_r + k_t)|t - t_0|]$. This effect is seen in Figure 5A. Both curves decay symmetrically to the baseline with similar time constants. The small difference in baseline for the two curves is a reflection of the fact that records chosen for cells that happen to be spinning in a given direction at an arbitrary time are more likely to belong to cells that are generally biased in that direction. If, however, the time t_0 is chosen to coincide with the time of the pulse, an intriguing result is obtained, as seen in Figure 5B. The two curves are back-correlated, as in Figure 5A, but now they follow an identical time course once cells that were spinning CW have had time to change their direction of rotation—that is, after an interval equal to the response latency. (The somewhat larger disparity in baselines for Figure 5B relative to Figure 5A also reflects the way in which the records were chosen, and is not statistically significant.) This implies that the response does not depend on the initial state of the

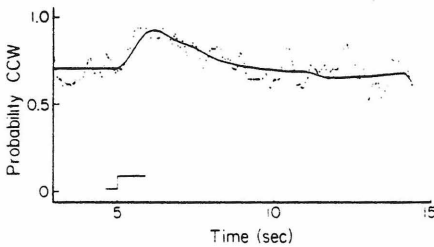


Figure 4. Small-Step Response of Wild-Type Cells

The probability of spinning CCW is shown as a function of time, with stimuli given at 5 sec (step mark). The data were smoothed, as described in the Experimental Procedures. The response to a small step increase in concentration of attractant (dotted line) is compared with the response predicted from integration of the impulse response (solid line). The pipette contained 0.1 mM L-aspartate. Steps were generated by switching the current from 0 to a value of -3 nA and maintaining that value for at least 10 sec. The experimental probability function was constructed from 34 records containing 417 events obtained with a single cell; 209 points are displayed. The impulse response was integrated from the beginning of the step onward in accordance with the convolution theorem (see text). The choices of baseline and amplitude for the predicted curve are arbitrary; they were scaled to match the baseline and amplitude of the experimental data. The impulse response used was similar to that shown in Figure 3A. It was derived from 237 records containing 4585 events obtained with 11 different cells.

motor, and that the mechanism responsible for the impulse response overrides the mechanism that generates spontaneous reversals.

Reversal Rate during Impulse Responses

As noted in the legend to Figure 1, the density of points along the time axis of the probability function provides an estimate of the average reversal rate. Such an estimate is shown in Figure 6, together with the repellent response from which it was derived. Once again, fluctuations around the baseline reflect the underlying statistical process; here, the amplitude of the fluctuations obeys a distribution related to the Poisson distribution, with a characteristically large variance. During the initial phase of the response, the reversal rate rose sharply, to a value of greater than 3 reversals/sec/cell, a consequence of the fact that cells that happened to be spinning CCW at the time of the pulse changed their direction of rotation within a narrow time interval. Shortly after the response minimum, the reversal rate fell to its lowest value, of approximately 0.3 reversals/sec/cell; the reversal rate is actively suppressed during the response. A subsidiary peak in the reversal rate occurred during the overshoot, whereafter the rate returned to its initial value. Reversal rates for attractant responses were nearly identical, but showed a somewhat less pronounced initial peak (1.5 reversals/sec/cell; data not shown). We will return to these data later when we discuss the two-state system (see Discussion).

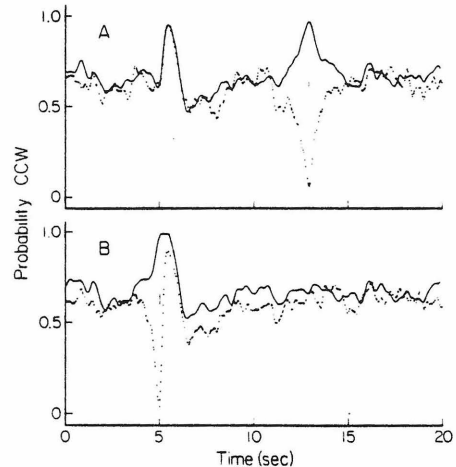


Figure 5. Stimulation during Either a CCW or a CW Interval

(A) The individual records used to compute Figure 3A were separated into two groups: those for cells that were rotating CCW (solid line) 8 sec after the pulse (at 13 sec; vertical line), and those that were rotating CW (dotted line). These groups were averaged separately to yield the graphs shown. The probability of being in the CCW or the CW mode is unity at 13 sec and decays exponentially in either direction to the baseline, as determined by the autocorrelation function (see text).

(B) The same records were separated into two different groups: those for cells that were rotating CCW (solid line) at the time of the stimulus pulse (5 sec; vertical line), and those that were rotating CW (dotted line). Both probabilities decay backwards in time, as in (A), but now the curves are nearly identical for times greater than 5.2 sec—that is, after an interval equal to the response latency.

Impulse Responses of Mutant Cells

The impulse response was determined for several generally nonchemotactic mutants, provided by J. S. Parkinson. Where possible, mutants with nonpolar deletions were used to ensure the null phenotype. The attractant response of cells carrying *cheR-cheB* double deletions is shown in Figure 7A. These mutants lack genes for both the methyltransferase and the methylesterase; they are defective in adaptation. Nevertheless, they have about the same directional bias as the wild-type and respond to large-step stimuli. Their impulse response was similar to that of the wild-type (Figure 3A); however, the initial peak was longer, and the undershoot was substantially smaller, in the mutant cells. The degree of undershoot varied from cell to cell; when examined individually, the cells whose average response is shown in Figure 7A showed different degrees of undershoot, ranging from none at all to a size comparable with that of the wild-type.

Mutants in *cheZ* have a large CW bias, high response thresholds and abnormally long response latencies (Parkinson, 1978; Parkinson and Parker, 1979; Segall et al., 1982). Very short impulses of L-aspartate failed to produce a response; however,

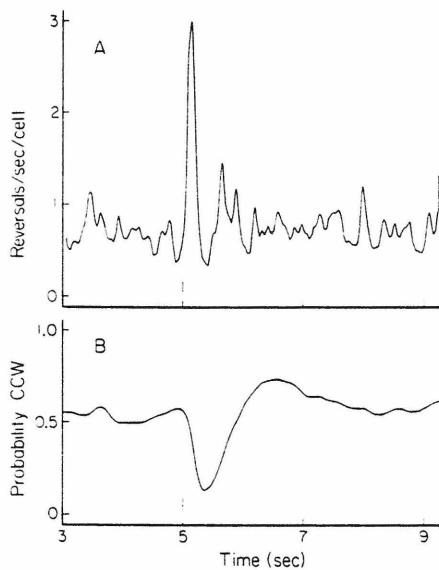


Figure 6. Reversal Rate during the Impulse Response
 (A) The instantaneous reversal rate for cells undergoing an impulse response, plotted as a function of time. Note the expanded time scale. The reversal rate was calculated from the density of points along the time axis in the data summarized in Figure 3B.
 (B) The curve of Figure 3B, shown on the same expanded time scale for comparison. Data were smoothed.

somewhat longer pulses proved effective, with the result shown in Figure 7B. The response latency was highly variable, ranging from 0.2 sec up to 5 sec or more. Typically, a cell changed its direction of rotation from CW to CCW after a relatively long (but variable) latency, spun CCW for a period of less than a second and then exhibited a few brief CCW intervals over the next 5 sec, before returning to its initial (CW) behavior. In some cases, responses continued over a much longer time period. Note (Figure 7B) that the response failed to return to baseline even 15 sec after the pulse. The low peak probability for CCW rotation apparent in the figure arose for the following reasons: some cells responded to every pulse, but with a variable time course, so that peak responses failed to add together in phase; and some cells responded with a probability less than unity—they continued to respond over the course of the experiment, but not to every pulse.

Mutants with *cheB* deletions are missing the methylesterase; they have a large CW bias and very high response thresholds (Parkinson, 1978; Sherris and Parkinson, 1981). Mutants with *cheR* deletions are missing the methyltransferase; they have a large CCW bias and high response thresholds (Goy et al., 1978; Parkinson and Revello, 1978). The responses of these mutants to attractants and repellents are shown in Figures 7C and 7D, respectively. These responses resembled those observed for the wild-type; in each case, the initial peak had a similar time course. The

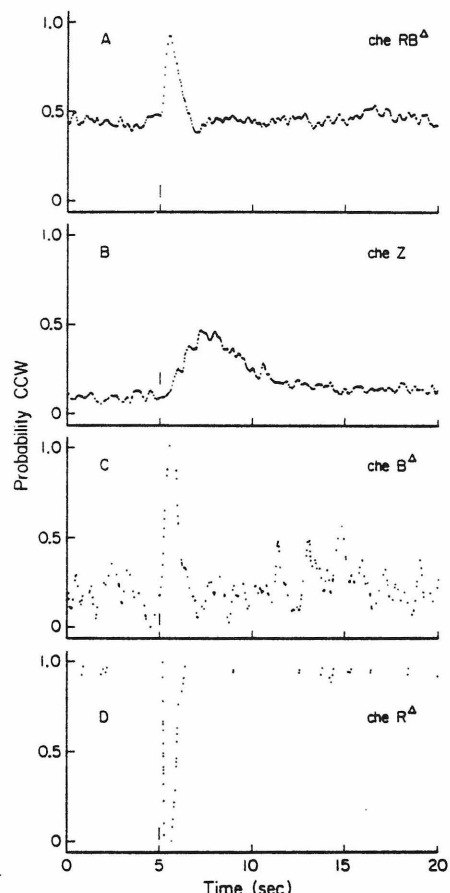


Figure 7. Impulse Responses of the *che* Mutants
 The probability of spinning CCW is shown as a function of time, with stimuli given at 5 sec (vertical lines). The data have been smoothed, as described in the Experimental Procedures.
 (A) Attractant response of cells carrying *cheR*-*cheB* double deletions. Pipettes contained 10 mM L-aspartate. Pulses were generated with currents ranging from -20 to -100 nA switched on for periods of 9–225 msec. The graph was constructed from 167 records containing 4260 events obtained with 11 different cells; 335 points are displayed.
 (B) Attractant response of the *cheZ* point and amber mutants. Pipettes contained 1 mM L-aspartate. Pulses were generated with currents of -10 to -100 nA switched on just long enough to give a response (0.2–1.8 sec). The graph was constructed from 132 records containing 2034 events obtained with five different cells; 339 points are displayed.
 (C) Attractant response of a cell carrying a *cheB* deletion. Pipettes contained 100 mM L-aspartate. Pulses were generated with a current of -100 nA switched on for 200–300 msec. The graph was constructed from 14 records containing 248 events obtained with a single cell. The mutant was CW-biased; noise in the baseline arose from occasional spontaneous reversals.
 (D) Repellent response of a cell carrying a *cheR* deletion. Pipettes contained 100 mM nickel chloride. Pulses were generated with currents of +2 nA switched on for 20 msec. The graph was constructed from 19 records containing 63 events obtained with a single cell. The mutant was CCW-biased; points on the baseline represent rare spontaneous reversals.

greater amplitude of this peak and the lack of undershoot (or overshoot) in the mutant cells may simply reflect the altered range available for changes in directional bias. A run-biased *cheR* point mutant (*cheR202*) gave a similar response to the *cheR* deletion mutant (data not shown). Mutants in *cheB* proved extremely hard to excite: only a small fraction of the cells responded reproducibly to stimulation by L-aspartate, even with relatively high concentrations in the pipette.

The records for the *cheR-cheB* and *cheZ* mutants were separated into two groups: those corresponding to cells that were stimulated while spinning CW, and those that were stimulated while spinning CCW. Although the probability functions differed from mutant to mutant (data not shown), it was clear in these mutants, as well as in the wild-type (Figure 5), that the mechanism determining the response to an impulse overrides the mechanism that generates spontaneous reversals.

Discussion

A conceptual distinction has been drawn in bacterial chemotaxis between excitation and adaptation (Goy et al., 1978; Springer et al., 1979). While the addition of an attractant or repellent causes an almost immediate response (excitation), that response gradually disappears with time, even if the attractant or repellent is still present (adaptation). In most cases, adaptation is complete: the behavior of the cell does not depend on the ambient concentration after a sufficiently long period of time (Macnab and Koshland, 1972; Tsang et al., 1973). There are some exceptions: for example, when cells in motility medium are exposed to serine (Berg and Brown, 1972), or when enough weak acid is added to cells in an acidic medium to perturb seriously the cytoplasmic pH (Kihara and Macnab, 1981). For the relatively large stimuli used in previous work, the time required for a cell to respond (the response latency) is about 0.2 sec (Segall et al., 1982). However, the time required for a cell to adapt (the adaptation time) ranges from several seconds to several minutes, depending on the magnitude of the change in receptor occupancy (Spudich and Koshland, 1975; Berg and Tedesco, 1975). These characteristic times are so different as to suggest that the pathways for excitation and adaptation are distinct. This notion is supported by the observation that cells carrying mutations in the *cheR* gene have normal response latencies (Segall et al., 1982) but fail to adapt (Goy et al., 1978; Parkinson and Revello, 1978). Alternatively, the disparity in characteristic times for excitation and adaptation might be an artifact of the step-stimulus paradigm, in which a large change in concentration rapidly drives the system into saturation. Measurements of the impulse response have allowed us to characterize the behavior of cells

in the small-signal domain. Our results suggest that the bacterial sensory system is matched to the task that it is required to perform. Both excitation- and adaptation-related phenomena occur on a time scale of seconds. The initial events in signal processing are similar in wild-type cells and in cells unable to methylate or demethylate, or both; however, they are markedly different in cells carrying *cheZ* mutations.

Characteristics of the Wild-Type Response

The impulse response shown in Figure 3A has a substantial width; it persists for about 4 sec. This means that a cell integrates stimuli that have occurred over the past few seconds in determining its present bias: variations in concentration that occur on a time scale much shorter than this average out. This is characteristic of a low-pass filter, a device that passes low frequencies in preference to high frequencies. The impulse response also is biphasic; one lobe is above the baseline and the other is below it. This means that the cell is sensitive to changes in concentration that have occurred over the past few seconds: variations in concentration that occur on a time scale much longer than this also average out. This is characteristic of a differentiator, or high-pass filter, a device that is sensitive to changes in input—that is, that passes high frequencies in preference to low frequencies. If the areas of the two lobes are equal, the output returns to its initial value after a stepwise change in input, as illustrated in Figure 4; the device is fully adaptive. In summary, the impulse response has bandpass properties; the cell is maximally sensitive to frequencies at which the low-pass and high-pass contributions overlap.

We could carry this analysis further by exposing the cell to sinusoidal stimuli and measuring the amplitude of the resultant swings in rotational bias as a function of frequency. But this is not necessary, because an equivalent result is obtained by decomposing the impulse response into its spectral components by means of the Fourier transform (Papoulis, 1977). A Bode (log-log) plot of this spectrum, shown in Figure 8, shows the bandpass properties. The system has a maximum pass frequency at 0.25 Hz, corresponding to a time span of 4 sec. A decomposition of the system into constituent filters is done by matching the slopes on either side of the pass frequency. Positive slopes indicate high-pass characteristics, and negative slopes indicate low-pass characteristics. The steepness of the slope determines the sharpness of the frequency cutoff: an asymptotic slope of $20n$ dB/decade indicates an n th order filter. The wild-type sensory system behaves roughly as a first order high-pass filter in cascade with a third order low-pass filter.

The 4 sec bandpass time implies that the system is maximally sensitive to changes occurring with this periodicity. This bandpass covers the range of frequencies that a cell generates by its motion when

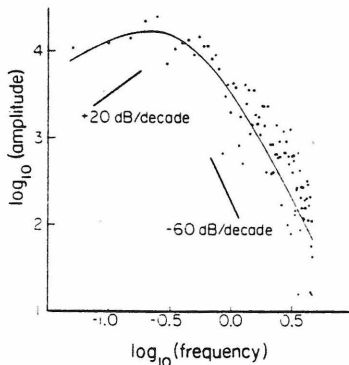


Figure 8. Fourier Transform of the Wild-Type Response

A Bode plot— \log_{10} (amplitude) versus \log_{10} (frequency)—of the absolute magnitude of the complex Fourier transform of the impulse response shown in Figure 3A. The transform peaks at approximately 0.25 Hz, corresponding to a bandpass centered at 4.0 sec. Slopes of +20 dB and -60 dB are shown for reference. The response system, if linear, is approximated by a first order high-pass filter in cascade with a third order low-pass filter. The response array of 1024 points was digitally filtered prior to transformation to reduce high-frequency contamination. Low-frequency trends were eliminated by subtracting out the baseline determined by a least-squares fit to the data obtained before and well after the response. The solid line is the transform of a nonlinear least-squares fit to the impulse response of a sum of four exponentials.

swimming in a spatial gradient. As we noted earlier, a swimming cell executes a random walk with steps (runs) averaging approximately 1 sec. The concentration rises and falls as the cell moves up and down the gradient; frequencies on the order of 0.25 Hz are prominent.

As noted above, the distributed nature of the impulse response indicates that cells make use of information over a time span extending at least 4 sec into the past. The Fourier analysis shows that they weight spectral components of stimuli with periods around 4 sec most heavily. Thus, while it can be said that a cell has "memory," it does not have a memory characterized by a single decay time. A time span of 2 sec is roughly equal to the persistence time of a cell swimming in a spatial gradient—that is, the mean time during which there is a component of cell motion up the gradient (Macnab and Koshland, 1973; Lovely and Dahlquist, 1975). This is another way of saying that the sensory system is optimized to sense those changes in concentration encountered when the cell swims in a gradient.

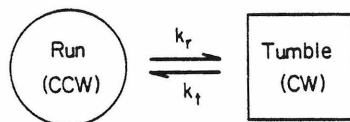
The question of memory time in bacterial chemotaxis has been addressed before. The long relaxation times for adaptation to steps in concentration imply a kind of "memory" in the limited sense that prior to adaptation, the cell continues to respond to a change made in the past (Macnab and Koshland, 1972). Adaptation times, however, are a function of the stimulus size (Spudich and Koshland, 1975; Berg and

Tedesco, 1975) and do not point to a particular characteristic memory time, t_m . Memory is not "useful" if it extends so far into the past that the information retained is not relevant to the current trajectory of the cell (Macnab and Koshland, 1973). Computer simulations of cells swimming in a spatial gradient show that a long memory is clearly detrimental (Brown and Berg, 1974). For cells with a memory that decayed exponentially with a time constant t_m , the rate of drift up the gradient fell off exponentially with a time constant of the order of $2t_r$, where t_r is the mean run interval. For values of $t_m > 5t_r$, chemotaxis was essentially abolished.

Why should the mean run interval be about 1 sec? On the one hand, runs must be long enough to allow the cell to sense changes in concentration in the presence of random fluctuations (noise); the precision with which such changes can be sensed improves with the square root of the measurement time (Berg and Purcell, 1977). On the other hand, the runs must not be so long that the curvature induced by rotational Brownian movement causes the cell to deviate significantly from its path before the measurement is complete. For a cell the size of *E. coli*, this is a serious problem for times on the order of 10 sec (Brown and Berg, 1974). The mean run interval must be shorter than this, so that when favorable runs are extended, they still fall within this limit. Hence the optimum run interval is determined by these physical constraints.

Modulation of a Two-State System

Very little is known about the machinery that generates the impulse response, but it is known that the baseline behavior of the cell involves random switching between two rotational modes. The underlying events that terminate CCW and CW intervals have constant probabilities in time. The simplest model that has this property is a two-state system, in which the states dictate either CCW rotation (runs) or CW rotation (tumbles). These states might represent alternate configurations of a protein that determine the direction of rotation, the binding and unbinding of a ligand on such a protein, or the like. Transitions between the two states are governed by first order rate constants k_r and k_t , which are the probabilities per unit time of terminating a run or a tumble, respectively.



In this system CCW intervals are distributed as $\exp(-k_r t)$ and CW intervals are distributed as $\exp(-k_t t)$. If k_r is greater than k_t , the motor spends most of its time in the tumble mode; if k_t is greater than k_r , the run mode predominates. In general, if both k_r and k_t are large, the reversal rate is high; if both k_r

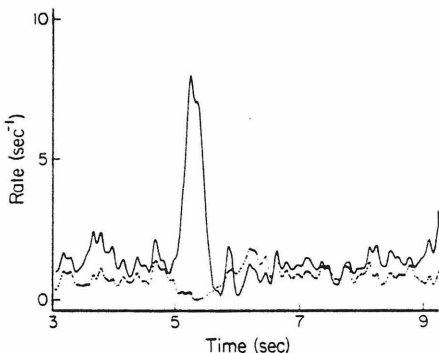


Figure 9. Rate Constants for the Two-State Model

The rate constants k_r (solid line) and k_t (dotted line) computed for the impulse response of Figure 3A and shown as a function of time. Note that k_r and k_t are anticorrelated during the positive phase of the impulse response, which lasts about 1 sec, as well as during the subsequent undershoot. The relatively high noise level reflects the large statistical variance in the reversal rate. This graph was prepared from the impulse response, its time derivative and the instantaneous reversal rate, as described in the text; see equations (3) and (4).

and k_t are small, the reversal rate is low. We suppose that the sensory system modulates k_r and k_t . The changes that occur during the impulse response can be derived from measurements of the probability of spinning CCW and the reversal rate, as outlined in Experimental Procedures. The results are shown in Figure 9. During the initial phase of the response, k_r rises and k_t drops. During the undershoot, k_r exceeds k_t , and tumbles are transiently favored. The response to a repellent gives essentially the same result, but with the roles of k_r and k_t interchanged (data not shown). If the cell actually works in this way, k_r and k_t must be controlled jointly by the sensory system, and they must be modulated in an antagonistic manner. If this modulation is to override the steady state reversal behavior, as implied by the results in Figure 5, the mechanism that controls the rate constants must act quite rapidly. Cells with different unstimulated biases (and different mean CCW and CW rotation intervals) give impulse responses with virtually identical time courses (data not shown). This suggests that the mechanism that controls the rate constants is quite similar from cell to cell, but distinct from the mechanism that sets the prestimulus values of these constants. The latter mechanism has a large biological variability (Berg and Tedesco, 1975; Spudich and Koshland, 1976).

Characteristics of Mutant Responses

It should be possible through the analysis of generally nonchemotactic mutants to work out the functions and interrelationships of different components of the signal-transduction pathway (see Parkinson, 1981; Boyd and Simon, 1982). One needs a combined assault with the use of genetics, biochemistry and physiology.

Although a great deal has been learned with slower methods, our results show that important physiological events occur on a relatively short time scale: a time scale not accessible to those methods. Defects in some mutants are so severe that the cells fail to respond to any stimuli; these strains are not amenable to the analysis undertaken here. Fortunately, other *che* mutants do respond, to varying degrees, and we have begun by examining some of these.

The impulse response of cells with a *cheR-cheB*-double deletion shown in Figure 7A is similar to that of wild-type cells (Figure 3A). It begins at roughly the same baseline, has essentially the same rise time and follows a similar time course for the first second or so, but it does not have as large an undershoot. As noted in the Results, this feature varied from cell to cell. The lack of a pronounced undershoot, on the average, for the mutant implies that it lacks some of the high-pass (adaptive) properties of the wild-type strain. This was confirmed through measurements of responses to small-step stimuli that unlike those for wild-type cells shown in Figure 4, failed to return to the baseline (in 10 sec, the longest period studied). These responses agreed with those predicted by convolution of a step stimulus with the mutant impulse response (data not shown).

The diminution in the undershoot is correlated with the absence of the enzymes that methylate and demethylate the MCPs. Therefore, it is likely that this aspect of the impulse response is caused by increased levels of methylation that accompany an increase in the concentration of attractant. This suggests that a transient burst of methylation initiated by the impulse feeds back in such a way as to depress the CCW bias.

We would expect these mutants to possess some chemotactic ability. As the cells move up a gradient, however, their CCW bias will become so great that the run intervals will soon exceed the limits of usefulness imposed by rotational Brownian movement (see above). In this limit, the cells will no longer be chemotactic. It is possible, at least in theory, to perform chemotaxis in the complete absence of adaptation. Runs up the gradient of an attractant will still be longer, and runs down will be shorter. In this case, however, chemotaxis will only be effective over a limited range in concentration, a range over which the rotational bias of the cell remains unsaturated and run lengths do not exceed the Brownian limit. Cells carrying *cheR-cheB* double deletions do, in fact, form chemotactic rings on soft agar containing tryptone (data not shown). These rings, although much smaller than those produced by wild-type cells, are substantially larger than swarms formed by completely non-chemotactic strains, such as *cheY* or *cheZ*. The possibility remains that the cells carrying *cheR-cheB* deletions are in fact adaptive, but only over a time span much longer than that probed by our measurements. (For examples of adaptation to other attrac-

tants not involving methylation, see Niwano and Taylor, 1982.)

Cells carrying mutations in either the *cheB* or *cheR* genes also have impulse responses that resemble that of the wild-type, at least for the first second or so (Figures 7C and 7D). The shape and duration of the first lobes are much the same, but any undershoot or overshoot is obscured by the baseline biases, which are almost exclusively CW or CCW, respectively. We conclude that the mechanisms responsible for generating the first lobe of the impulse response do not involve methylation or demethylation.

The *cheZ* mutants appear to be defective in excitation and to have a very long "memory time." The response shows a long rise time and a very slow recovery (Figure 7B). An undershoot, if it exists, did not develop on the time scale of our measurements. Short impulses of the kind used to stimulate wild-type cells had essentially no effect. Longer pulses (still short on the time scale of the response) set in motion a characteristic sequence of brief CCW bursts; some of these sequences lasted for many seconds. The response did not return to baseline, even 15 sec after the onset of a pulse. As noted earlier, a cell that averages temporal information with such a long time base cannot be chemotactic, because the older information is not relevant to the current trajectory. There exist *cheZ-cheC* double mutants that fail to move up gradients, even though their tumbling rates are normal (Parkinson and Parker, 1979). They are likely to be nonchemotactic both because of a slow response and because of an excessive memory time.

Preliminary measurements of responses of *cheZ* mutants to step stimuli did not agree with those predicted by convolution with the impulse response. The discrepancy might be due to long-range behavior occurring outside the time domain that we investigated, to a nonlinearity in the *cheZ* response or to the fact that the limited amount of step-stimulus data available was not representative of the population of *cheZ* cells as a whole. Further work on these mutants is in progress.

Epilogue

In a recent review, Boyd and Simon (1982) discussed the implications of evolution for chemotaxis. They suggested that chemotaxis initially arose as a response to a transient change in the cellular state (such as perturbation of pH or protonmotive force). Cellular mechanisms of homeostasis restored that state, thus providing a primitive form of adaptation within a limited range. Other mechanisms of adaptation, involving methylation, developed later, allowing adaptation to occur over a wider dynamic range. The components of this system then became sensitive to specific sensory inputs. Our data on responses to aspartate are consistent with this view. Even without methylation or demethylation, *E. coli* has the ability to integrate in-

formation over lengths of time comparable with the duration of a run and has a limited capacity to adapt. The imperfections inherent in this process might have been compensated for by the development of a system that restores the rotational bias of the motor, so that a cell that has drifted up a gradient remains able to respond. Reversible carboxymethylation of the MCPs might provide a basis for such a system, with the primary function of range adjustment. In any event, it is clear from our results that *E. coli* contains sophisticated machinery for chemotaxis. This machinery processes sensory information over a time span of a few seconds, making maximal use of the information available. The iontophoretic technique provides a means of defining the physiological properties of mutants with defects in this machinery, and thus of learning more about how signal transduction works.

Experimental Procedures

Chemicals

α -Methyl-D,L-aspartate and D,L-leucine were obtained from Sigma; other L-amino acids (A grade) were obtained from Calbiochem; nickel chloride was obtained from Fisher; benzoic and lactic acids (reagent grade) were obtained from Mallinckrodt; and thorium chloride was obtained from ICN-K&K Pharmaceuticals. Tetraethylpentamine (tetroen; technical grade) was obtained from Aldrich and purified according to the method of Reiley and Vavoulis (1959).

Bacterial Strains

The wild-type strain was AW405, an *E. coli* K12 derivative auxotrophic for threonine, leucine and histidine, obtained from J. Adler (Armstrong et al., 1967). Mutant strains were: *cheR* deletion, RP4968; *cheB* deletion, RP4972; *cheR-cheB* double deletions, RP1273 (Sherris and Parkinson, 1981), RP4969, RP4970; *cheZ* point mutants, RP5007 (*cheZ293*) and RP5008 (*cheZ278*) (Parkinson, 1978). All *che* mutants were provided by J. S. Parkinson.

Preparation of Tethered Cells

Cells were grown to saturation in a minimal growth medium containing glycerol and essential amino acids (Hazelbauer et al., 1969), diluted 1:100 and grown again in the same medium, and harvested at mid-exponential phase. The cells were grown at 35°C in a rotary incubator; collected by centrifugation; washed once or twice in a motility medium containing 90 mM NaCl, 10 mM KCl, 10 mM Tris-Cl (pH 7.0 at 32°C), 10 mM sodium lactate, 0.1 mM tetroen and 0.001 mM methionine; and resuspended in this medium at one-fifth the original volume. The cells were sheared by passage of this suspension 60 times between two syringes equipped with 26-gauge needles connected with an 8 cm length of polyethylene tubing (0.58 mm internal diameter). The cells were washed twice more, and tethered to a coverslip as described by Berg and Tedesco (1975).

Data Acquisition

The coverslip to which the cells were tethered was sealed to the bottom of a stainless-steel chamber mounted on the stage of a phase-contrast microscope. The cells were viewed through a 40X water-immersion objective (Zeiss). Both the stage and the objective were heated to 32.0°C. The objective was thermally and electrically isolated from the microscope body. The preparation was slowly perfused with motility medium during the entire experiment. Iontophoretic pipettes filled with motility medium containing 0.01 mM thorium chloride and either attractants or repellents were prepared as described by Segall et al. (1982). Pipette resistances were 15–50 megohms. A current-injection circuit (Dreyer and Peper, 1974) was used to pass current (1–200 nA) through the pipettes via Ag/AgCl wires. Control experiments, in which no attractant or repellent was added to the

medium in the pipettes, yielded no response (Segall et al., 1982). The microscope was equipped with an optoelectronic device that extracts the x and y coordinates of the centroid of the image of a spinning cell, $x = \sin(\omega t)$ and $y = \sin(\omega t \pm \phi)$, where ω is the angular velocity of the cell and ϕ is a 90° phase shift, the sign of which indicates the handedness of the rotation (apparatus of Kobayashi et al., 1977, as modified by Berg et al., 1982). Cells that were monitored with this device met several criteria: they were tethered around a point near one end; they rotated with a regular, circular motion; their center of rotation did not change appreciably when they underwent reversals; and their angular velocity was between 5 and 12 Hz. Cells were stimulated about once a minute. Records of the x and y coordinates were made on a strip-chart recorder (Gould Brush 220; run at 25 mm/sec), together with event markers indicating the sign of ϕ and the timing of the stimulus current, as illustrated in Figure 1 of Segall et al. (1982). The positions of the phase discontinuities, evident in the x and/or y signals, were digitized with a strip-chart digitizer built for the purpose. The data, a list of numbers representing the times of CW-to-CCW or CCW-to-CW transitions, measured relative to the onset of the stimulus, were stored as records in a PDP 11/34 computer for subsequent analysis. These numbers were accurate to within about 55 msec, with errors arising from delays due to the electronics, from uncertainties in the positions of the phase discontinuities on the strip-chart records or from random slippage of the paper in the digitizing apparatus.

Data Analysis

Over 1700 records, containing more than 35,000 events, were digitized in all. An array of computer programs was developed to collate, analyze and display data reduced from these records. Each record contained a list of numbers corresponding to the times at which reversals in the direction of rotation occurred. A chronological list of all such numbers in a set of n records was compiled by concatenating the records and sorting the numbers with the Shell-Metzner algorithm (see, for example, Wirth, 1976). A function was constructed whose initial value was taken to be equal to the total number of records in which the cell was spinning CCW at time zero. The value of the function for subsequent times was computed by changing the previous value by unity at every reversal: +1 for a CW-to-CCW transition, -1 for a CCW-to-CW transition. An estimate of the probability of spinning CCW was obtained by dividing all the values in this function by n (Figure 1). Prior to display, this probability function was passed to a cubic spline-fit smoothing routine (Reinsch, 1967, 1971), which fits an array of cubic segments to the data. The endpoints of each segment are constrained to pass close to (but not necessarily through) the data, in such a way that the spline-fit curve fits the data in a least-squares sense. A smoothing parameter, specifying a χ^2 measure of the fit, governs the degree of smoothing. The routine was used to smooth data and to perform interpolation (see below).

The (uneven) density of points along the time axis in the probability function provided a measure of the total number of reversals occurring in the group of records at any instant. The average number of reversals per second per cell is this density divided by n . The density was computed by counting the total number of events up to a given time, and treating that number as a function of time. The time derivative (slope) of this curve gives the density of reversals. The derivative was computed by fitting the function with cubic splines, the coefficient of the linear term for each cubic giving the derivative. Smoothing was used to eliminate discontinuities in the density function.

The two-state model described in the text can be solved to give the fraction of time that a cell runs, f_r , and the reversal rate, ρ . When the system is at equilibrium, one obtains $f_r = k_r/(k_r + k_b)$ and $\rho = 2k_rk_b/(k_r + k_b)$. Even when the system is out of equilibrium, these quantities can be derived from a knowledge of f_r , its time derivative, df_r/dt , and ρ . Since

$$df_r/dt = -k_r f_r + k_b(1 - f_r) \quad (1)$$

and

$$\rho = k_r f_r + k_b(1 - f_r), \quad (2)$$

it follows that

$$k_r = \frac{\rho - df_r/dt}{2f_r} \quad (3)$$

and

$$k_b = \frac{\rho + df_r/dt}{2(1 - f_r)}. \quad (4)$$

The rate constants in Figure 9 were calculated according to equations (3) and (4) with the use of the impulse response, its time derivative and the reversal rate. The impulse response and reversal rate were determined as previously described. The time derivative of the impulse response was obtained from the cubic spline-fit to the rotational data by a method similar to that described for the reversal rate. Both the reversal rate and the impulse response data were smoothed prior to the computation; no smoothing was performed on the result.

The Fourier transform of the impulse response was performed on an array of 1024 points with a Fast Fourier Transform Module (Digital Equipment Corporation). The magnitude of the transform was computed from the real and complex parts. The input array of equally spaced points was obtained by interpolation of 400 unevenly spaced points from Figure 3A with the cubic spline-fit smoothing routine. Some smoothing was done to eliminate excessive noise at high frequencies. Low-frequency trends were eliminated by choosing a baseline and subtracting out the best-fit straight line prior to transformation. Aliasing was reduced by choosing the length of the transformed record (20 sec) to be close to an integral multiple of the impulse response period (approximately 4 sec).

The predicted response to a small step was computed by a routine that performs the convolution integral of an experimentally determined impulse response with a step function of adjustable amplitude. The impulse response was interpolated and smoothed as described above, and the integration was carried out numerically by Romberg extrapolation (Acton, 1970).

Acknowledgments

S. M. B. and J. E. S. contributed equally to the work. We are grateful to Robert Smyth for discussion and for providing computer routines. We also thank Markus Meister for theoretical contributions to the two-state model, and Paul Meyer for discussion of small-step stimuli. This work was supported by a grant from the National Institute of Allergy and Infectious Diseases. J. E. S. acknowledges support as an NSF predoctoral fellow.

The costs of publication of this article were defrayed in part by the payment of page charges. This article must therefore be hereby marked "advertisement" in accordance with 18 U.S.C. Section 1734 solely to indicate this fact.

Received July 13, 1982

References

- Acton, F. S. (1970). Numerical Methods That Work. (New York: Harper & Row), pp. 100–129.
- Armstrong, J. B., Adler, J. and Dahl, M. M. (1967). Nonchemotactic mutants of *Escherichia coli*. *J. Bacteriol.* 93, 390–398.
- Berg, H. C. and Brown, D. A. (1972). Chemotaxis in *Escherichia coli* analysed by three-dimensional tracking. *Nature* 239, 500–504.
- Berg, H. C. and Purcell, E. M. (1977). Physics of chemoreception. *Biophys. J.* 20, 193–219.
- Berg, H. C. and Tedesco, P. M. (1975). Transient response to chemotactic stimuli in *Escherichia coli*. *Proc. Nat. Acad. Sci. USA* 72, 3235–3239.
- Berg, H. C., Manson, M. D. and Conley, M. P. (1982). Dynamics and energetics of flagellar rotation in bacteria. *Symp. Soc. Exp. Biol.* 35, 1–31.
- Boyd, A. and Simon, M. (1980). Multiple electrophoretic forms of methyl-accepting chemotaxis proteins generated by stimulus-elicited methylation in *Escherichia coli*. *J. Bacteriol.* 143, 809–815.

- Boyd, A. and Simon, M. (1982). Bacterial chemotaxis. *Ann. Rev. Physiol.* **44**, 501–517.
- Brown, D. A. and Berg, H. C. (1974). Temporal stimulation of chemotaxis in *Escherichia coli*. *Proc. Nat. Acad. Sci. USA* **71**, 1388–1392.
- Chesky, D. and Dahlquist, F. W. (1980). Structural studies of methyl-accepting chemotaxis proteins of *Escherichia coli*: evidence for multiple methylation sites. *Proc. Nat. Acad. Sci. USA* **77**, 2434–2438.
- DeFranco, A. L. and Koshland, D. E., Jr. (1980). Multiple methylation in processing of sensory signals during bacterial chemotaxis. *Proc. Nat. Acad. Sci. USA* **77**, 2429–2433.
- Dreyer, F. and Peper, K. (1974). Iontophoretic application of acetyl-choline: advantages of high resistance micropipettes in connection with an electronic current pump. *Pflügers Arch. ges. Physiol.* **348**, 263–272.
- Engström, P. and Hazelbauer, G. L. (1980). Multiple methylation of methyl-accepting chemotaxis proteins during adaptation of *E. coli* to chemical stimuli. *Cell* **20**, 165–171.
- Goy, M. F., Springer, M. S. and Adler, J. (1977). Sensory transduction in *Escherichia coli*: role of a protein methylation reaction in sensory adaptation. *Proc. Nat. Acad. Sci. USA* **74**, 4964–4968.
- Goy, M. F., Springer, M. S. and Adler, J. (1978). Failure of sensory adaptation in bacterial mutants that are defective in a protein methylation reaction. *Cell* **15**, 1231–1240.
- Hazelbauer, G. L., Mesibov, R. E. and Adler, J. (1969). *Escherichia coli* mutants defective in chemotaxis toward specific chemicals. *Proc. Nat. Acad. Sci. USA* **64**, 1300–1307.
- Kihara, M. and Macnab, R. M. (1981). Cytoplasmic pH taxis and weak-acid repellent taxis of bacteria. *J. Bacteriol.* **145**, 1209–1221.
- Kobayashi, S., Maeda, K. and Imae, Y. (1977). Apparatus for detecting rate and direction of rotation of tethered bacterial cells. *Rev. Sci. Instr.* **48**, 407–410.
- Kondoh, H., Ball, C. B. and Adler, J. (1979). Identification of a methyl-accepting chemotaxis protein for the ribose and galactose chemoreceptors of *Escherichia coli*. *Proc. Nat. Acad. Sci. USA* **76**, 260–264.
- Kort, E. N., Goy, M. F., Larsen, S. H. and Adler, J. (1975). Methylation of a membrane protein involved in bacterial chemotaxis. *Proc. Nat. Acad. Sci. USA* **72**, 3939–3943.
- Koshland, D. E., Jr. (1981). Biochemistry of sensing and adaptation in a simple bacterial system. *Ann. Rev. Biochem.* **50**, 765–782.
- Larsen, S. H., Reader, R. W., Kort, E. N., Tso, W.-W. and Adler, J. (1974). Change in direction of flagellar rotation is the basis of the chemotactic response in *Escherichia coli*. *Nature* **249**, 74–77.
- Lovely, P. S. and Dahlquist, F. W. (1975). Statistical measures of bacterial motility and chemotaxis. *J. Theor. Biol.* **50**, 477–496.
- Macnab, R. M. (1978). Bacterial motility and chemotaxis: the molecular biology of a behavioral system. *CRC Crit. Rev. Biochem.* **5**, 291–341.
- Macnab, R. M. and Koshland, D. E., Jr. (1972). The gradient-sensing mechanism in bacterial chemotaxis. *Proc. Nat. Acad. Sci. USA* **69**, 2509–2512.
- Macnab, R. and Koshland, D. E., Jr. (1973). Persistence as a concept in the motility of chemotactic bacteria. *J. Mechanochem. Cell. Motil.* **2**, 141–148.
- Marmarelis, P. Z. and Marmarelis, V. Z. (1978). *Analysis of Physiological Systems*. (New York: Plenum), pp. 11–130.
- Niwano, M. and Taylor, B. L. (1982). Novel sensory adaptation mechanism in bacterial chemotaxis to oxygen and phosphotransferase substrates. *Proc. Nat. Acad. Sci. USA* **79**, 11–15.
- Papoulis, A. (1977). *Signal Analysis*. (New York: McGraw-Hill), pp. 3–25, 56–138.
- Parkinson, J. S. (1978). Complementation analysis and deletion mapping of *Escherichia coli* mutants defective in chemotaxis. *J. Bacteriol.* **135**, 45–53.
- Parkinson, J. S. (1981). Genetics of bacterial chemotaxis. *Symp. Soc. Gen. Microbiol.* **31**, 265–290.
- Parkinson, J. S. and Parker, S. R. (1979). Interaction of the *cheC* and *cheZ* gene products is required for chemotactic behavior in *Escherichia coli*. *Proc. Nat. Acad. Sci. USA* **76**, 2390–2394.
- Parkinson, J. S. and Revello, P. T. (1978). Sensory adaptation mutants of *E. coli*. *Cell* **15**, 1221–1230.
- Reiley, C. N. and Vavoulis, A. (1959). Tetraethylenepentamine, a selective titrant for metal ions. *Anal. Chem.* **31**, 243–248.
- Reinsch, C. H. (1967). Smoothing by spline functions. *Numerische Mathematik* **10**, 177–183.
- Reinsch, C. H. (1971). Smoothing by spine functions II. *Numerische Mathematik* **16**, 451–454.
- Segall, J. E., Manson, M. D. and Berg, H. C. (1982). Signal processing times in bacterial chemotaxis. *Nature* **296**, 855–857.
- Sherris, D. and Parkinson, J. S. (1981). Posttranslational processing of methyl-accepting chemotaxis proteins in *Escherichia coli*. *Proc. Nat. Acad. Sci. USA* **78**, 6051–6055.
- Silverman, M. and Simon, M. (1974). Flagellar rotation and the mechanism of bacterial motility. *Nature* **249**, 73–74.
- Silverman, M. and Simon, M. (1977). Chemotaxis in *Escherichia coli*: methylation of *che* gene products. *Proc. Nat. Acad. Sci. USA* **74**, 3317–3321.
- Springer, M. S., Goy, M. F. and Adler, J. (1977). Sensory transduction in *Escherichia coli*: two complementary pathways of information processing that involve methylated proteins. *Proc. Nat. Acad. Sci. USA* **74**, 3312–3316.
- Springer, M. S., Goy, M. F. and Adler, J. (1979). Protein methylation in behavioral control mechanisms and in signal transduction. *Nature* **280**, 279–284.
- Springer, W. R. and Koshland, D. E., Jr. (1977). Identification of a protein methyltransferase as the *cheR* gene product in the bacterial sensing system. *Proc. Nat. Acad. Sci. USA* **74**, 533–537.
- Spudich, J. L. and Koshland, D. E., Jr. (1975). Quantitation of the sensory response in bacterial chemotaxis. *Proc. Nat. Acad. Sci. USA* **72**, 710–713.
- Spudich, J. L. and Koshland, D. E., Jr. (1976). Non-genetic individuality: chance in the single cell. *Nature* **262**, 467–471.
- Stock, J. B. and Koshland, D. E., Jr. (1978). A protein methylesterase involved in bacterial sensing. *Proc. Nat. Acad. Sci. USA* **75**, 3659–3663.
- Tsang, N., Macnab, R. and Koshland, D. E., Jr. (1973). Common mechanism for repellents and attractants in bacterial chemotaxis. *Science* **181**, 60–63.
- Wirth, N. (1976). *Algorithms + Data Structures = Programs*. (Englewood Cliffs, N. J.: Prentice-Hall), pp. 56–124.

Additional data

The data base for wild-type impulse responses has more than doubled since the publication of the preceding paper, corresponding to an improvement in average signal-to-noise in the response by the square root of two. Approximately six times as many small steps have been performed, reducing uncertainties there by about a factor of 2.5. The attractant impulse response based on the current data base clearly shows that the undershoot is not a random fluctuation in baseline, and that it persists for approximately three seconds following the first lobe of the response. This response is shown in Text-figure 5, together with a fit to the sum of four exponentials.

The asymptotic slopes of the Bode plot in Fig. 8 of Block et al. (1982) imply that the overall sensory system behaves as a first-order (one pole) high pass filter in cascade with a third-order (three pole) low pass filter; a fourth-order bandpass overall. The general transfer function of such a system, $H(s)$, may be written as:

$$H(s) = H(i\omega) = \frac{s \phi(s)}{(c_4 s^4 + c_3 s^3 + c_2 s^2 + c_1 s + c_0)}$$

where the denominator is a fourth-order polynomial in the Laplace transform variable, s , $\phi(s)$ is a phase term of unit magnitude, and the c_i are constants (Marmarelis and Marmarelis, 1978). The polynomial expression may be expanded as a sum of partial fractions of the form $b_i/(s-r_i)$ and $b_i s/(s-r_i)$, where the b_i are constants and the r_i are roots of the polynomial.

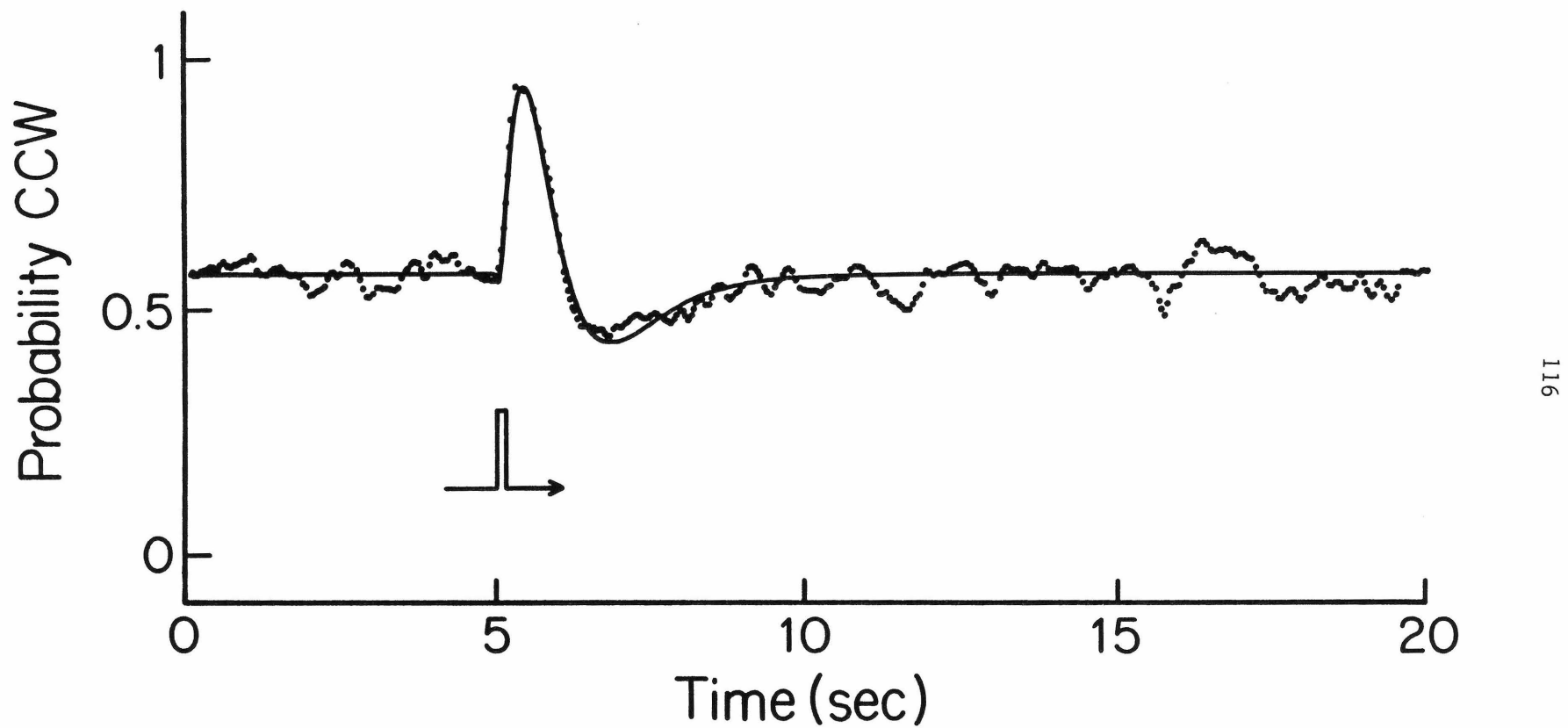
The impulse response is given by the inverse transform of the transfer function. For real roots r_i , the partial fractions $b_i/(s-r_i)$ transform as exponentials, giving a sum of exponentials as a representation (the transform is a linear operator): this was a rationale for attempting to fit such a function to the impulse response in Text-figure 5. The best-fit values for the exponential amplitudes and

Text-figure 5. The wild-type attractant impulse response.

The probability of spinning CCW is shown as a function of time, with stimuli given at 5 sec (shown schematically by the pulse mark). The data were smoothed, as described in Block et al. (1983).

Dotted curve: the response of wild-type cells to impulses of an attractant, either L-aspartate or α -methyl-D,L-aspartate, is shown. Pulses were generated with currents ranging from -1 to -100 nA switched on for periods of 20-100 msec. The graph was constructed from 378 records containing 7,566 events obtained with 17 different cells; 398 points are plotted. These data are a superset of the attractant impulses in Block et al. (1983).

Smooth curve: a weighted nonlinear least-squares fit of a sum of four exponentials to the impulse response. The fit was made to the region from $t = 5$ sec to $t = 20$ sec. Weights were calculated at each point from estimates of the standard deviation in bias expected from an average of 378 records; fluctuations in bias were assumed to be binomially distributed. The fitting function was constructed to have equal areas for the positive and negative response lobes, i.e., it had a time integral of zero; this constraint insures that the function is adaptive. The fit therefore has only seven free parameters out of eight. Best-fit amplitudes (a_i) and time constants (τ_i) for the four exponentials: $a_1, \tau_1 = 40.56, -0.540$ sec; $a_2, \tau_2 = -26.82, -0.261$ sec; $a_3, \tau_3 = -27.63, -0.640$; $a_4, \tau_4 = 13.84, -0.201$ sec.



time constants are given in the figure legend. A high pass (adaptive) characteristic was built into the fit by constraining the positive and negative response lobes to cancel in area; this reduced the number of free parameters in the fit by one.

The small step attractant response

Text-figure 6 reproduces the impulse response data on an expanded time scale (without the fit), together with the predicted and measured responses to small steps in concentration. Coincidence of predicted and measured responses is a test of linearity, since the step response may be considered as an infinite superposition of identical impulses. The integrated impulse response accurately predicts the time course for recovery from a small step. Note that the baseline bias and response amplitude were scaled. Random noise in the small step response makes it difficult to compare the rising edge with the prediction, but the time to peak is roughly the same; the system is acceptably linear.

The exact change in chemoreceptor occupancy induced by impulses is difficult to determine, since the timing and amount of chemical ejected from the pipet during the short current pulse is subject to uncertainty. However, the amplitude scaling factor used to match the integral of the impulse response to the small step response (Fig. 4 of Block et al., 1982, and Text-figure 6) can be used to calculate this value, provided that the corresponding change in receptor occupancy is known for small steps. The occupancy change for small steps, in turn, may be determined by measuring transition times to pipet currents of various magnitudes (Segall et al., 1982). Since transition times are related to the absolute change in receptor occupancy by the apparent dissociation constant of the chemoreceptor (Berg and Tedesco, 1975; Spudich and Koshland, 1975), knowledge of this constant, together with the scaling factor above, is sufficient to predict both the time course and change in bias produced by an arbitrary stimulus from the impulse response by

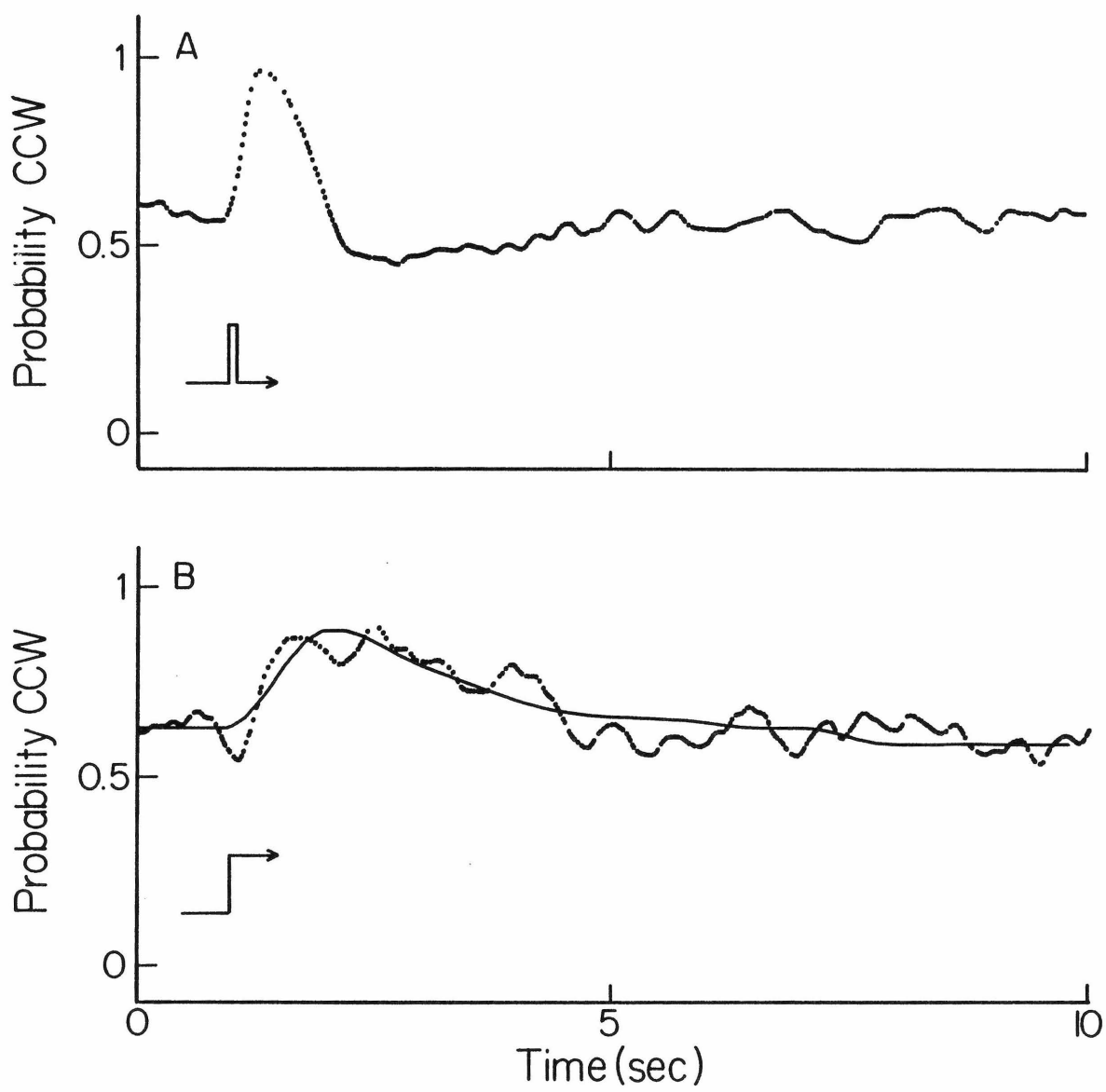
Text-figure 6. Small-step response of wild-type cells.

The probability of spinning CCW is shown as a function of time, with stimuli given at the time shown by the pulse and step marks.

A) The wild type attractant impulse response, as in Text-figure 5, but re-plotted on a time scale of zero to ten seconds. The impulse (shown schematically by the pulse mark) occurs at time $t = 1$ sec on this scale. The graph was constructed from the same data: 3,831 of the 7,566 events lie in this time interval; 383 are plotted. Data have been smoothed.

B) Dotted line: the wild type response to a small step of L-aspartate. Steps were generated by switching the current from 0 to -3nA, where it was maintained for at least 10 sec. The experimental probability function was constructed from 198 records containing 1,992 events obtained with 8 cells; 399 points are displayed. These data are a superset of the small-step responses in Block et al. (1983).

Smooth line: the impulse response shown in (A) was integrated from the beginning of the step onward; this generates the predicted step response. The choices of baseline and amplitude for the predicted curve were arbitrary; they were scaled to match the baseline and amplitude of the experimental data. The amplitude scaling factor, once established, can be used together with the convolution theorem to predict responses to an arbitrary stimulus (e.g., exponential ramps). See text.



convolution. The procedure just described produces a "calibration" of the impulse response in terms of absolute changes in bias.¹⁰

Convolutions of the attractant impulse response with exponential ramps in concentration of the type used in Block et al. (1983) have been performed. Rotational bias was predicted to shift for the duration of such ramps by an amount related to the steepness of the ramp; this corroborates the experimental findings. The relaxation time to the new bias is roughly four seconds. A graph of bias versus ramp rate (of the form shown in Fig. 6 of Block et al., 1983) is a straight line, passing through the unstimulated bias value at zero ramp rate. The slope of this theoretical curve agrees to within 20% with the experimental value reported in the ramp experiments (J. Segall, personal communication); the agreement is consistent within statistical errors. However, the offsets seen in the experimental ramp data are not predicted; this is due to the linear nature of impulse response analysis. The overall correspondence of the two independent approaches is nevertheless encouraging.

The small step repellent response

The effects of nonlinearities are more severe for repellent responses, which have experimental ramp thresholds at least twice as large as the corresponding values for attractants. When repellent impulse responses are integrated and compared with the response to small steps down in the concentration of attractant (equivalent to repellent steps), the agreement is less satisfactory than in the case of attractant steps, especially for times up to one second after the stimulus: the measured response peaks somewhat before the prediction. The approximate time course for return to baseline bias after the step, however, is given correctly by the integrated impulse. The positive and negative lobes of the repellent impulse

¹⁰This calibration scheme was developed by J. Segall, who used it to perform the convolutions described here.

response do not seem to cancel completely as they do for attractants. The relative size of the overshoot in the repellent impulse response seems to be a function of the stimulus size (J. Segall, personal communication) and is currently under study. The large offset seen for experimental ramps down is not predicted by convolution of the impulse response with an exponential change in concentration. These convolutions do, however, predict a slope of bias versus ramp rate with about half of the sensitivity of the measured value. Since the linear convolution cannot show offsets, the decreased sensitivity may result from a linear approximation to the curve in Figure 6B of Block et al. (1983).

Mutant data

CheZ mutants (unlike cheR and cheB) adapt to chemicals in flow cell experiments, albeit with different kinetics than the wild type. When tethered, their unstimulated bias is heavily CW. The impulse response of cheZ (Figure 7 of Block et al., 1982) did not display an undershoot, and consequently integration of the response does not predict adaptation. Several hypotheses for this discrepancy were suggested in the paper, including the possibility that cheZ was somehow nonlinear or that adaptive behavior was reflected in an undershoot occurring at times later than we measured. It was equally possible that the extreme CW bias of cheZ obscured any undershoots (i.e., that no "room at the bottom" existed for changes in bias). Preliminary experiments with cheZ-cheC double mutants suggest that a combination of the latter two possibilities may indeed be the case (J. Segall, personal communication). The unstimulated bias of the double mutant is closer to that of the wild type¹¹ than to cheZ. These mutants have an impulse response with

¹¹For comparison, the CCW mean unstimulated bias found in the experiments of Block et al. (1982) for wild type cells was 0.64. The cheZ mutant used in that study had a mean unstimulated bias of 0.06. The cheZ-cheC double mutant currently under study (Strain RP2734, a gift of S. Parkinson) has a mean unstimulated bias of 0.37.

an initial positive lobe similar to that of cheZ, lasting about 13 seconds. The bias returns to baseline, undershoots, and remains below the unstimulated bias level for as long as 20 seconds. Impulses affect the bias of cheZ mutants for longer than 30 seconds. Further studies using cheZ-cheC double mutants are in progress.

The constraints of chemotaxis

Data collected using the programmed gradients cover the response of tethered E. coli to slowly-varying chemical signals of the sort encountered by swimming cells as they drift up spatial gradients during chemotaxis. In this domain, the response is characterized by a proportional control mechanism in which adaptation takes place with first-order kinetics. This mechanism takes the time derivative of the input (Text-figure 5).

During individual runs in a gradient, however, the apparent concentration fluctuates. The source of the apparent fluctuation is the diffusion of molecules in the neighborhood of chemoreceptors. In order to make a reliable measurement, cells must time-integrate the instantaneous chemoreceptor occupancy over a suitable period.

A sample calculation of integration time is illuminating. The relative error made in a determination of concentration by a spherical cell with chemoreceptors distributed over its surface is given by

$$\Delta C_{\text{rms}}/C = [2 \pi D C N s a \tau_{\text{meas}}^{(1-P)/(Ns + \pi a)}]^{-1/2},$$

where τ_{meas} is the integration time, D is the diffusion constant for the compound sensed, a is the radius of the cell, P is the mean fraction of chemoreceptors bound, and s is the effective radius of each of the N chemoreceptors (Berg and Purcell, 1977). An efficient number of chemoreceptors for a cell to produce occurs for $N = \pi a/s$, the number at which half of the theoretical flux to the cell is detected. In

the Weber-Fechner region $C = K_D$, and the value of $P = C/(C + K_D)$ is close to 1/2.

Placing these numbers in the equation gives:

$$\Delta C_{\text{rms}}/C = [(\pi D C a \tau_{\text{meas}})/2]^{-1/2}$$

For a determination of concentration with 1% uncertainty, assuming $D = 5 \times 10^{-6}$ cm²/sec, $a = 1 \mu\text{m}$, and $C = 10^{-7}$ M, a time of approximately 0.2 sec is needed.

The relative error improves as the inverse square root of the measurement time.

It is in the best interest of cells to integrate for as long as possible, but only up to a certain limit. The upper limit for this integration is set, in theory, by the time required to randomize the motion of a bacterium steering up a gradient. Were a bacterium to proceed without tumbling, this time would be given by the relaxation time for rotational Brownian motion about the run axis of the cell. Relaxation time can be estimated from $\tau_{\text{rot}} = \langle \theta \rangle^2 / 4D_r$, where $\langle \theta \rangle^2$ is the mean square angle and D_r is the rotational diffusion constant of a bacterium. Setting $\langle \theta \rangle^2 = \pi^2/4$ and choosing $D_r \approx 0.05 \text{ sec}^{-1}$, appropriate for a 1.5μ dia. sphere in water at room temperature,¹² one obtains $\tau_{\text{rot}} \approx 13$ seconds. The run length for a bacterium the size of E. coli, therefore, is theoretically bracketed by a minimum integration time (τ_{meas}) of around 0.2 sec and a maximum directional steering (τ_{rot}) time of around 10 sec. In fact, the mean unstimulated run time is about 0.9 seconds. Tumbles randomize the direction of the new run, but the angular distribution function for the new direction is a bit skewed towards smaller angles (Berg and Brown, 1972); this introduces a "persistence", or directional memory (Macnab and Koshland, 1972), so that the effective mean time prior to loss of directional information is somewhat longer than the run time.

¹²The rotational diffusion constant is given by the rotational version of the Einstein-Smoluchowski relation: $D_r = KT/f_r$, where f_r is the rotational drag coefficient, equal to $8\pi\eta a^3$ for a sphere of radius a immersed in a fluid of viscosity η . Choosing $KT = 4.11 \times 10^{-14}$ gm-cm²/sec, $\eta = 0.01$ gm/cm-sec, and $a = 1.5 \times 10^{-4}$ cm gives $D_r = 0.048 \text{ sec}^{-1}$.

It is this effective mean time, τ_{eff} , over which a cell should integrate. An optimal sensory system, therefore, would differentiate stimuli (i.e., adapt) for characteristic times long compared to τ_{eff} , but should integrate stimuli (i.e., signal average) for characteristic times comparable or shorter than τ_{eff} . The rejection of stimuli which vary rapidly compared to τ_{meas} should be strong, since these fluctuations are thermal in origin and extend to high frequencies.

The response spectrum of bacteria

The measured response of bacteria, Text-figure 7, shows that the bacterial sensory system is optimized for the task it performs over roughly four decades of frequency. At the low frequency end, the response has been measured by experiments with slowly-varying concentration that gather data over a long baseline. At the high frequency end, the spectrum has been measured with a technique having a superior time resolution, i.e., by iontophoresis and signal-averaging. The composite plot charts the behavior over a frequency domain covered by the combination of the two approaches.

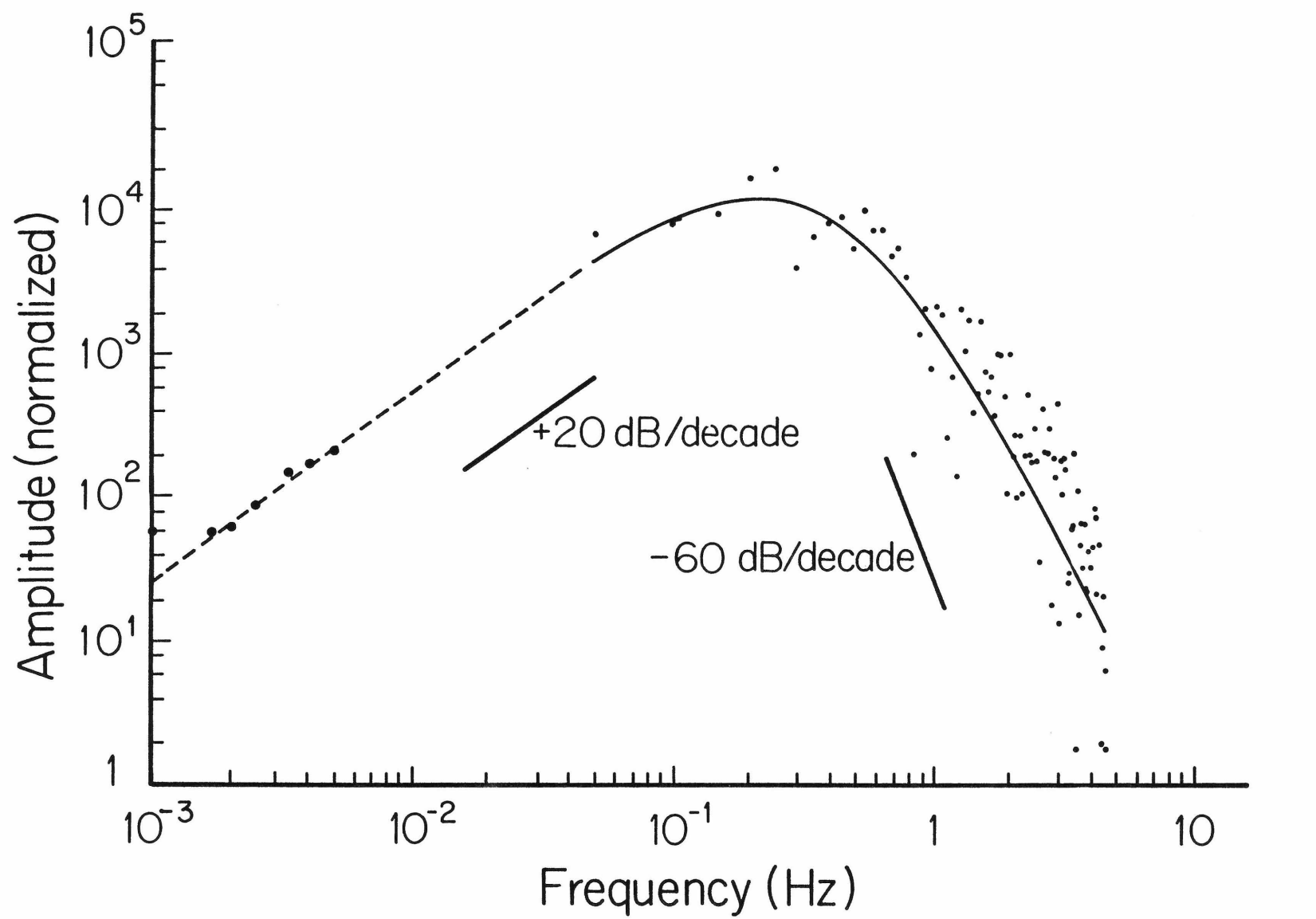
The amplitudes of the sinusoidal ramp data have been scaled to place them on the diagram, since the exact correspondence between impulse response amplitudes and concentration change is unknown. However, using the "calibration" method described previously for small steps, a crude, absolute estimate of the scaling factor can be made. Unfortunately, sinusoidal stimulation is biphasic, and the calibration for stimuli depends on the sign of dP/dt . Assuming that negative values for dP/dt are far less effective than positive values (rectification), a correction can be made to the predicted sine response. Applying this correction to a convolution of a sine wave with the best-fit analytical solution produces a set of points which lie very close to the dashed line in the figure (J. Segall, personal communication); this provides a consistency check on the two sets of measurements.

Text-figure 7. Spectral sensitivity of tethered bacteria.

A composite Bode plot demonstrating the spectral sensitivity of tethered E. coli to chemotactic stimuli over a dynamic range of almost 10^4 . The graph combines data obtained from programmed gradients and from iontophoresis experiments, and shows the bandpass properties of the response. The sensitivity has a first order high-pass (adaptive) filter characteristic for frequencies in the range of 0.001 Hz up to 0.1 Hz. The peak of sensitivity lies at approximately 0.25 Hz, and falls off with roughly a third order low pass (integrative) filter characteristic until about 10 Hz.

The small dots and smooth curve are data reproduced from Block et al. (1982). The dots represent the magnitude of the Fourier transform of the impulse response data as in Fig. 8 of the paper. The smooth curve is the transform of a nonlinear least-squares fit to the impulse response of the sum of four exponentials.

The heavy dots are reproduced from Block et al. (1983) and show the response to exponentiated sine waves in attractant concentration, as in Fig. 8 of that paper. Only data points representing unsaturated responses have been redrawn. The dashed line is an extrapolation of the smooth curve with a first-order high pass characteristic. The amplitude scaling factor for the sine data is, to a large degree, arbitrary (see text). It has been chosen to place the data point at 0.0025 Hz on the dashed line.



Post-script

The reaction mechanisms that underlie the response spectrum of bacteria are unknown. A key role is certainly played by the covalent modification of the MCPs; their methylation is presumably involved in completing the sensory feedback loop. The impulse response undershoot is likely to be a reflection of the methylation process. Asymmetries in the response to positive and negative stimuli suggest that adaptation proceeds along different pathways depending on the sign of the stimulus. The cheZ gene product affects signal timing and excitation, since point and amber mutants show abnormal impulse response patterns. It is possible that the cheZ gene product plays a role in the integration phase of the response. The nature of the signal that is passed to the motor remains a profound mystery. The evidence developed here suggests that this signal works indirectly by affecting the stochastic process of motor reversal. Models in which a noisy signal is compared to a threshold value are not as successful in predicting CW/CCW interval statistics as ones in which the signal modulates the probability of spontaneous motor reversal. The modulation of these probabilities is likely to be complex, since tethered cells can show changes in both mean CW and CCW intervals without concomitant changes in rotational bias. The seconds-long duration of the impulse response is quite slow on the time scale of many enzyme reactions; these rates may have evolved to produce the band-pass characteristics required. The overall chemical response of bacteria is tailor-made to extract the maximum amount of information from the noisy chemical environment in which bacteria swim.

REFERENCES

- Adler, J.** (1969). Chemoreceptors in bacteria. *Science* **166**, 1588-1597.
- Aneshanesley, D. J.** (1980). Digital readouts superposed electronically on televised pictures. *Behav. Res. Meth. Instrum.* **12**, 451-454.
- Bachmann, B. J. and Low, K. B.** (1980). Linkage map of Escherichia coli K-12, edition 6. *Microbiol. Rev.* **44**, 1-56.
- Berg, H. C.** (1971). How to track bacteria. *Rev. Sci. Instr.* **42**, 868-871.
- Berg, H. C.** (1974). Dynamic properties of bacterial flagellar motors. *Nature* **249**, 77-79.
- Berg, H. C.** (1975a). Bacterial behaviour. *Nature* **254**, 389-392.
- Berg, H. C.** (1975b). Bacterial movement. In: *Swimming and Flying in Nature*, Vol. 1 (Plenum Publishing, N. Y.), Wu, T. Y.-T., Brokaw, C. J., Brennen, C. (eds.), 1-11.
- Berg, H. C. and Anderson, R. A.** (1973). Bacteria swim by rotating their flagellar filaments. *Nature* **245**, 380-382.
- Berg, H. C. and Brown, D. A.** (1972). Chemotaxis in Escherichia coli analysed by three-dimensional tracking. *Nature* **239**, 500-504.
- Berg, H. C. and Brown, D. A.** (1974). Chemotaxis in Escherichia coli analyzed by the three-dimensional tracking. *Antibiot. Chemother. (Basel)* **19**, 55-78.
- Berg, H. C. and Purcell, E. M.** (1977). Physics of chemoreception. *Biophys. J.* **20**, 193-219.
- Berg, H. C. and Tedesco, P. M.** (1975). Transient response to chemotactic stimuli in Escherichia coli. *Proc. Nat. Acad. Sci. U.S.A.* **72**, 3235-3239.
- Berg, H. C., Manson, M. D. and Conley, M. P.** (1982). Dynamics and energetics of flagellar rotation in bacteria. *Symp. Soc. Exp. Biol.* **35**, 1-31.
- Block, S. M., Segall, J. E. and Berg, H. C.** (1982). Impulse responses in bacterial chemotaxis. *Cell* **31**, 215-226,

- Block, S. M., Segall, J. E. and Berg, H. C.** (1983). Adaptation kinetics in bacterial chemotaxis. *J. Bacteriol.* **154**, 312-323.
- Boeckh, J., Kaissling, K. E. and Schneider, D.** (1965). Insect olfactory receptors. *CSH Symp. Quant. Biol.* **30**, 263-280.
- Boring, E.** (1956). Gustav Theodor Fechner. In: *The World of Mathematics*, V. 2 (Simon and Schuster, New York), J. R. Newman (ed.), 1148-1166.
- Boyd, A. and Simon, M.** (1982). Bacterial chemotaxis. *Ann. Rev. Physiol.* **44**, 501-517; 9895-9902.
- Boyd, A., Kendall, K. and Simon, M. L.** (1983). Structure of the serine chemo-receptor in Escherichia coli. *Nature* **301**, 623-626.
- Boyd, A., Krikos, A. and Simon, M.** (1981). Sensory transducers of E. coli are encoded by homologous genes. *Cell* **26**, 333-343.
- Brown, D. A. and Berg, H. C.** (1974). Temporal stimulation of chemotaxis in Escherichia coli. *Proc. Nat. Acad. Sci. U.S.A.* **71**, 1388-1392.
- Clarke, S. and Koshland, D. E., Jr.** (1979). Membrane receptors for aspartate and serine in bacterial chemotaxis. *J. Biol. Chem.* **254**, 9695-9702.
- Dahlquist, F. W., Elwell, R. A. and Lovely, P. S.** (1976). Studies of chemotaxis in defined concentration gradients. *J. Supramol. Struct.* **4**, 329-342.
- Dahlquist, F. W., Lovely, P. and Koshland, D. E., Jr.** (1972). Quantitative analysis of bacterial migration in chemotaxis. *Nature New Biol.* **236**, 120-123.
- Delbrück, M. and Reichardt, W.** (1956). System analysis for the light growth response of Phycomyces. In: *Cellular Mechanisms in Differentiation and Growth* (Princeton Univ. Press, Princeton, N. J.), D. Rudnick (ed.), 3-44.
- DePamphilis, M. L. and Adler, J.** (1971a,b). Fine structure and isolation of the hook-basal body complex from Escherichia coli and Bacillus subtilis. *J. Bacteriol.* **105**, 376-395.

Dobell, C. (1958). In: *Antony van Leeuwenhoek and his "Little Animals"* (Russell and Russell, New York), Chapter 2, p. 188. **Also published:** (1932, John Bale, Sons and Danielsson, Ltd., Cambridge, England; 1960, Dover Publications, New York), C. Dobell (ed.).

Engelmann, T. W. (1883). Bacterium photometricum. Ein Beitrag zur vergleichenden Physiologie des Licht- und Farbensinnes. *Pflügers Arch. Gesamte Physiol. Menschen Tiere* **30**, 95-124.

Goy, M. F., Springer, M. S. and Adler, J. (1977). Sensory transduction in Escherichia coli: Role of a protein methylation reaction in sensory adaptation. *Proc. Nat. Acad. Sci. U.S.A.* **74**, 4967-4968.

Hazelbauer, G. L. (1975). The maltose chemoreceptor of Escherichia coli. *J. Bacteriol.* **122**, 206-214.

Hedblom, M. L. and Adler, J. (1960). Genetic and biochemical properties of Escherichia coli mutants with defects in serine chemotaxis. *J. Bacteriol.* **144**, 1048-1060.

Iino, T. (1977). Genetics of structure and function of bacterial flagella. *Ann. Rev. Genet.* **11**, 161-182.

Ishihara, A., Segall, J. E., Block, S. M. and Berg, H. C. (1983). Coordination of flagella on filamentous cells of Escherichia coli. *J. Bacteriol.*, in press.

Khan, S. and Macnab, R. M. (1980). The steady-state counterclockwise/clockwise ratio of bacterial flagellar motors is regulated by protonmotive force. *J. Mol. Biol.* **138**, 563-597.

Komeda, Y. (1982). Fusion of flagellar operons to lactose genes on a Mu-lac bacteriophage. *J. Bacteriol.* **150**, 16-26.

Kondoh, H., Ball, C. B. and Adler, J. (1979). Identification of a methyl-accepting chemotaxis protein for the ribose and galactose chemoreceptors of Escherichia coli. *Proc. Nat. Acad. Sci. U.S.A.* **76**, 260-264.

- Larsen, S. H., Reader, R. W., Kort, E. N., Tso, W.-W. and Adler, J.** (1974). Change in direction of flagellar rotation is the basis of the chemotactic response in Escherichia coli. *Nature* **249**, 74-77.
- Lovely, P. S. and Dahlquist, F. W.** (1975). Statistical measures of bacterial motility and chemotaxis. *J. Theor. Biol.* **50**, 477-496.
- Macnab, R. M.** (1976). Examination of bacterial flagellation by dark-field microscopy. *J. Clin. Microbiol.* **4**, 258-265.
- Macnab, R. M. and Koshland, D. E., Jr.** (1972). The gradient-sensing mechanism in bacterial chemotaxis. *Proc. Nat. Acad. Sci. U.S.A.* **69**, 2509-2512.
- Macnab, R. M. and Koshland, D. E., Jr.** (1973). Persistence as a concept in the motility of chemotactic bacteria. *J. Mechanochem. Cell. Motil.* **2**, 141-148.
- Manson, M. D., Tedesco, P., Berg, H. C., Harold, F. M. and van der Drift, C.** (1977). A protonmotive force drives bacterial flagella. *Proc. Nat. Acad. Sci. U.S.A.* **74**, 3060-3064.
- Marmarelis, P. and Marmarelis, V.** (1978). Analysis of physiological systems: the white noise approach. (Plenum Press, N. Y.), Chapter 3, pp. 71-128.
- Parkinson, J. S.** (1981). Genetics of bacterial chemotaxis. *Soc. Gen. Microbiol. Symp.* **31**, 265-290.
- Parkinson, J. S.** (1982). Genetics of bacterial chemotaxis. *Symp. Soc. Exp. Biol.* **35**, 264-290.
- Parkinson, J. S. and Hazelbauer, G. L.** (1984). Bacterial chemotaxis: molecular genetics of sensory transduction and chemotactic gene expression. (Cold Spring Harbor, in press).
- Pfeffer, W.** (1884). Locomotorische Richtungsbewegungen durch chemische Reize. *Untersuch. Botan. Inst. Tübingen* **1**, 363-482.
- Pfeffer, W.** (1888). Über chemotactische Bewegungen von Bakterien, Flagellaten und Volvocinen. *Untersuch. Botan. Inst. Tübingen* **2**, 582-663.

- Purcell, E. M.** (1977). Life at low Reynold's number. *Am. J. Phys.* **45**, 3-11.
- Rollins, C. and Dahlquist, F. W.** (1981). The methyl-accepting chemotaxis proteins of E. coli: a repellent-stimulated covalent modification distinct from methylation. *Cell* **25**, 333-340.
- Segall, J. E., Manson, M. D., and Berg, H. C.** (1982). Signal processing times in bacterial chemotaxis. *Nature* **296**, 855-857.
- Sherris, D. and Parkinson, J. S.** (1981). Post-translational processing of methyl-accepting chemotaxis proteins in Escherichia coli. *Proc. Nat. Acad. Sci. U.S.A.* **78**, 6051-6055.
- Silverman, M. and Simon, M.** (1974). Flagellar rotation and the mechanism of bacterial motility. *Nature* **249**, 73-74.
- Silverman, M. and Simon, M. L.** (1977). Bacterial flagella. *Ann. Rev. Microbiol.* **31**, 397-419.
- Silverman, M., Matsumura, P. and Simon, M.** (1976). The identification of the mot gene product with Escherichia coli-lambda hybrids. *Proc. Nat. Acad. Sci. U.S.A.* **73**, 3126-3130.
- Springer, M., Goy, M. F. and Adler, J.** (1977). Sensory transduction in Escherichia coli: two complementary pathways of information processing that involve methylated proteins. *Proc. Nat. Acad. Sci. U.S.A.* **74**, 3312-3316.
- Springer, M. S., Goy, M. F. and Adler, J.** (1979). Protein methylation in behavioural control mechanisms and in signal transduction. *Nature* **280**, 279-284.
- Spudich, J. L. and Koshland, D. E., Jr.** (1975). Quantitation of the sensory response in bacterial chemotaxis. *Proc. Nat. Acad. Sci. U.S.A.* **74**, 710-713.
- Watson, J. D.** (1977). Molecular biology of the gene. (W. A. Benjamin, Menlo Park), Chapter 3, pp. 59-82.